Stability Analysis of Large-Scale Power Electronics Systems

by

Phuong Huynh

Dissertation submitted to the Faculty of the

Virginia Polytechnic Institute and State University

in partial fulfillment of the requirements for the degree of

Doctor of Philosophy

in

Electrical Engineering

APPROVED:

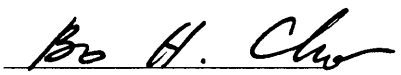

Bo H. Cho, Chairman

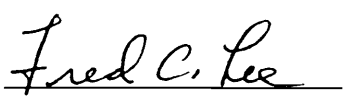

Fred C. Lee

Dan Sable

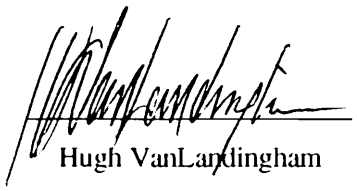

Hugh VanLandingham

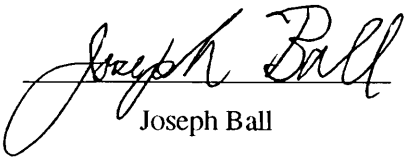

Joseph Ball

December 1994

Blacksburg, Virginia

Stability Analysis of Large-Scale Power Electronics Systems

by

Phuong Huynh

Bo H. Cho, Chairman

Electrical Engineering

(ABSTRACT)

A new methodology is proposed to investigate the large-signal stability of interconnected power electronics systems. The approach consists of decoupling the system into a source subsystem and a load subsystem, and stability of the entire system can be analyzed based on investigating the feedback loop formed by the interconnected source/load system. The proposed methodology requires two stages: (1) since the source and the load are unknown nonlinear subsystems, system identification, which consists of isolating each subsystem into a series combination of a linear part and a nonlinear part, must be performed, and (2) stability analysis of the interconnected system is conducted thereafter based on a developed stability criterion suitable for the nonlinear interconnected-block-structure model. Applicability of the methodology is verified through stability analysis of PWM converters and a typical power electronics system.

Acknowledgments

I would like to express my sincere appreciation to my advisor, Dr. Bo H. Cho, for his encouragement, support, and guidance which allowed me to complete this work during the course of my stay at the Virginia Power Electronics Center (VPEC). Special thanks to Dr. Fred C. Lee for providing me the opportunity to do research at VPEC. I would like to thank also my committee members, Dr. Dan Sable, Dr. Hugh VanLandingham, and Dr. Joseph Ball for their suggestions and comments. I would like to thank my fellow members at VPEC for their friendship and help.

I would like to acknowledge the supports provided by National Science Foundation.

Thanks to my parents and my cousins for their endless support; and with much love and gratitude, I wish to thank also my fiancee, My-Hanh, for her deepest understanding, love, and support during my stay at Virginia Tech. I dedicate this dissertation to her in token of my love and appreciation.

Table of Contents

Chapter 1: Introduction **1**

1.1 Background 1

1.2 Methodology for the Stability Analysis of Large-Scale Power Electronics Systems 4

1.3 Objective and Outline 7

Chapter 2: Methodology for the Stability Analysis of Large-Scale Power Electronics Systems **11**

2.1 Source and Load Subsystem Identification 14

2.1.1 Perturbation Signals for Source and Load Subsystem Identification 15

2.1.2 Sampling Effect and Experiment Design 15

2.1.3 Factorization of Linear and Nonlinear Parts 17

2.1.4 Linear Part Identification 22

2.1.5 Sector Gain Identification of the Nonlinear Part 23

2.2 A Large-Signal Stability Criterion for the Interconnected Source/Load System 27

2.3 Summary 32

Chapter 3: Stability Analysis of PWM Converters **33**

3.1 State-Space Averaging of PWM Converters 34

3.2 Large-Signal Stability Analysis in Voltage-Mode Control 36

3.2.1 Effect of Duty Cycle Saturation on the Converter Stability 36

3.2.2 Effect of Saturation in the Feedback Loop on the Converter Stability 49

3.2.3 Combined Saturation Nonlinearities 49

3.3 Large-Signal Stability Analysis in Current-Injection Control 50

3.3.1 Effect of Duty Cycle Saturation on the Converter Stability 56

3.3.2 Effect of Saturation in the Feedback Loop on the Converter Stability 57

3.3.3 Combined Saturation Nonlinearities 57

3.4 Large-Signal Stability Analysis of a Boost Converter 63
3.4.1 Stability Analysis of a Boost Converter as a Bilinear System 63
3.4.2 Effect of Duty Cycle Saturation on the Boost Converter 69
3.5 Summary 78

Chapter 4: Stability Analysis of a Large-Scale Power Electronics System 79
4.1 DDCU and a Load Subsystem 80
4.1.1 Small-Signal Identification of the DDCU and the Load Subsystem 84
4.1.2 Sector Gain Identification of the DDCU and the Load Subsystem 87
4.1.2.1 Selection of a CSRS for Large-Signal Perturbation 88
4.1.2.2 Sector Gain Identification 92
4.1.2.3 Multiplier Insertion and Identification of a New Sector Gain for the DDCU 93
4.1.3 Stability Analysis of the Interconnected DDCU and Load Subsystem 99
4.2 Graphical Design Insights of the Small-Signal Loop Gain Leading to Large-Signal Stability .108
4.3 Summary 109

Chapter 5: Conclusions 111

References 113

Appendix A: Input-Output Stability Theory for Nonlinear Systems 119
A.1 Signals and Systems 120
A.1.1 Norms 120
A.1.2 Systems 122
A.1.2.1 Gain of a System 122
A.1.2.2 BIBO Stability 123
A.1.2.3 Sectoricity 123
A.1.2.4 Conicity 124
A.1.2.5 Linear Systems 124
A.1.2.6 Nonlinear Systems 127
A.2 Input-Output Stability of Single-Loop Systems 128
A.2.1 A Small-Gain Theorem for Single Loop Systems 128
A.2.2 Margin of Boundedness 131

A.2.3 Loop Transformation Theorem 131
A.2.4 The Circle Criterion 134
A.2.5 Graphical Interpretation of the Margin of Boundedness 139
A.2.6 Local Stability 140
A.2.7 Multiplier Theory 140
A.2.7.1 Sector Products 143
A.2.7.2 Improved Stability Criteria 144
A.2.7.3 The Off-Axis Circle Criterion 146
A.3 Input-Output Stability of Multiple-Loop Systems 148
A.3.1 M-Matrices 148
A.3.2 A Small-Gain Theorem for Multiple-Loop Systems 150

Appendix B: Perturbation Signals for Nonlinear System Identification 152

Appendix C: Stability of a Single-Loop Nonlinear System 157

Appendix D: MATLAB Programs 161
D.1 Small-Signal ARMA Modeling 161
D.2 Sector Gain Identification of Nonlinear Part 163

Vita 165

List of Illustrations

Fig. 1.1: Source/Load Decoupling at Interface 1 9
Fig. 1.2: Feedback Connection at an Interface 10
Fig. 2.1: Feedback Connection of Source and Load Subsystems 13
Fig. 2.2: Sampling Effect on the Input Signal 18
Fig. 2.3: Spectrum of the System Output 19
Fig. 2.4: Series Representation of an Unknown System 20
Fig. 2.5: Feedback Connection of Source and Load in Factorization Form 26
Fig. 2.6: Existence of Two Nonlinear Feedback Loop 29
Fig. 3.1: Voltage-Mode-Controlled Buck Converter 37
Fig. 3.2: Block Diagram Representations of the Closed-Loop Buck Converter With Inclusion of the Duty Cycle Saturation Nonlinearity 38
Fig. 3.3: Graphical Interpretation of the Off-Axis Circle Criterion 41
Fig. 3.4: Design for the Unstable Mode 44
Fig. 3.5: Graphical Interpretation of the Large-Signal Stability Analysis 45
Fig. 3.6: Design for the Stable Mode 46
Fig. 3.7: Block Diagram Representations of the Closed-Loop Buck Converter With Inclusion of the Opamp Saturation Nonlinearity 47
Fig. 3.8: Block Diagram Representations of the Closed-Loop Buck Converter With Inclusion of the Duty Cycle Saturation and the Opamp Saturation 48
Fig. 3.9: A Current-Injection-Controlled Buck Converter 51
Fig. 3.10: Block Diagram Representation of the Closed-Loop Buck Converter With Inclusion of the Duty Cycle Saturation Nonlinearity 52
Fig. 3.11: System Loop Gains 53
Fig. 3.12: Simulation Results for an Unstable Closed-Loop Buck Converter 54

Fig. 3.13: Block Diagram Representation of the Closed-Loop Buck Converter With Inclusion of the Opamp Saturation Nonlinearity 55
Fig. 3.14: Block Diagram Representation of the Closed-Loop Buck Converter With Inclusion of the Duty Cycle Saturation and the Opamp Saturation 59
Fig. 3.15: Simplified Block Diagram Representation of the Buck Converter 60
Fig. 3.16: A Current-Injection-Controlled Boost Converter 64
Fig. 3.17: Stability Conditions for a Closed-Loop Boost Converter 67
Fig 3.18: Block Diagram Representation of a Closed-Loop Boost Converter With Inclusion of the Duty Cycle Saturation Nonlinearity 70
Fig 3.19: Loop Gains of the Closed-Loop Boost Converter 74
Fig. 3.20: Simulation Results For an Unstable Boost Converter 75
Fig 3.21: Loop Gains of the Closed-Loop Boost Converter 76
Fig. 3.22: Simulation Results For a Stable Boost Converter 77
Fig. 4.1: Circuit Diagram of the DDCU and a Load Converter 82
Fig. 4.2: Large-Signal Instability Results for the Interconnected System 83
Fig. 4.3: DDCU Output Impedance 85
Fig. 4.4: Load Output Admittance 86
Table. 4.1: Log (RMS error) for Different System Orders 87
Fig. 4.5: Nonlinearity Detection 90
Fig. 4.6: Power Spectra of CSRSs with Different Dts 91
Fig. 4.7: Data Generation for Sector Gain Identification 94
Fig. 4.8: Conic Radius-Center Conic Relationship 95
Fig. 4.9: Insertion of a Multiplier 96
Fig. 4.10: New Sector Gain for the DDCU 97
Table 4.2: Key Parameters for the Stability Analysis 101
Fig. 4.11: Stability Results for Load Power = 6250 W 103
Fig. 4.12: Stability Results for Load Power = 3125 W 104
Fig. 4.13: Stability Results for Load Power = 240 W 105
Fig. 4.14: Case 1 - New Load Subsystem Characteristics and Stability Results 106
Fig. 4.15: Case 2 - New Load Subsystem Characteristics and Stability Results 107
Fig 4.16: Graphical Interpretation of Designing the Small-Signal Loop-Gain Leading to Large-Signal Stability 110

Fig. A.1: Sectoricity and Conicity 125
Fig. A.2: A Basic Single Loop System 129
Fig. A.3: Graphical Interpretation of the Loop Transformation Technique 132
Fig. A.4: Circle Criterion 136
Fig. A.5: Graphical Interpretation of the Margin of Boundedness 137
Fig. A.6: A Redefined Sector for Local Stability 138
Fig. A.7: Multiplier Insertion 142
Fig. A.8: Off-Axis Circle Criterion 147
Fig. A.9: A Basic Multiple Loop System 149
Table B.1: Stages That Can Be Combined with the Last Stage to Generate Maximum-Length Pseudorandom Binary Sequence 154
Fig. B.1: Pseudorandom Binary Signals Characteristics 155
Fig. B.2: CSRS characteristics 156
Fig. C.1: Single Loop Nonlinear Systems 160

Chapter 1

Introduction

1.1 Background

Presently, existing methods for the stability analysis of large-scale power electronics systems are based on linearization around the system steady-state operating point, from which linear analysis can be performed. Even though the linearization technique is a powerful tool, it can only predict the system local stability. New techniques are needed to investigate the large-signal behaviors and the global stability of large-scale power electronics systems.

Power electronics systems are known to be highly nonlinear. The nonlinear interactions between subsystems make the stability analysis of large-scale power electronics systems a difficult task. Presently, in order to analyze the stability of power electronics systems, linear analysis– the so-called *impedance comparison technique*– has to be conducted. The overall system stability can be investigated based on the comparison of the source impedance and the load admittance at each interface of the system. Middlebrook has used this technique to design input filters for the switching regulators [Middlebrook, 1976], and applications of the impedance comparison technique have been seen thereafter in the stability analysis of distributed power systems [Lewis, 1989], [Liu, 1989], and [Schulz, 1990]; spacecraft power systems [B. H. Cho, 1988s]. The

impedance comparison technique is considered the principal technique for designing and analyzing power electronics systems.

The main advantage of using linear analysis is evident because of its elegance and versatility. However, linear analysis and control are by no means a universal technique that can achieve system global stability. In fact, due to the system linearization around the steady-state operating point, the resulting small-signal analysis can only predict stability in the neighborhood of the system operating point. Then, one must resort to computer simulations in order to investigate any large-signal instability in the system. Yet, uncertainty in the system large-signal stability remains still. Indeed, computer simulations are, in a sense, a tool for "final product" verification and not for analysis and design. A successful computer test-case on a system does not necessarily mean that the system is stable in the large-signal sense, and it is possible that other types of input disturbance can render the system unstable. Thus, new tools that are suitable for the nonlinear system stability analysis are needed to back up the deficiency of the linear analysis in establishing large-signal stability criteria for power electronics systems.

For the nonlinear stability analysis of large-scale systems, three approaches have been proposed in the control literature: the Lyapunov approach, the passivity approach, and the input-output approach. When analyzing a large-scale system, the common technique observed in all the approaches is to decompose the entire system into smaller interconnected subsystems. Then, stability of the entire system can be investigated based on the properties of each subsystem and the interconnection structures.

The Lyapunov approach consists of finding a Lyapunov function for each subsystem, and stability of the overall system is guaranteed if a Lyapunov function, which composes all the subsystem's Lyapunov functions, exists for the overall system. Developments of this approach can be found in [Araki, 1978], and [Michel, 1978].

The passivity approach is based on the existing dissipative (a more general term for passivity) criteria. Since a passive system is a stable system, the emphasis of this approach is to determine the passivity property of the entire system based on the passivity properties of each subsystem. Major developments in this area can be found in [Vidyasagar, 1977 and 1979], [Sundareshan, 1977], and [Moylan, 1978].

The input-output approach emphasizes input/output properties of each subsystem. This approach identifies the subsystem inputs and outputs and the interconnection structure of the overall system and applies various properties of the so-called M-matrices to assess the overall system stability. The input-output approach for large-scale systems is an extension of the well-known nonlinear stability criteria for single-loop feedback systems: the Circle criterion and Popov criterion. The major contributors are [Porter, 1974], [Lasley, 1975], and [Michel, 1978].

Unfortunately, these stability criteria are difficult to apply to power electronics systems because they require specific information about the subsystems as well as the interconnection structure, which may not be available. Furthermore, these criteria become more complex to apply as the size of the system increases.

It is within the scope of this work that another approach is proposed to investigate the stability of large-scale power electronics systems. The new approach follows along the line of the input-output approach in an attempt to improve the impedance comparison technique mentioned previously.

1.2 Methodology for the Stability Analysis of Large-Scale Power Electronics Systems

In general, design and analysis of power electronics systems adopt a modular approach. A large-scale power electronics system consists of several interconnected subsystems or modules. First, each module is designed and optimized for stability at the subsystem level; then, the next step is to integrate these modules. However, integration of these modules does not guarantee that the interconnected system is stable due to interaction among modules. Therefore, interaction analysis at each connection point (or system interface) is needed to ensure the overall system stability. A common approach for the interaction analysis is to decouple the large-scale system into a source that comprises all the upstream modules and a load that consists of all the downstream modules, as illustrated in Fig. 1.1. Then, the overall system stability can be predicted based on investigating any possible interaction between the source and the load. This process is repeated at all the interfaces of the interconnected system to ensure the overall system stability.

First, it is necessary to review the classical impedance comparison technique and the meaning of interconnected subsystems in terms of stability before development of the new approach. When a source subsystem is connected to a load subsystem, a feedback loop is formed. Emergence of this feedback loop due to the interconnection means that instability can arise in the interconnected source/load system.

To show existence of the feedback loop, consider both source and load as unterminated one-port networks, as shown in Fig. 1.2(a), where the directions of the source and the load currents are specified as entering the ports. When the source and the load are connected as in Fig. 1.2(b), where v_p and i_p denote the system perturbations at the interface, a feedback loop is formed. Indeed, let the operator Z represent the source subsystem and the operator Y represent the load subsystem, then

$$v_s = Zi_s, \tag{1.1}$$

$$i_l = Y v_l. \tag{1.2}$$

Also, according to Fig. 1.2(b), interconnection of the source and the load yields

$$i_s = i_p - i_l, \tag{1.3}$$

$$v_l = v_p + v_s. \tag{1.4}$$

Equations 1.1, 1.2, 1.3, and 1.4 can be translated into an equivalent block diagram, as shown in Fig. 1.2(c), and the existence of a feedback loop due to the source/load interconnection is obvious.

According to Fig. 1.2(c), use of the impedance comparison technique for the small-signal stability analysis of interconnected source/load systems become clear. If the operator Z represents the impedance of the source and the operator Y represents the admittance of the load, small-signal stability can be assured by investigating the Nyquist plot of the loop gain ZY. Consequently, this technique is appropriate for the small-signal stability analysis of large-scale power electronics systems: an interface is selected, and the system is decoupled into a source subsystem and a load subsystem; then the source impedance, Z, and the load admittance, Y, are measured; and the overall system small-signal stability can be investigated based on the Nyquist plot of the loop gain ZY. Nevertheless, in dealing with input-output stability, the observability properties of the source and the load subsystems are important because it is possible that stability can be assured at an interface of the system while an oscillation, which cannot be observed at the analyzed interface, can occur elsewhere in the system. Consequently, it is necessary to analyze the stability at all the interfaces of the interconnected system.

However, the impedance comparison analysis can only assure stability of the interconnected system within a small neighborhood around the system operating point, since both Z and Y represent the linearized small-signal transfer functions of the nonlinear source and the nonlinear load. Thus, a new approach must be developed to overcome the deficiency of this impedance comparison technique.

At this point, it is realized that the above interface analysis can be applied to investigate the nonlinear large-signal stability of the interconnected system as well, if Z and Y are considered nonlinear operators, which represent the large-signal behaviors of the source and the load. This is the cornerstone of the proposed methodology for analyzing the large-signal stability of power electronics systems. The new approach follows all the rigorous arguments discussed earlier regarding the impedance comparison technique, except for the fact that Z and Y are treated as nonlinear operators.

Even though this methodology is similar to the impedance comparison technique, several issues can arise. Due to the nonlinear characteristics of the operators Z and Y, the first complication is that the Nyquist criterion and the linear stability theory are not applicable. Also, it is not obvious how to characterize Z and Y. Therefore, departure of this methodology from the impedance comparison analysis technique is evident, and this methodology requires proper characterization of the nonlinear operators Z and Y and a new stability criterion for the nonlinear feedback loop in Fig. 1.2(c).

Thus, to make this methodology a feasible approach, two stages are required: (1) characterization of Z and Y in such a way that they are suitable for the interconnected system stability analysis, and (2) development of a nonlinear stability criterion based on the input-output stability theory outlined in Appendix A for the stability analysis of the interconnected source/load system.

1.3 Objective and Outline

As mentioned above, large-signal stability of power electronics systems has always been the main concern. Many nonlinearities existing in power electronics systems make the impedance comparison technique inappropriate in assuring the system large-signal stability. The scope of this work is motivated by a need of new tools and techniques, based on the modular approach, that can be used to ensure large-signal stability of power electronics systems.

The main objective of the research is to conduct stability analysis of large-scale power electronics systems based on the nonlinear input-output stability theory, which is presented in Appendix A for consultation, and the system identification theory. First, charaterization of both load and source is necessary: Z and Y must be represented in a particular structure that can be used for the stability analysis of the interconnected source/load system. If knowledge of Z and Y, such as state space representation or input-output representation, is available, then they can be rearranged into the particular structure for the stability analysis. Otherwise, the characterization can adopt an input-output data analysis point of view: it presumably treats the source and the load as "black boxes" and identifies their structures based on their input/output responses. Once both source and load structures are identified, stability analysis of the interconnected system can be conducted. However, since these are nonlinear systems, the Nyquist criterion is not applicable, and a new stability criterion must be developed. The input-output theory provides a foundation for the development of a new stability criterion that is suitable for the analysis of interconnected source/load systems.

In Chapter 2, theoretical development of the proposed methodology is presented. First, source and load subsystem characterization is discussed. The identification process consists of isolating the linear part and the nonlinear part of the subsystem. This process is commonly known as block structure identification where the nonlinear part is cascaded after the linear part. Initially, perturbation signals are injected into the source and the load subsystems, and the output response

is collected. Then, characterization of source and load is performed based on the measured data. Next, a new stability criterion suitable for the stability analysis of an interconnected source/load system is developed based on the input-output stability theory. The outcome is a set of three sufficient conditions which have to be fulfilled in order to assure large-signal stability of the entire system.

Chapter 3 addresses the large-signal stability of PWM converters based on the input-output stability theory discussed in Appendix A. Since the structures of PWM converters are well-known, identification process is not necessary. Only application of existing input-output stability criteria is performed to assess stability properties of PWM converters. The objective of this chapter is twofold: (1) to illustrate feasibility of the input-output stability theory outlined in Appendix A as applied in the large-signal stability analysis of power electronics systems, and (2) to investigate the large-signal stability of PWM converters- an issue that has not been addressed widely in the literature.

In Chapter 4, a typical power electronics system is selected to illustrate feasibility of the proposed methodology developed in Chapter 2. Practical consideration of the approach is outlined as well. Assuming that the given system has an unknown structure, the procedure consists of decoupling the system into a source subsystem and a load subsystem, performing subsystem identification, and investigating the feedback loop formed by the interconnection to assess stability property of the integrated system.

Conclusions are presented in Chapter 5.

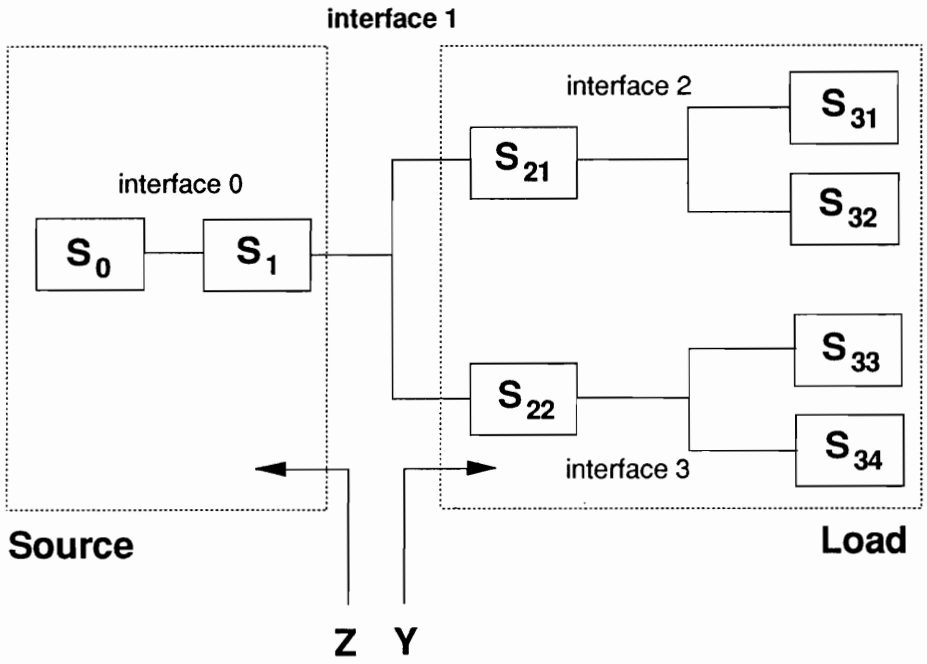

Fig. 1.1: Source/Load Decoupling at Interface 1

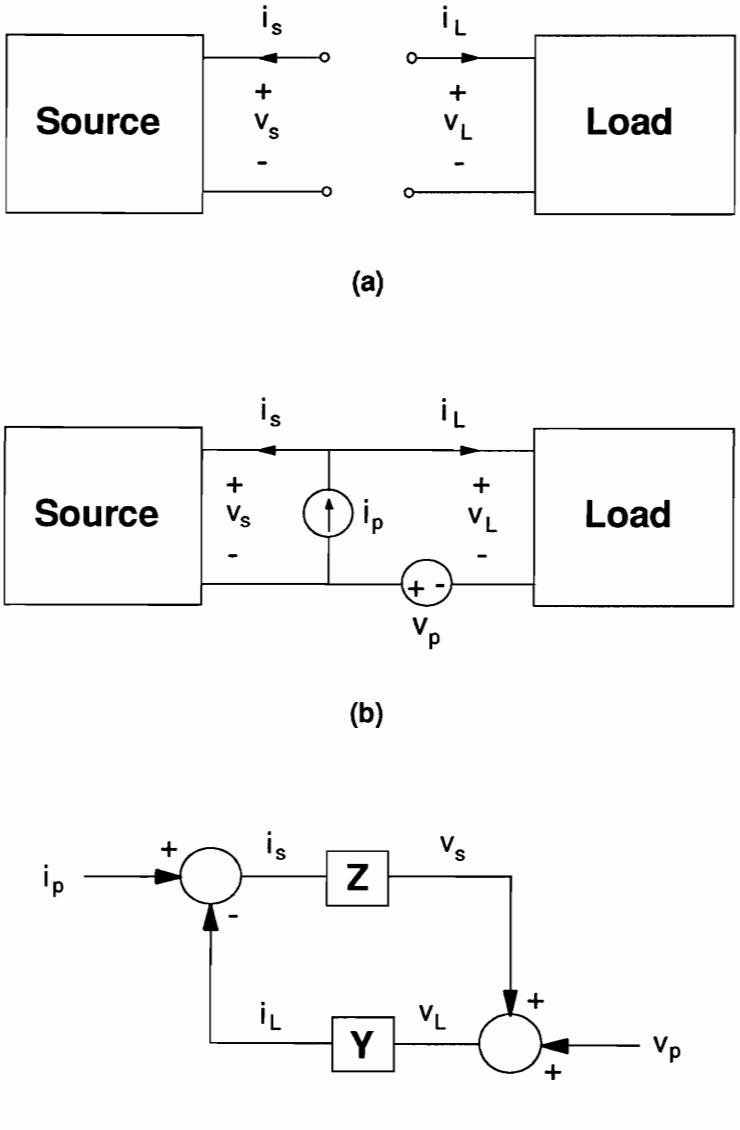

Fig. 1.2: Feedback Connection at an Interface
(a) Source and Load Unterminated Models
(b) Source and Load Interconnection
(c) Equivalent Feedback Representation

Chapter 2

Methodology for the Stability Analysis of Large-Scale Power Electronics Systems

In this chapter, a new methodology for the stability analysis of large-scale power electronics systems is represented. It has been pointed out in Chapter 1 that a large-scale power electronics system can be viewed as an interconnection of a source subsystem and a load subsystem, which gives rise to the feedback loop shown in Fig. 2.1(a). Under large-signal disturbance, the source subsystem, Z, and the load subsystem, Y, are nonlinear; therefore, Nyquist criterion is not applicable to the feedback loop formed by the source/load interconnection.

First, characterization of Z and Y is necessary. Assuming that Z and Y are stable subsystems, it is claimed that both Z and Y are factorizable into a series combination of a stable linear part, L, and a stable nonlinear part, N; namely

$$v_s = Zi_s \Rightarrow v_s = N_z L_z i_s, \tag{2.1}$$

and

$$i_l = Yv_l \Rightarrow i_l = N_y L_y v_l, \tag{2.2}$$

where L represents the linearized system around the steady-state operating point, and N represents the large-signal nonlinear dynamic. This implies that under small-signal input perturbation, N has

little contribution to the output response and becomes an identity operator, I. The reason for the factorization is to improve the conservativeness of the to-be-developed nonlinear stability criterion and to establish stability conditions that are in similar format to Nyquist criterion. Figure 2.1(b) illustrates the feedback loop with both Z and Y factorized into $Z = N_z L_z$ and $Y = N_y L_y$.

Given this particular feedback structure, the first step in the stability analysis is identification of L_z, N_z, L_y, and N_y. Since both L_z and L_y are linear operators, they can be represented by the system transfer functions. If the structures of Z and Y are not known in advance, linear system identification, which will be presented in Section 2.1.4, can be performed to obtain equivalent ARMA models for L_z and L_y. However, N_z and N_y are nonlinear operators and must be characterized differently. In the input-output stability theory, which is presented in Appendix A for consultation, a nonlinear operator can be characterized by a sector gain, a pair of real numbers $\{a,b\}$. Recall from Appendix A that a nonlinear operator, N, belonging to the sector $\{a,b\}$ means that the gain the operator N must be confined within a and b; namely, if u is the input to the system N, then

$$a \le \frac{\|Nu\|}{\|u\|} \le b. \tag{2.3}$$

Once L_z, N_z, L_y, and N_y are determined, the next step is to analyze the stability of the interconnected system based on investigation of the feedback loop. A new large-signal stability criterion for the interconnected source/load system is developed for this purpose.

The next section will address identification of L_z, N_z, L_y, and N_y.

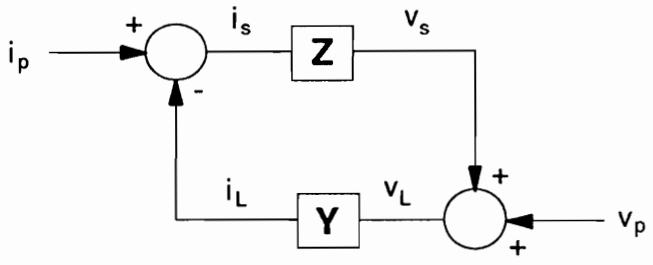

(a)

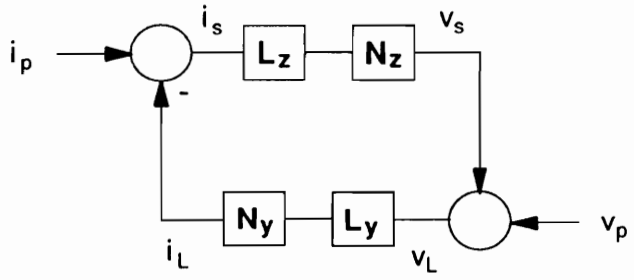

(b)

Fig. 2.1: Feedback Connection of Source and Load Subsystems
(a) Theoric Operator Representation
(b) Feedback Representation in Factorization Form

2.1 Source and Load Subsystem Identification

Since the source and the load subsystems are given as black boxes with only an accessible input u and an accessible output y, the first step in the system identification is to obtain a meaningful set of measured input/output data, $\{u,y\}$, which characterizes fully the system. Selection of perturbation signals for nonlinear system identification is therefore important because the perturbation signal must excite all the dynamics and nonlinearities that exist in the unknown system. According to the Volterra series theory [Schetzen, 1980], the concept of nonlinear transfer functions suggests that a nonlinearity in a system can be excited more considerably at a certain frequency than at other frequencies. For instance, it is possible that a step input does not excite the nonlinearities in a system, while a sinusoidal input at the exciting frequency can have a greater impact on the nonlinear effects in the system. Thus, interpretation of signals and nonlinear systems in the frequency domain seems to be more suitable than in the time domain. Consequently, let us introduce the following important concepts that will become useful in the forthcoming sections.

Definition: *The average power of a signal x(t), denoted by P(x), is defined as*

$$P(x)=\lim_{T\to\infty}\frac{1}{T}\int_0^T x(t)^2\,dt. \tag{2.4}$$

Definition: *The power spectral density of a signal x(t), denoted by $\mathcal{P}_x(f)$, is a real nonnegative function of frequency and describes distribution of the signal power over the frequency span. Also, the average power of the signal x, P(x), is given by*

$$P(x)=\int_{-\infty}^{\infty}\mathcal{P}_x(f)df. \tag{2.5}$$

Theorem: *For a linear system with an input u and an output y, the magnitude of the system transfer function, $H(j2\pi f)$, can be computed from [Couch, 1993]*

$$|H(j2\pi f)|=\sqrt{\frac{\mathcal{P}_y(f)}{\mathcal{P}_x(f)}}. \tag{2.6}$$

2.1.1 Perturbation Signals for Source and Load Subsystem Identification

Since the principle of superposition does not hold for nonlinear systems, application of sinusoidal inputs is certainly unpromising because the response of the system to two such inputs of different frequencies is different in general from the sum of the responses due to each input separately- so no additional information is gained besides the sinusoidal behavior. In general, the same will hold true for other types of inputs such as steps, pulses, etc.

On the other hand, provided that the system is subjected to a Gaussian white-noise (random perturbation with normal distribution) input for a long enough time, there is a finite probability that any given input waveform will be represented arbitrarily closely (over a finite time interval) by some sample of this white-noise signal. This is true because the Gaussian white-noise signal contains every possible frequency and all amplitudes within the Gaussian distribution of signal amplitude. Therefore, Gaussian white-noise input is a more preferable perturbation signal.

However, Gaussian white-noise is not a physically realizable signal since it has an infinite power bandwidth and, consequently, infinite average power [Couch, 1993]. Consequently, two other types of signals (Appendix B), which preserve most of the important properties of the Gaussian white-noise and which can be easily generated by software or hardware, have been proposed: pseudorandom binary signals (PRBS) [Godfrey, 1993], and constant-switching-pace symmetric random signals (CSRS) [Marmarelis, 1978].

2.1.2 Sampling Effect and Experiment Design

The information collected from the unknown system is in the form of measured input-output data, $\{u,y\}$, which are recorded at a specific sampling period, T_d. Consequently, the spectra of the measured signals u and y consist of replication of the true spectra of the signals u and y at multiple of the sampling frequency, $1/T_d$- a phenomenon known as sampling effect. If the sampling

frequency is selected to be smaller than half of the bandwidth of the signals u and y, the replicated spectra will overlap, and aliasing will occur, resulting in erroneous characterization of the unknown system. Thus, during the data acquisition process, two key parameters need to be specified in order to characterize the unknown system properly: the sampling frequency and the perturbing frequency of the random input signal.

First, selection of the perturbation frequency for the PRBSs or the CSRSs is important. If the perturbation period, Δt, is the same as the sampling period, T_d, Fig. 2.2(a) indicates that there is still considerable power within the input signal above the Nyquist frequency ($1/2\Delta t$) and aliasing errors will occur. However, setting $\Delta t = 2T_d$ would move the replicated spectrum toward higher frequency, and the amount of overlap between the original spectrum and the replicated spectrum would be significantly reduced, as illustrated in Fig. 2.2(b). Thus, the illustration in Fig. 2.2 suggests that the perturbation period, Δt, should be at least two times larger than T_d to avoid the problem of aliasing when sampling the input data.

The next issue concerns selection of T_d. Ljung [Ljung, 1987] suggests that a sampling frequency that is about ten times the bandwidth of the system should be a good choice in most cases. However, for a source or load subsystem, the outputs are usually an output voltage or an input current, and often, they can be periodic waveforms with a fundamental period T_s. Note that for a switching regulator, T_s can be the switching period of the regulator; or for a power factor correction circuit, T_s can be the period of the 120 Hz ripple. When dealing with such periodic signals, selection of the sampling period must be made carefully.

Since the subsystem output, says $y(t)$, is periodic, it can be represented by a Fourier series expansion,

$$y(t) = \sum_{n=-\infty}^{n=\infty} c_n e^{jn2\pi f_s t}, \tag{2.7}$$

where $f_s = 1/T_s$. When the input is perturbed with a signal of bandwidth B, the Fourier coefficients of $y(t)$, c_n, become time-varying. According to the modulation theory [Couch, 1993], the spectrum of $y(t)$, as illustrated in Fig. 2.3, consists of replicated spectra of the baseband spectrum centered at multiple of the fundamental frequency, f_s. Therefore, if the bandwidth of the input perturbation signal, B, is larger than $f_s/2$, it will excite the output signal to have a bandwidth larger than $f_s/2$ and the replicated spectra will overlap, resulting in an aliasing problem. Thus, this means that the linear response beyond $f_s/2$ cannot be recovered by sampling the system faster than f_s, since the aliasing problem is inherent in systems with periodic outputs. Consequently, a sampling frequency equal to or less than f_s should be used for system identification. However, the sampling frequency should be high enough to detect all different modes in the system. Therefore, setting the sampling frequency at f_s should be a proper choice.

2.1.3 Factorization of Linear and Nonlinear Parts

As mentioned previously, in order to reduce the conservativeness of the sufficient condition for stability, one should factorize the operators Z and Y in such a way as to isolate the linear part and the nonlinear part in each. It was claimed that if both Z and Y are stable subsystems, their factorization will result in stable linear and nonlinear operators. This section will show that the above argument is true.

Recall from the Volterra series theory [Schetzen, 1980] that any time-invariant nonlinear system with memory can be represented by a Volterra series. If u and y are the input and output of the system, respectively, then the system is represented by

$$y = \sum_{i=1}^{\infty} H_i u, \tag{2.8}$$

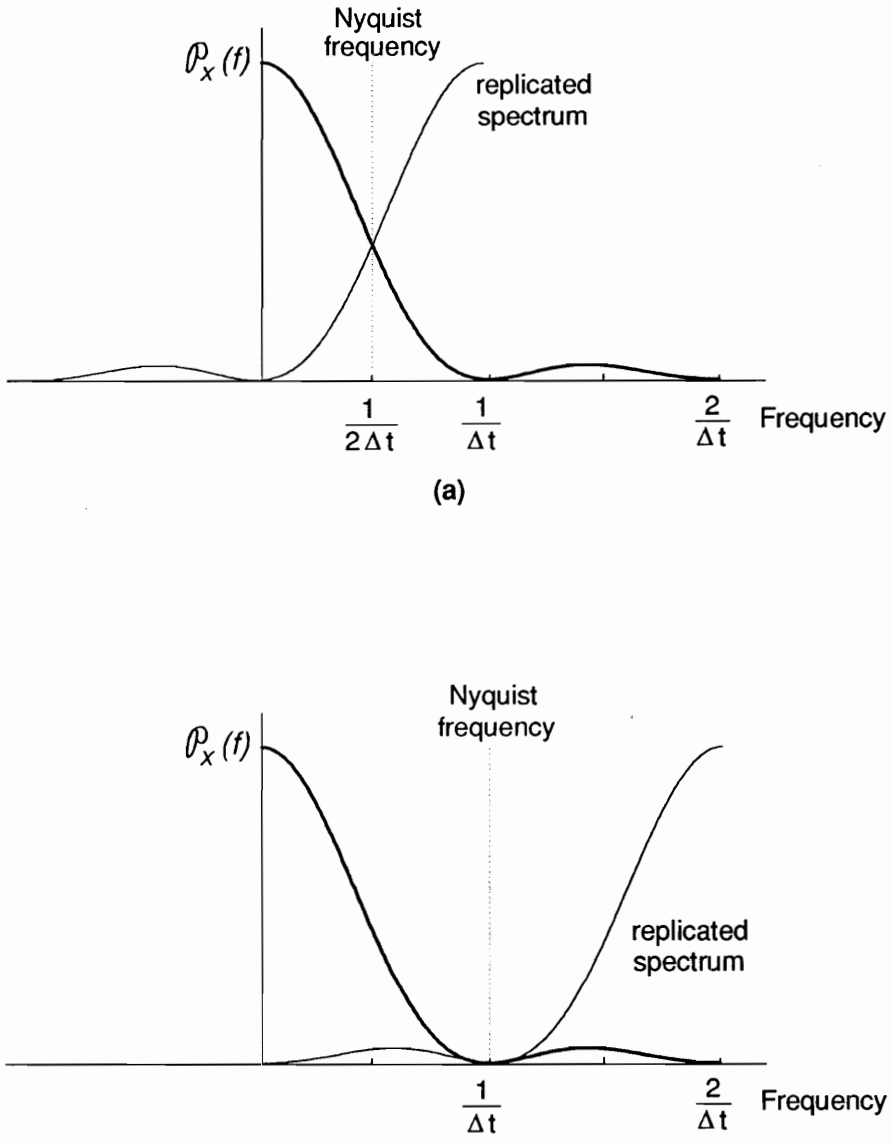

Fig. 2.2: Sampling Effect on the Input Signal
(a) $\Delta t = T_s$
(b) $\Delta t = 2T_s$

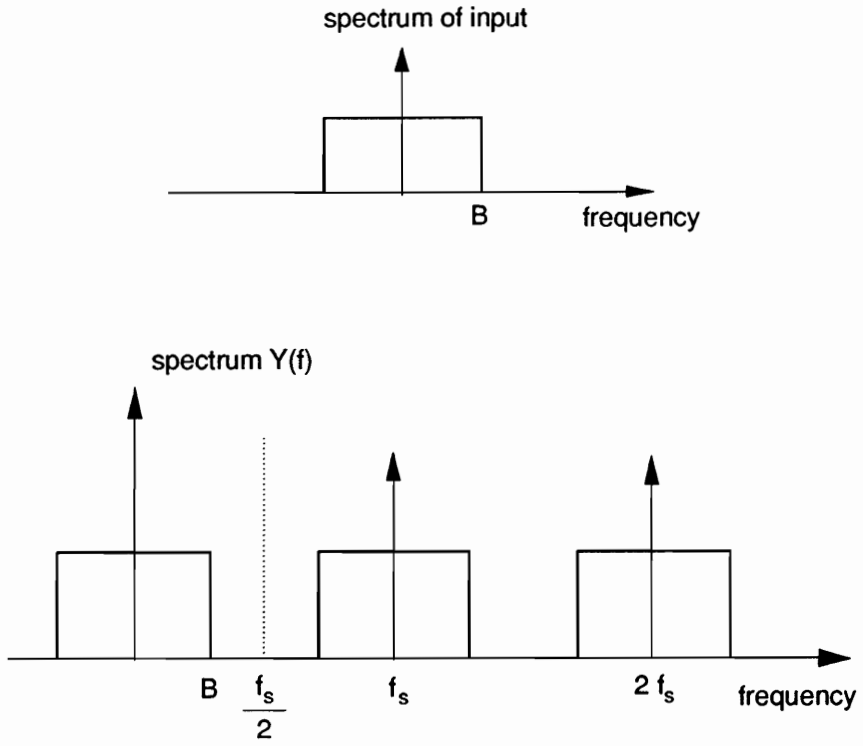

Fig. 2.3: Spectrum of the System Output

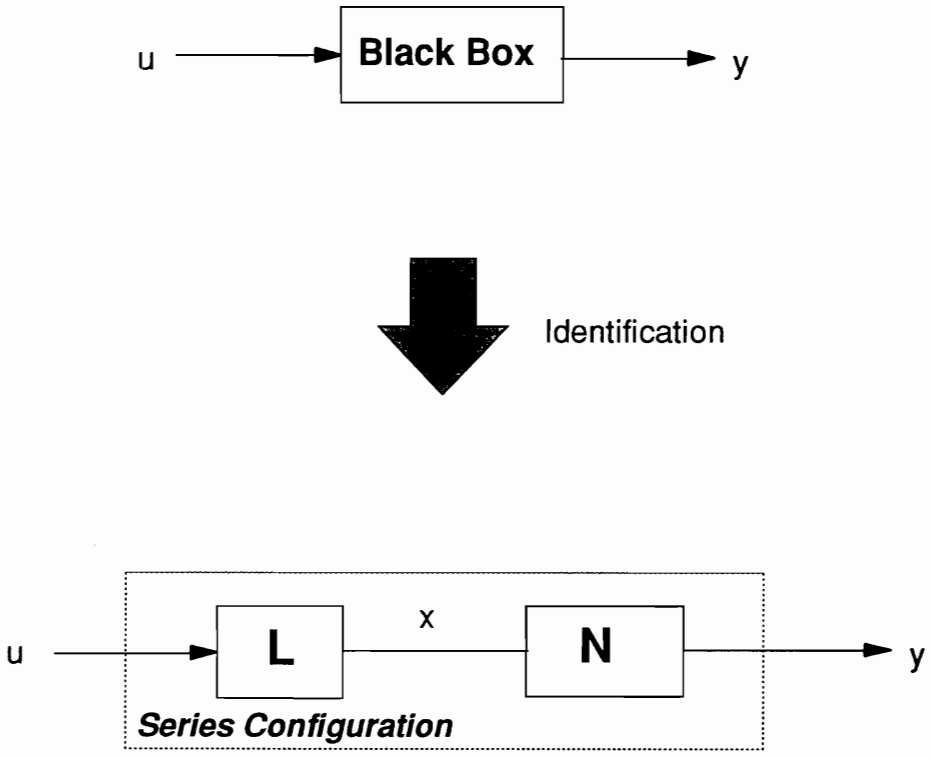

Fig. 2.4: Series Representation of an Unknown System

where the first-order operator, H_1, represents the linearized system around the steady-state operating point, and all the higher-order operators, H_i ($i > 1$), represent the nonlinear expansion from the steady-state operating point. Therefore, let S represents either the source subsystem, Z, or the load subsystem, Y; then S can be represented by

$$S = H_1 + (H_2 + H_3 + \ldots) = L_{parallel} + N_{parallel}, \tag{2.9}$$

where $L_{parallel} = H_1$ represents the linearized system of S around the steady-state operating point, and $N_{parallel}$ represents the sum of higher-order operators $H_2 + H_3 + \ldots$. Consequently, if S is a stable operator, both $L_{parallel}$ and $N_{parallel}$ must be stable also.

On the other hand, for the series configuration (the configuration that one is interested in for the stability analysis of the interconnected source/load system, as illustrated in Fig. 2.4) L_{series} represents the linearized system of S ($L_{series} = L_{parallel}$), and the nonlinear part, N_{series}, represents the large-signal dynamic of the system. Since $L_{series} = L_{parallel}$, this establishes that L_{series} must be stable.

In order to show that N_{series} is also a stable operator, notice that N_{series} can also be expanded into a Volterra series model of the form $N_{series} = K_1 + K_2 + K_3 + \ldots$ where K_1 is the 1st-order linear operator and K_i ($i > 1$) is the higher-order nonlinear operator. Thus, the system, S, can be represented by

$$S = N_{series} L_{series} = (K_1 + K_2 + K_3 + \ldots) L_{series} = K_1 L_{series} + K_2 L_{series} + K_3 L_{series} + \ldots. \tag{2.10}$$

Under small-signal disturbance, the nonlinear part N_{series} has a null effect on the system S; and therefore, $S = L_{series}$. This implies that K_1 must be an identity operator, $K_1 = I$ (the fundamental property of an identity operator is $Ix = x$.) Consequently, for the series-configuration block structure model, the unknown system is represented by $S = L_{series} + (K_2 + K_3 + \ldots) L_{series}$; and therefore, since $S = L_{parallel} + N_{parallel}$ for the parallel configuration, the relationship between $N_{parallel}$ and N_{series} is

$$N_{parallel} = (N_{series} - I)L_{series}. \tag{2.11}$$

Since it is known that L_{series} is a stable operator, N_{series} being unstable would imply that $N_{parallel}$ is also unstable. Thus, from contrapositive argument, N_{series} must also be stable, since $N_{parallel}$ is a stable operator.

2.1.4 Linear Part Identification

Knowing that an unknown stable system can be factorized into a series combination of a stable linear part and a stable nonlinear part, one can proceed to identify L_{series} and N_{series} independently. Since L_{series} represents the linearized system around a steady-state operating point of the nonlinear system S, injecting small-signal perturbation around the stead-state operating point would nullify the nonlinear effects in N_{series} and would be appropriate for identifying L_{series}. Thus, the first step in the identification process is to identify L_{series}. Given a data set $\{u_{small}, y_{small}\}$ that represents the small-signal response of the system around a steady-state operating point, one can apply existing technique in the literature to obtain a small-signal linear model for the unknown system. One of the approach is based on the least-squares fit [Norton, 1986]. Consider an AutoRegressive Moving Average (ARMA) model of order n

$$\begin{aligned} y(k) = {} & a_0 + a_1 y(k-1) + \ldots + a_{n-1} y(k-n+1) \\ & + b_0 u(k) + b_1 u(k-1) + \ldots + b_n u(k-n) \\ & + e(k) \end{aligned}, \tag{2.12}$$

where $e(k)$ represents the error between the exact response and the approximated response of the ARMA model. It is desirable to estimate the parameters $[a_0, a_1, \ldots, a_{n-1}, b_0, b_1, \ldots, b_n]$ in such a way that the identified ARMA model will mimic the linear response of the unknown system based on the measured sequence $\{u,y\}$. Substituting N sampled data points of the set $\{u,y\}$ in Eq. 2.12 yields

$$\mathbf{Y} = \mathbf{U}\boldsymbol{\theta} + \mathbf{E}, \tag{2.13}$$

where

$$\mathbf{Y} = \begin{bmatrix} y(n) \\ y(n+1) \\ \vdots \\ y(N) \end{bmatrix} \quad \mathbf{U} = \begin{bmatrix} 1 & y(n-1) & \cdots & y(1) & u(n) & \cdots & u(0) \\ 1 & y(n) & \cdots & y(2) & u(n+1) & \cdots & u(1) \\ \vdots & \vdots & \vdots & \vdots & \vdots & \vdots & \vdots \\ 1 & y(N-1) & \cdots & y(N-n+1) & U(N) & \cdots & U(N-n) \end{bmatrix},$$

$\boldsymbol{\theta} = [a_0, a_1, ..., a_{n-1}, b_0, b_1, ..., b_n]^T$, and $\mathbf{E}$ is the error vector. Let $\mathbf{S}$ denote the sum square error,

$$\mathbf{S} = \mathbf{E}^T\mathbf{E} = (\mathbf{Y}^T - \boldsymbol{\theta}^T\mathbf{U}^T)(\mathbf{Y} - \mathbf{U}\boldsymbol{\theta}). \tag{2.14}$$

Then, it is desirable to find $\boldsymbol{\theta}$ such that $\mathbf{S}$ is minimized. This can be accomplished by taking the derivative of $\mathbf{S}$ with respect to $\boldsymbol{\theta}$ and setting it to zero; namely

$$\frac{\delta \mathbf{S}}{\delta \boldsymbol{\theta}} = -2\mathbf{U}^T\mathbf{Y} + 2\mathbf{U}^T\mathbf{U}\boldsymbol{\theta} = 0. \tag{2.15}$$

Therefore, one obtains

$$\left[\mathbf{U}^T\mathbf{U}\right]\boldsymbol{\theta} = \mathbf{U}^T\mathbf{Y} \quad \text{or} \quad \boldsymbol{\theta} = \left[\mathbf{U}^T\mathbf{U}\right]^{-1}\mathbf{U}^T\mathbf{Y}. \tag{2.16}$$

Equation 2.16 represents the general solution for an ARMA model given a set of measured data $\{u,y\}$. However, straight application of Eq. 2.16 will yield an ill-conditioned solution. $\boldsymbol{\theta}$ can be solved using the Gaussian elimination technique with partial pivoting or better techniques that can be found in [Norton, 1986]. This algorithm has been shown to be quite effective in [Huynh, 1994] and can identify accurately the unknown system.

2.1.5 Sector Gain Identification of the Nonlinear Part

Given a measured set of input/output data $\{u,y\}$ that represents the system, the sector gain of the nonlinear part can be identified. Recall from Appendix A that a nonlinear system can be represented by a sector gain $\{a,b\}$ or equivalently by a conic sector $\{c,r\}$. Also, the nonlinear

system with an input u and an output y, which belongs to the sector $\{a,b\}$ or equivalently interior conic $\{c,r\}$, must satisfy

$$\|y - cu\| \le r\|u\|. \tag{2.17}$$

Therefore, the conic radius r as a function of the center conic c is given by

$$r(c) \ge \sqrt{\frac{\|y - cu\|^2}{\|u\|^2}}. \tag{2.18}$$

According to the definition of the 2-norm, Eq. 2.18 can be expanded to

$$r(c) \ge \sqrt{\frac{\int_0^\infty [y(t) - cu(t)]^2\, dt}{\int_0^\infty u(t)^2\, dt}} = \sqrt{\frac{\lim_{T\to\infty} \frac{1}{T}\int_0^T [y(t) - cu(t)]^2\, dt}{\lim_{T\to\infty} \frac{1}{T}\int_0^T u(t)^2\, dt}}, \tag{2.19}$$

or

$$r(c) \ge \sqrt{\frac{P(y - cu)}{P(u)}}, \tag{2.20}$$

where $P(.)$ denotes the average power of the signal (.), and Eq. 2.20 must hold true for all input u. Consequently, Eq. 2.20 dictates that the sector gain of a system is determined by the square root of the ratio of the average powers of the system output and input. Furthermore, according to Eq. 2.5, Eq. 2.20 becomes

$$r(c) \ge \sqrt{\frac{\int_{-\infty}^{\infty} \wp_{y-cu}(f)df}{\int_{-\infty}^{\infty} \wp_u(f)df}} \approx \sqrt{\frac{\sum_i \wp^i_{y-cu}(f_i)}{\sum_i \wp^i_u(f_i)}}. \tag{2.21}$$

The topic of approximating the power spectral density of a signal is part of the signal processing field and is beyond the scope of this work. However, one should be satisfied with many existing

robust algorithms, such as the FFT algorithm, in the literature for computing the power spectral density of a signal.

Thus, once L_{series} is identified, the sector gain of N_{series} can be approximated. Under large-signal perturbation, the nonlinear effects in N_{series} cannot be neglected. Consequently, if $\{u_{large}, y_{large}\}$ represents the large-signal response of the unknown system around a steady-state operating point, then the output of the linear part, x (Fig. 2.4), can be computed from $x_{large} = L_{series} u_{large}$. Then, given $\{x_{large}, y_{large}\}$, the sector gain of N_{series} can be computed based on Eq. 2.21. The outcome is a set of conic radii for different conic centers. It will be illustrated in Chapter 4 that there exists an optimum pair $\{c,r\}$ that satisfies the stability condition.

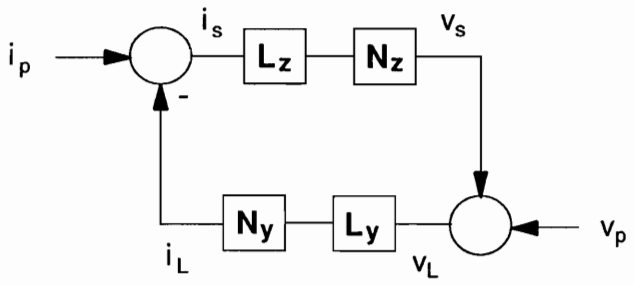

(a)

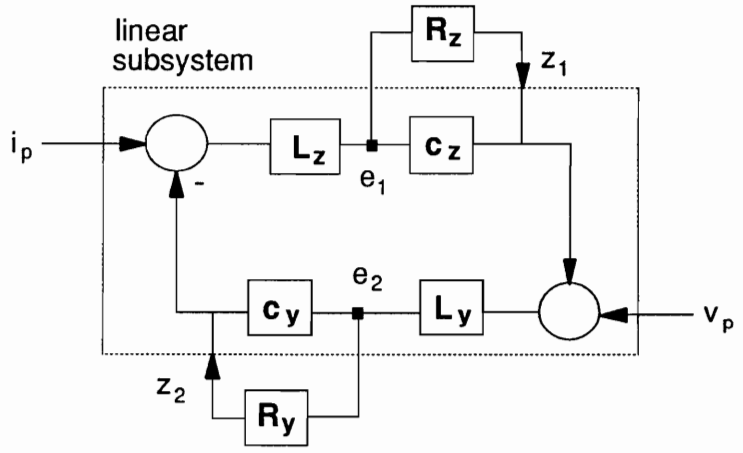

(b)

Fig. 2.5: Feedback Connection of Source and Load in Factorization Form
(a) Feedback Connection in Series Configuration Form
(b) Conicity Decomposition of the Nonlinear Parts

2.2 A Large-Signal Stability Criterion for the Interconnected Source/Load System

As stated in Chapter 1, interconnection of the source and the load results in a closed-loop system. However, Nyquist criterion is not applicable to the stability analysis at a source/load interface because the operators Z and Y are nonlinear operators. Consequently, a new stability criterion is needed for the interconnected source/load system.

Given that both Z and Y are factorizable into linear and nonlinear operators, as shown in Fig. 2.5(a), let us assume furthermore that the nonlinear parts N_z and N_y have conic sectors $\{c_z,r_z\}$ and $\{c_y,r_y\}$ (Appendix A, Fig A.1), respectively; then expanding $N_z = R_z + c_z$ and $N_y = R_y + c_y$ and regrouping the linear blocks yield the block structure representation in Fig. 2.5(b), where R_z and R_y represent the nonlinear operators that have gains of r_z and r_y, respectively. According to Fig. 2.5(b), the lumped linear subsystem, which has four inputs, z_1, z_2, i_p and v_p, and two outputs, e_1 and e_2, has the following input-output representation

$$e_1 = L_z i_p - L_z z_2 - L_z L_y c_y v_p - L_z L_y c_y z_1 - L_y L_z c_y c_z e_1, \tag{2.22}$$

$$e_2 = L_y v_p + L_y z_1 + L_y L_z c_z i_p - L_y L_z c_z z_2 - L_y L_z c_y c_z e_2. \tag{2.23}$$

Also, the input-output representations of the two nonlinear operators, R_z and R_y, are given by

$$z_1 = R_z e_1, \tag{2.24}$$

$$z_2 = R_y e_2. \tag{2.25}$$

Rearranging Eqs. 2.22 and 2.23 and substituting Eqs. 2.24 and 2.25 into Eqs. 2.22 and 2.23 yield

$$\begin{bmatrix} e_1 \\ e_2 \end{bmatrix} = \begin{bmatrix} \dfrac{-Tc_y}{1+Tc_zc_y} R_z & \dfrac{L_z}{1+Tc_zc_y} R_y \\ \dfrac{-L_y}{1+Tc_zc_y} R_z & \dfrac{-Tc_z}{1+Tc_zc_y} R_y \end{bmatrix} \begin{bmatrix} e_1 \\ e_2 \end{bmatrix} + \begin{bmatrix} \dfrac{Tc_y}{1+Tc_zc_y} & \dfrac{L_z}{1+Tc_zc_y} \\ \dfrac{L_y}{1+Tc_zc_y} & \dfrac{-Tc_z}{1+Tc_zc_y} \end{bmatrix} \begin{bmatrix} i_p \\ v_p \end{bmatrix}, \tag{2.26}$$

where T represents the small-signal loop gain and is given by $T = L_z L_y$. Applying the norm, the triangular inequality, and regrouping $\left[\|e_1\| \|e_2\|\right]^T$ leads to

$$\begin{bmatrix} 1-g\left(\frac{Tc_y}{1+Tc_zc_y}\right)r_z & -g\left(\frac{L_z}{1+Tc_zc_y}\right)r_y \\ -g\left(\frac{L_y}{1+Tc_zc_y}\right)r_z & 1-g\left(\frac{Tc_z}{1+Tc_zc_y}\right)r_y \end{bmatrix}\begin{bmatrix}\|e_1\| \\ \|e_2\|\end{bmatrix} \le \begin{bmatrix} g\left(\frac{Tc_y}{1+Tc_zc_y}\right)g\left(\frac{L_z}{1+Tc_zc_y}\right) \\ g\left(\frac{L_y}{1+Tc_zc_y}\right)g\left(\frac{Tc_z}{1+Tc_zc_y}\right)\end{bmatrix}\begin{bmatrix}\|i_p\| \\ \|v_p\|\end{bmatrix}, \quad (2.27)$$

where $g(.)$ denotes the gain of (.), and r_z and r_y are the gains of the nonlinear operators, R_z and R_y, respectively. Equation 2.27 has the following representation

$$\mathbf{R}\begin{bmatrix}\|e_1\| \\ \|e_2\|\end{bmatrix} \le \mathbf{W}\begin{bmatrix}\|i_p\| \\ \|v_p\|\end{bmatrix}. \quad (2.28)$$

Therefore, if $\mathbf{R}$ is invertible and all elements of $\mathbf{R}^{-1}$ are positive, which means that $\mathbf{R}$ must be an M-matrix (Appendix A), then

$$\begin{bmatrix}\|e_1\| \\ \|e_2\|\end{bmatrix} \le \mathbf{R}^{-1}\mathbf{W}\begin{bmatrix}\|i_p\| \\ \|v_p\|\end{bmatrix}, \quad (2.29)$$

and the system is input-output stable. The conditions required for $\mathbf{R}$ to be an M-matrix are

$$\delta_z \equiv 1-g\left(\frac{Tc_y}{1+Tc_zc_y}\right)r_z > 0, \quad (2.30)$$

$$\delta_y \equiv 1-g\left(\frac{Tc_z}{1+Tc_zc_y}\right)r_y > 0, \quad (2.31)$$

$$\delta_z\delta_y - g\left(\frac{L_z}{1+Tc_zc_y}\right)g\left(\frac{L_y}{1+Tc_zc_y}\right)r_zr_y > 0. \quad (2.32)$$

Thus, following the above three stability conditions, the system is closed-loop BIBO stable in the 2-norm sense if

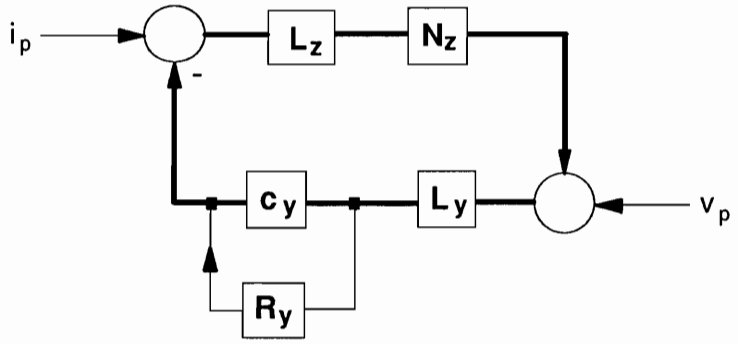

(a)

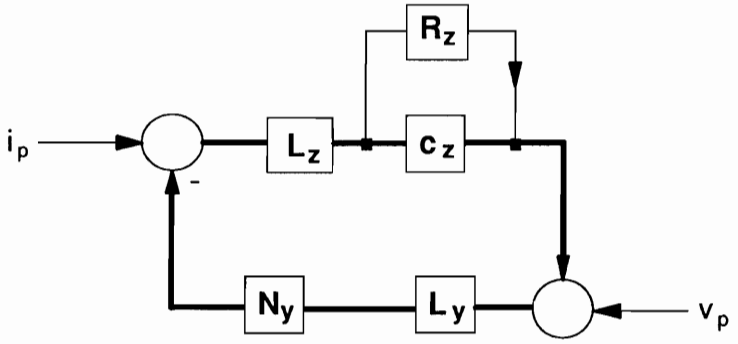

(b)

Fig. 2.6: Existence of Two Nonlinear Feedback Loop
(a) First Nonlinear Feedback Loop
(b) Second Nonlinear Feedback Loop

$$\delta_z \equiv 1 - \left| \frac{T(s)c_y}{1 + c_z T(s) c_y} \right| r_z > 0, \tag{2.33}$$

$$\delta_y \equiv 1 - \left| \frac{T(s)c_z}{1 + c_y T(s) c_z} \right| r_y > 0, \tag{2.34}$$

$$\left| \frac{T(s)}{[1 + c_z c_y T(s)]^2} \right| < \frac{\delta_z \delta_y}{r_y r_z}. \tag{2.35}$$

Equations 2.33 and 2.34 have structured similar to the Circle criterion discussed in Appendix A. In fact, the above three sufficient conditions can be interpreted as follows: notice that the nonlinear feedback loop in Fig. 2.5(a) can be decomposed into two feedback loops that contain one linear element and one nonlinear element, as illustrated in Fig. 2.6. The first feedback loop contain a nonlinear element, N_z, and a lumped linear element, $c_y L_z L_y$, while the second feedback loop contain N_y and $c_z L_z L_y$. Consequently, Eqs. 2.33 and 2.34 result from applying the Circle criterion on the first and the second feedback loop, respectively. Also, Eq. 2.35 is needed to take into account the interaction between the two nonlinear feedback loops. Therefore, the graphical interpretations of Eqs. 2.33 and 2.34 are similar to the one from the Circle criterion; namely let $a_z = (c_z - r_z)/2$, $b_z = (c_z + r_z)/2$, $a_y = (c_y - r_y)/2$, and $b_y = (c_y + r_y)/2$; Eq. 2.33 is satisfied if the Nyquist plot of $c_y T(s)$ satisfies the Circle criterion with regard to the disc $D(a_z, b_z; \delta_z)$. Also, Eq. 2.34 is satisfied if the Nyquist plot of $c_z T(s)$ satisfies the Circle criterion with respect to the disc $D(a_y, b_y; \delta_y)$.

Inspection of the above three stability conditions reveals that the new stability criterion is an extension of the Nyquist criterion. Indeed, the less both Z and Y become nonlinear, the more N_z and N_y become negligible, that is both r_z and $r_y \to 0$, and both c_z and $c_y \to 1$. Consequently, all the three stability conditions from Eqs. 2.33, 2.34 and 2.35 reduce to

$$|1 + T(s)| > 0, \tag{2.36}$$

which represents the Nyquist criterion [Vidyasagar, 1993]. The graphical interpretation of Eq. 2.36 is that the Nyquist plot of $T(s)$ must encircle the (-1, j0) point as many times as there are poles of $T(s)$ in the right half plane, and the encirclement, if any, must be made in the clockwise direction [Kuo, 1987]. Thus, when Z and Y represent the large-signal dynamic of the source and the load subsystems, respectively, N_z and N_y must be taken into account, and the critical (-1, j0) point expands to forbidden regions defined by the sets $\{c_z,r_z\}$ and $\{c_y,r_y\}$ that the Nyquist plot of $T(s)$ must avoid in order to assure large-signal stability of the interconnected system.

Nevertheless, the principal difference between the Nyquist criterion and this stability criterion is that the Nyquist criterion results in both necessary and sufficient conditions, whereas according to the derivation, the new stability criterion yields only a set of three sufficient conditions. How far the outcome of this criterion is from the necessary condition depends upon systems. However, it will be illustrated in Chapters 3 and 4 that in general, this new stability criterion is not too conservative. Also, the other difference between the Nyquist criterion and the new stability criterion is that the latter ensures large signal stability, while the Nyquist criterion ensures only small-signal stability.

2.3 Summary

This chapter discusses the theoretical background of the proposed methodology for the stability analysis of large-scale power electronics systems. The large-signal stability properties of any power electronics system can be analyzed based on decoupling the system into a source subsystem and a load subsystem and investigating the feedback loop formed by the source/load interconnection

First, it is necessary that both source and load subsystems be factorizable into series combinations of a linear part and a nonlinear part. It has been shown that, if both source and load are stable subsystems, the linear parts and the nonlinear parts resulting from the factorization are also stable. The linear part can be identified by injecting small-signal random perturbation, collecting the response data, and applying the least-square-fit algorithm to determine an equivalent ARMA model. The nonlinear part sector gain can be identified also based on square root of the ratio of the average power of the output signal over the average power of the input perturbation.

Since both source and load are assumed to be nonlinear, the Nyquist criterion is not applicable. However, by factorizing both subsystems into series combinations of a linear part and a nonlinear part, a new stability criterion suitable for the nonlinear interconnected source/load system is derived. This new stability criterion is a set of three sufficient conditions, which are not too conservative in general; nevertheless, unlike the Nyquist criterion, they can ensure large-signal stability of the interconnected source/load system.

Chapter 3

Stability Analysis of PWM Converters

This chapter presents the large-signal stability of PWM converters. The objective of this chapter is twofold: (1) to illustrate feasibility of the input-output stability theory as applied in the large-signal analysis of PWM converters, and (2) to investigate the large-signal stability of PWM converters– an issue that has not been addressed widely in the literature.

Even though small-signal analysis has been commonly used for the design and optimization of power converters, the linear analysis technique in conjunction with the Nyquist criterion becomes handicapped for the nonlinear large-signal stability analysis. Linear characterization of power converters is performed for the closed-loop design. Consequently, inherent nonlinearities in the system such as duty cycle saturation and opamp saturation, which can be a source of instability, are neglected in the design process. The large-signal stability analysis, which employs the input-output stability theory presented in Appendix A, includes all the nonlinearities existing in the system and provides design insight and optimization of power converters.

Large-signal characterization of different nonlinearities in PWM converters is considered, and the large-signal stability of the closed-loop converters with regards to theses nonlinearities is investigated. First the state-space averaging method for PWM converters is reviewed, from which a large-signal average model representing the low-frequency dynamics of PWM converters is

derived. This large-signal average model will be utilized for the large-signal stability analysis of PWM converters. Saturation effects in voltage-mode control and current-injection control are investigated. Also, the bilinear structure of the PWM converters due to state-space averaging and its effect on the large-signal stability of the system are analyzed. The last section will address the mutual effects of all the above nonlinearities on the stability properties of PWM converters.

3.1 State-Space Averaging of PWM Converters

In general, an analytical model structure of a system must be available for the design and analysis process. PWM converters can be characterized by a combination of an ON-time linear model and an OFF-time linear model. State-space averaging has been widely used to obtain an average model for PWM converters. It has been known to be accurate up to half of the switching frequency, and it can provide great insights into the low frequency dynamic of PWM converters. Since the control bandwidths of closed-loop converters are usually set at much lower frequencies than the switching frequency, the average modeling technique is sufficient to provide a nonlinear characterization of PWM converters. Let

$$\begin{aligned} \dot{\xi} &= \mathbf{A}_1\xi + \mathbf{B}_1\upsilon \\ \dot{\xi} &= \mathbf{A}_2\xi + \mathbf{B}_2\upsilon \end{aligned} \tag{3.1}$$

be the state-space representation of PWM converters during the ON-time and the OFF-time, respectively (operation in Continuous Conduction Mode), where ξ represents the state vector, and υ represents the input vector. Then state-space averaging Eq. 3.1 results in

$$\dot{\bar{\mathbf{x}}} = (\mathbf{A}_1\bar{d} + \mathbf{A}_2\bar{d}')\bar{\mathbf{x}} + (\mathbf{B}_1\bar{d} + \mathbf{B}_2\bar{d}')\upsilon, \tag{3.2}$$

where $\bar{\mathbf{x}}$ denotes the average of the state ξ, $\bar{d}$ is the average of the duty cycle over one switching period, and $\bar{d}' = 1 - \bar{d}$. Equation 3.2 represents the general equivalent large-signal average model

of PWM converters, which can predict the converter dynamic up to half of the switching frequency.

Input-output boundedness refers to disturbance around a steady-state operating point; therefore, to make Eq. 3.2 suitable for the input-output stability analysis purpose, it is necessary to make a change of variables by introducing perturbation $\mathbf{x} = \bar{\mathbf{x}} - \mathbf{X}_0$, $\mathbf{u} = \upsilon - \mathbf{U}_0$, and $d = \bar{d} - D$, where D is the steady-state duty cycle, and the pair ($\mathbf{U}_0$, $\mathbf{X}_0$) denotes the steady-state operating point of the system. Substituting these variables into Eq. 3.2 yields

$$\dot{\mathbf{x}} = (\mathbf{A}_1 D + \mathbf{A}_2 D')\mathbf{x} + \left[(\mathbf{A}_1 - \mathbf{A}_2)\mathbf{X} + (\mathbf{B}_1 - \mathbf{B}_2)\mathbf{U}\right]d + (\mathbf{B}_1 D + \mathbf{B}_2 D')\mathbf{u} + (\mathbf{A}_1 - \mathbf{A}_2)\mathbf{x}d + (\mathbf{B}_1 - \mathbf{B}_2)\mathbf{u}d \quad , \tag{3.3}$$

or

$$\dot{\mathbf{x}} = \mathbf{A}\mathbf{x} + \mathbf{B}d + \mathbf{C}\mathbf{u} + \mathbf{G}\mathbf{x}d + \mathbf{F}\mathbf{u}d . \tag{3.4}$$

Equation 3.4 represents the general large-signal open-loop average model of PWM converters and is a bilinear system because of the product of the state and the input, $\mathbf{x}d$. When the perturbation is small, the cross-product terms $\mathbf{x}d$ and $\mathbf{u}d$ can be neglected, and Eq. 3.4 becomes a small-signal model. In practical applications, the small-signal model of Eq. 3.4 is often used as an analytical model for the feedback design and optimization. However, it is realized that because of the cross-product terms, which cannot be neglected under large-signal disturbance, the designed closed-loop system based on the small-signal optimization may not be globally stable. This issue will be addressed later. The nonlinear effects due to saturation nonlinearities are investigated first based on the input-output stability.

3.2 Large-Signal Stability Analysis in Voltage-Mode Control

This section addresses the effects of the saturation nonlinearities on the performance of PWM converters in voltage-mode control. A buck converter is selected for the analysis because it is known that the large-signal state-space averaging model of a buck converter is linear; therefore, emphasis can be placed solely on the saturation nonlinearities. Two important saturation nonlinearities are investigated: duty cycle saturation and opamp-saturation in the feedback loop.

3.2.1 Effect of Duty Cycle Saturation on the Converter Stability

One of the most important nonlinearities often ignored in the design and analysis is the duty cycle saturation. It will be shown that the duty cycle saturation can affect the performance of power converters, and a criterion for system stability will be established.

Consider a closed-loop buck converter in voltage-mode control, as illustrated in Fig. 3.1(a). Under the assumption that $R_c << R$, the ON-time and OFF-time state space representations of the system are given by

ON-time ***OFF-time***

$$\begin{bmatrix} \frac{di_l}{dt} \\ \frac{dv_c}{dt} \end{bmatrix} = \begin{bmatrix} \frac{-R_c}{L} & \frac{-1}{L} \\ \frac{1}{C} & \frac{-1}{RC} \end{bmatrix} \begin{bmatrix} i_l \\ v_c \end{bmatrix} + \begin{bmatrix} \frac{1}{L} \\ 0 \end{bmatrix} v_g \qquad \begin{bmatrix} \frac{di_l}{dt} \\ \frac{dv_c}{dt} \end{bmatrix} = \begin{bmatrix} \frac{-R_c}{L} & \frac{-1}{L} \\ \frac{1}{C} & \frac{-1}{RC} \end{bmatrix} \begin{bmatrix} i_l \\ v_c \end{bmatrix} + \begin{bmatrix} 0 \\ 0 \end{bmatrix} v_g$$

$$v_o = \begin{bmatrix} 1 & R_c \end{bmatrix} \begin{bmatrix} i_l \\ v_c \end{bmatrix}. \tag{3.5}$$

Applying state-space averaging and introducing perturbation around the steady-state operating point of the system, as in Eq. 3.3, yield

$$\begin{bmatrix} \frac{di_l}{dt} \\ \frac{dv_c}{dt} \end{bmatrix} = \begin{bmatrix} -R_c / L & -1/L \\ 1/C & -1/RC \end{bmatrix} \begin{bmatrix} i_l \\ v_c \end{bmatrix} + \begin{bmatrix} V_g / L \\ 0 \end{bmatrix} d + \begin{bmatrix} D/L \\ 0 \end{bmatrix} v_g + \begin{bmatrix} 1/L \\ 0 \end{bmatrix} v_g d$$

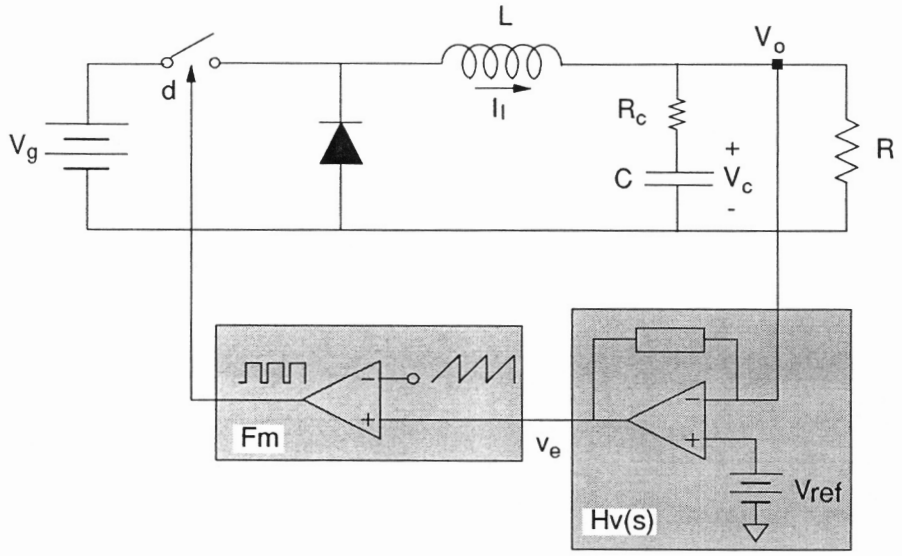

(a)

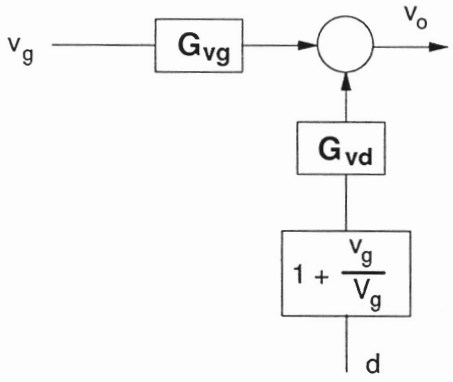

(b)

Fig. 3.1: Voltage-Mode-Controlled Buck Converter
(a) Circuit Diagram of a Closed-Loop Buck Converter
(b) Open-Loop Large-Signal Average Model of the Buck Converter

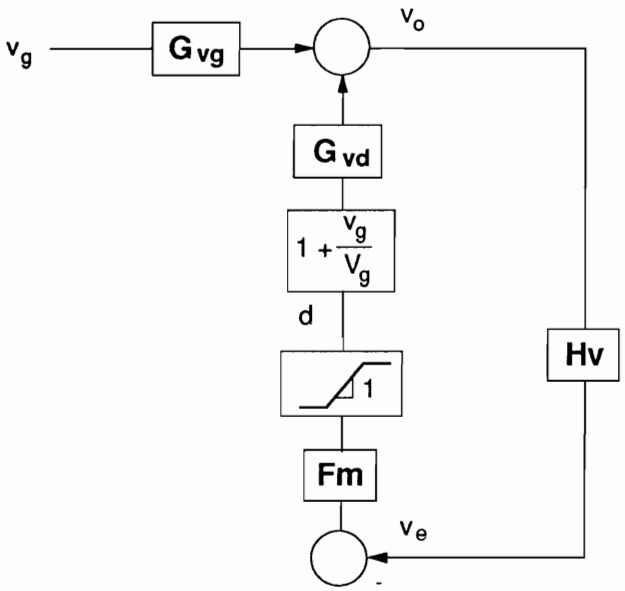

(a)

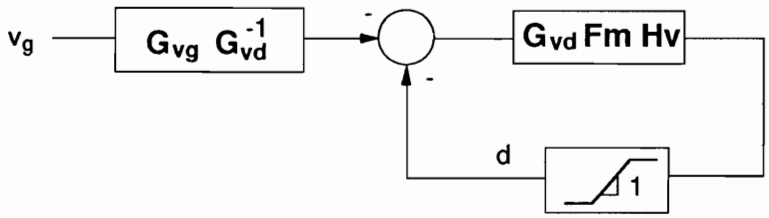

(b)

Fig. 3.2: Block Diagram Representations of the Closed-Loop Buck Converter With Inclusion of the Duty Cycle Saturation Nonlinearity
(a) Equivalent Block Diagram Representation
(b) Reduced Block Diagram Representation

$$v_o = \begin{bmatrix} 1 & R_c \end{bmatrix} \begin{bmatrix} i_l \\ v_c \end{bmatrix}, \tag{3.6}$$

which can be rearranged as

$$\begin{bmatrix} \frac{di_l}{dt} \\ \frac{dv_c}{dt} \end{bmatrix} = \begin{bmatrix} -R_c / L & -1/L \\ 1/C & -1/RC \end{bmatrix} \begin{bmatrix} i_l \\ v_c \end{bmatrix} + \begin{bmatrix} V_g / L \\ 0 \end{bmatrix} \left(1 + \frac{v_g}{V_g}\right) d + \begin{bmatrix} D/L \\ 0 \end{bmatrix} v_g$$

$$v_o = \begin{bmatrix} 1 & R_c \end{bmatrix} \begin{bmatrix} i_l \\ v_c \end{bmatrix}. \tag{3.7}$$

Equation 3.7 has an equivalent representation in the frequency domain , as shown in Fig. 3.1(b), where G_{vd} is the duty-cycle-to-output transfer function,

$$G_{vd} = V_g \frac{1 + sR_cC}{1 + s\left(\frac{L}{R} + R_cC\right) + s^2LC}, \tag{3.8}$$

G_{vg} is the input-to-output transfer function,

$$G_{vg} = D \frac{1 + sR_cC}{1 + s\left(\frac{L}{R} + R_cC\right) + s^2LC}, \tag{3.9}$$

and D, V_g are the steady-state duty cycle and steady-state input voltage, respectively. Notice also that the large-signal average model of the open-loop buck converter in Fig. 3.1(b) contains the cross-product term of both inputs d and v_g.

For output regulation, a feedback loop is closed upon the open-loop buck, as illustrated in Fig. 3.2(a), where *Fm* is the modulator gain, *Hv* is the compensation circuit, and effect of the duty cycle saturation is also included. In order to optimize the loop gain, T, which is defined as

$$T = FmHv(s)G_{vd}(s), \tag{3.10}$$

one employs a three-pole, two-zero compensation circuit; that is

$$Hv(s) = \frac{w_i(1+\frac{s}{w_{z1}})(1+\frac{s}{w_{z2}})}{s(1+\frac{s}{w_{p1}})(1+\frac{s}{w_{p2}})}. \tag{3.11}$$

The two low-frequency zeroes, w_{z1} and w_{z2}, are used to boost the phase up; the first pole w_{p1} is used to cancel the zero of $G_{vd}(s)$; and w_{p2} is used to provide attenuation at high frequency.

At this point, it is questionable whether the small-signal design can assure also large-signal stability of the closed-loop buck converter. Since Fig. 3.2(a) represents a large-signal average model of the closed-loop buck, it can be used to investigate the large-signal stability property of the closed-loop buck converter. In other words, the system is input-output stable if for any bounded v_g, the output v_o must also be bounded. According to Fig. 3.2(a), the feedback loop contains two nonlinearities: (1) the term $(1 + v_g/V_g)$ and (2) the duty cycle saturation. However, it is proved in Appendix C that the term v_g/V_g has no effect on the stability property of the system and can be ignored. Thus, Fig. 3.2(a) can be rearranged as in Fig. 3.2(b), where T is the loop gain as defined in Eq. 3.10. Since the feedback loop contains a linear transfer function and a memoryless nonlinearity, the Off-Axis Circle criterion, which is stated in the following, can be employed to investigate the stability properties of the closed-loop buck converter.

Theorem (Off-Axis Circle Criterion):

Consider the basic single loop feedback system in Fig. 3.3(a), where L and N are a linear operator and a nonlinear operator, respectively. Let N be *memoryless*, time invariant, and inside the sector $\{a,b\}$ where $b > 0$. Then the closed-loop system is BIBO stable if

Case 1: a > 0 *The Nyquist plot of L(s) lies outside a circle passing through -1/a and -1/b (note that the center need not be on the negative real axis as in the Circle criterion) and encircle it as many times as the number of RHP poles of L(s) (Fig. 3.3(b)).*

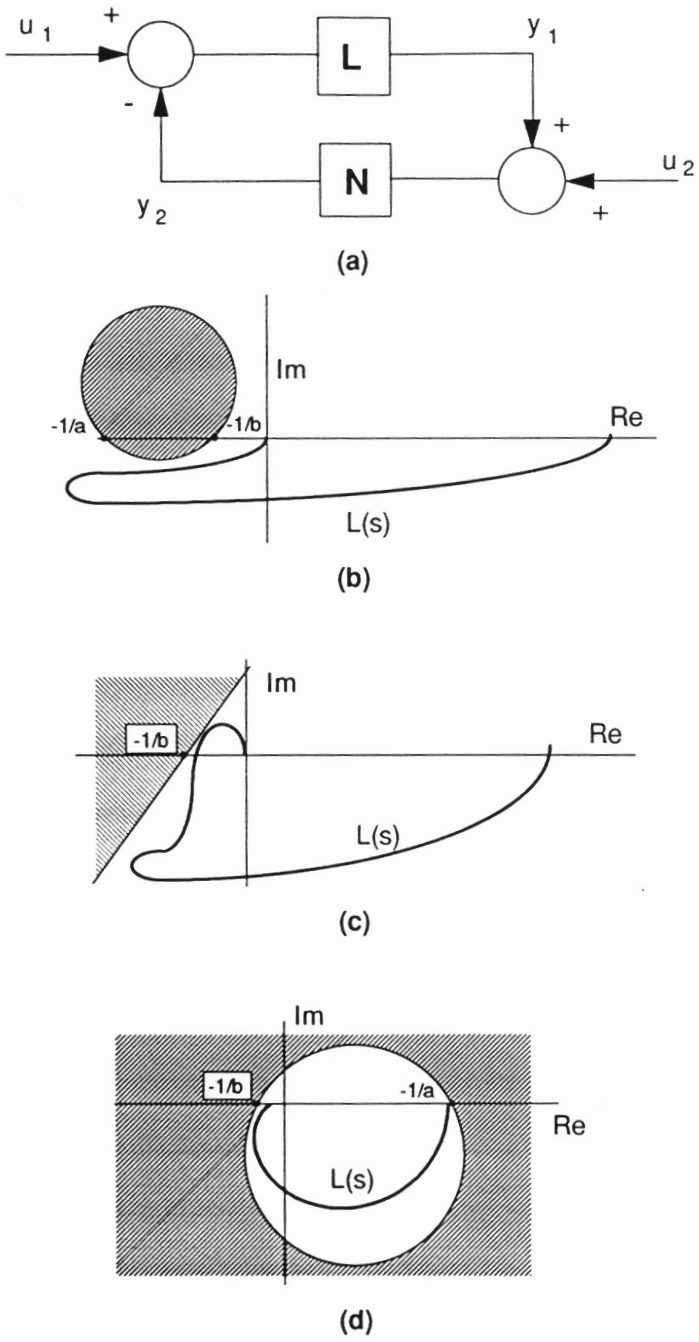

Fig. 3.3: Graphical Interpretation of the Off-Axis Circle Criterion
(a) A Single-Loop Feedback System
(b) $a > 0$
(c) $a = 0$
(d) $a < 0$

Case 2: a = 0 *The Nyquist plot of L(s) must stay on the right of a line of any slope passing through -1/b (Fig. 3.3(c)).*

Case 3: a < 0 *The Nyquist plot of L(s) lies inside a circle passing through -1/a and -1/b (Fig. 3.3(d))*

Assuming the following design parameters for the buck converter: L = 80 μH, C = 300 μF, R_c = 0.05 Ω, R = 6.25 Ω, Fm = 1, V_g = 30 V, V_o = 25 V, and the switching frequency is 80 KHz, and if $Hv(s)$ is chosen as

$$Hv(s) = \frac{6000(1+s/17000)(1+s/17000)}{s(1+s/10^5)(1+s/2\times10^5)}, \tag{3.12}$$

then Fig. 3.4(a) illustrates the resulting loop gain T. The Bode plot of T shows that, even though T has an adequate phase margin and gain margin, the system is conditionally stable and the time-domain simulation in Fig. 3.4(b) shows that under a random disturbance (a CSRS) of the input voltage v_g, the output v_o oscillates.

Prediction of such instability can be performed based on the off-axis circle criterion stated above. If the Bode plot of the loop gain T is translated into a Nyquist plot as shown in Fig. 3.5(a), it is observed that T cuts the negative real axis at two points within the segment $(-\infty, -1]$. Note that since the duty cycle saturation nonlinearity is restricted to a straight line of slope 1 and the horizontal line (slope 0), it belongs to the sector $\{0,1\}$. Therefore, if one applies Case 2 of the Off-Axis Circle criterion , it follows that the system is globally stable if the Nyquist plot of T stays completely to the right of a straight line of any slope passing through the $(-1,j0)$ point. Consequently, it is observed that the above design does not meet the stability condition because the Nyquist plot of T intersects the negative real axis at the points $(-1,j0)$ and $(-5,j0)$; and therefore, it is impossible to draw any straight line passing though the $(-1,j0)$ point such that $T(j2\pi f)$ stays entirely to the right of it.

However, the buck converter can be stable in a neighborhood around the steady-state operating point, because according to Fig. 3.5(a), one can fit a circle that intersects the negative real axis at the points $(-1,j0)$ and $(-5,j0)$, which implies that Case 1 of the Off-Axis Circle criterion is satisfied. It follows that the saturation nonlinearities must belong to the sector $\{1/5 = 0.2, 1\}$. Figure 3.5(b) illustrates a smaller sector gain $\{0.2, 1\}$, where the origin is taken to be the steady-state duty cycle. Such restriction on the sector gain implies that the duty cycle perturbation around the steady-state duty cycle must be confined to within a certain Δd_{max}. However, if some input disturbance can cause the duty cycle perturbation to exceed Δd_{max}, the requirement for stability is violated and the system may become unstable, as observed in the time-domain simulation in Fig. 3.4(b). Consequently, two conclusions can be drawn regarding application of the Off-Axis Circle criterion to this particular problem. First, the farther the intersection points of the Nyquist plot of T with the negative real axis is from the $(-1,j0)$ point, the larger the sector gain becomes, and the more the instability problem alleviates. At the extreme, if the Nyquist plot of T does not intersect the negative real axis within the segment $(-\infty, -1]$ at all, the sector gain of the saturation nonlinearity expands to $\{0,1\}$; case 2 of the Off-Axis Circle criterion is met; and the system is globally stable. Note that the Off-Axis Circle criterion provides only a sufficient condition. However, because this criterion is derived based on the Circle criterion with inclusion of a multiplier (Appendix A), it is not conservative in general, and in most cases, it can yield results that are very near the necessary condition [Y. S. Cho, 1968b].

To validate the above argument, the feedback compensation circuit is redesigned so that conditional stability can be avoided. The two zeroes of $Hv(s)$ are moved toward lower frequencies with readjustment of w_{p2} to provide good attenuation at high frequencies. Then $Hv(s)$ becomes

$$Hv(s) = \frac{6000(1+s/7000)(1+s/15000)}{s(1+s/10^5)(1+s/10^5)}. \tag{3.13}$$

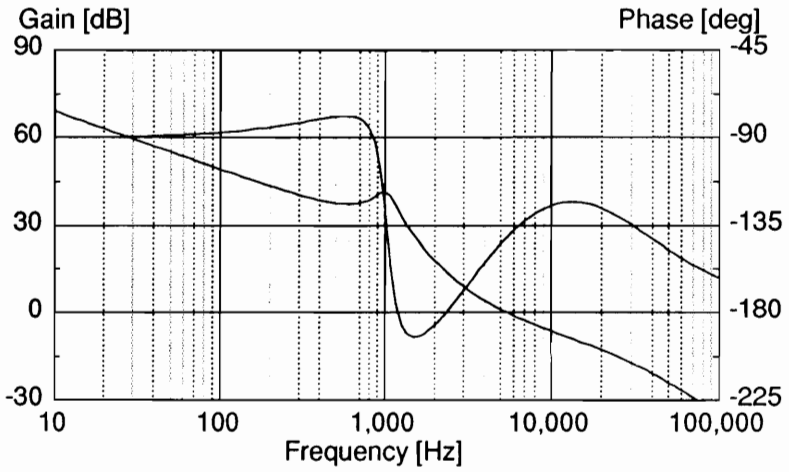

(a)

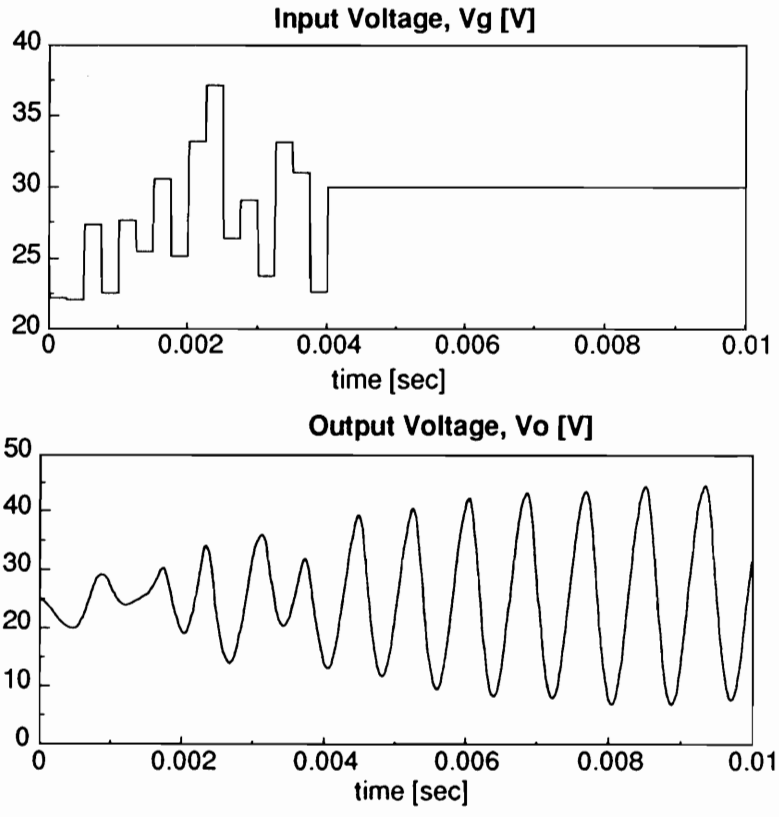

(b)

Fig. 3.4: Design for the Unstable Mode
(a) Loop Gain T
(b) Time-Domain Simulation Results

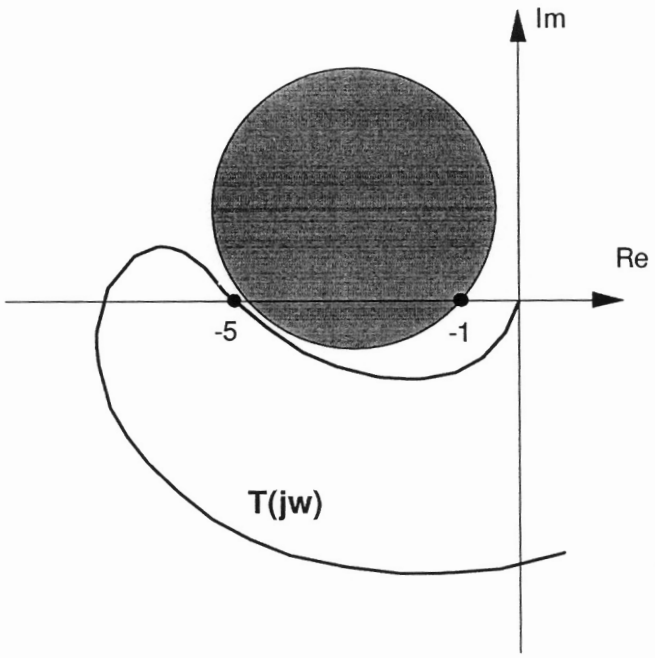

(a)

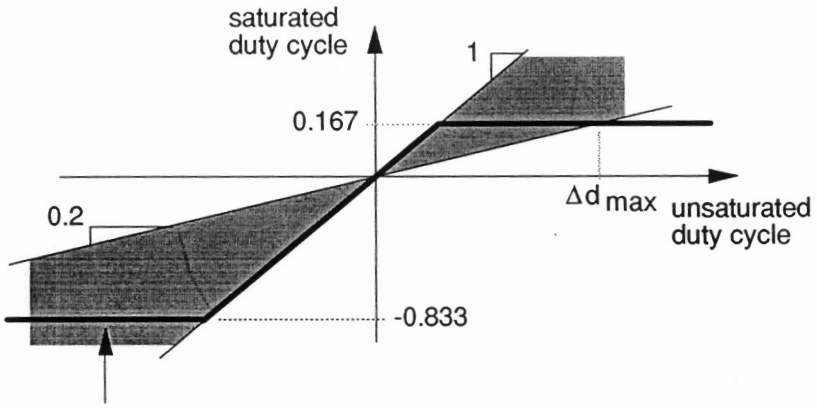

(b)

Fig. 3.5: Graphical Interpretation of the Large-Signal Stability Analysis
(a) Nyquist Plot of the Loop Gain T
(b) Sector Gain Analysis

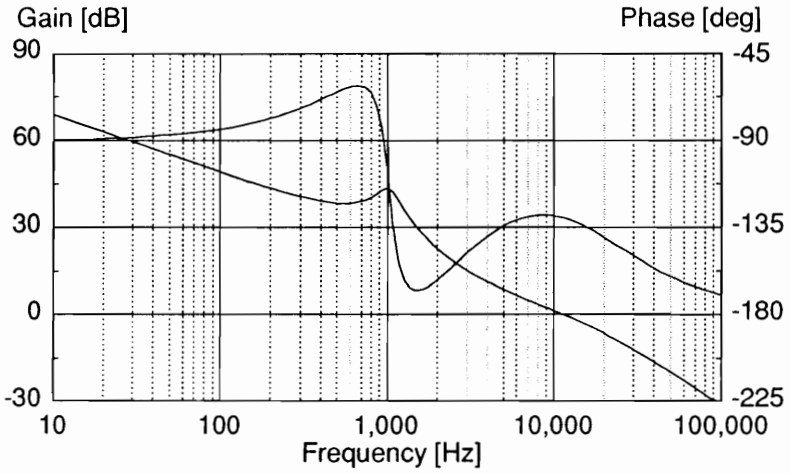

(a)

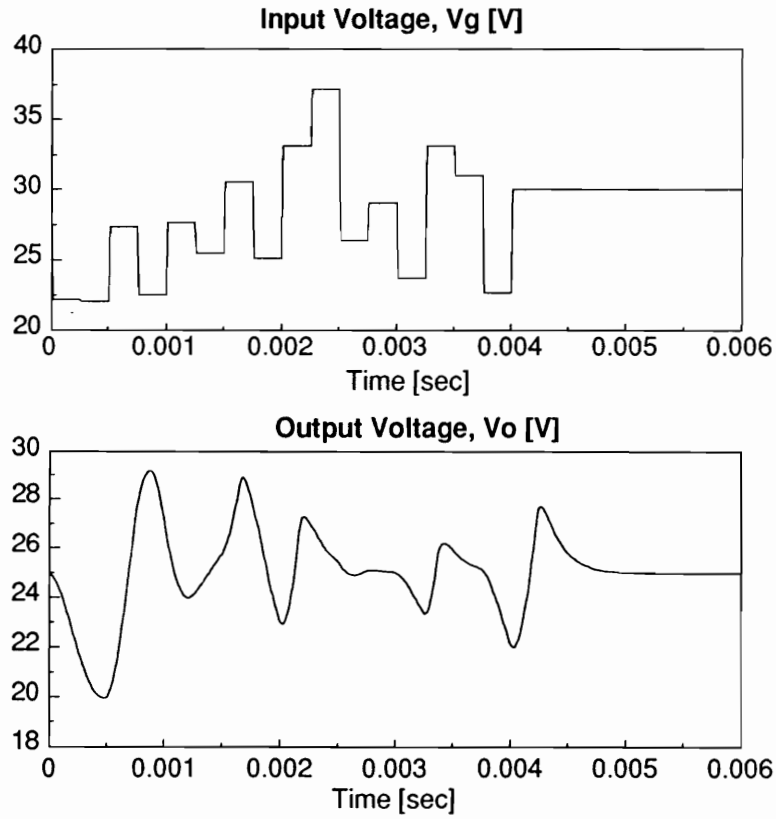

(b)

Fig. 3.6: Design for the Stable Mode
(a) Loop Gain T
(b) Time-Domain Simulation Results

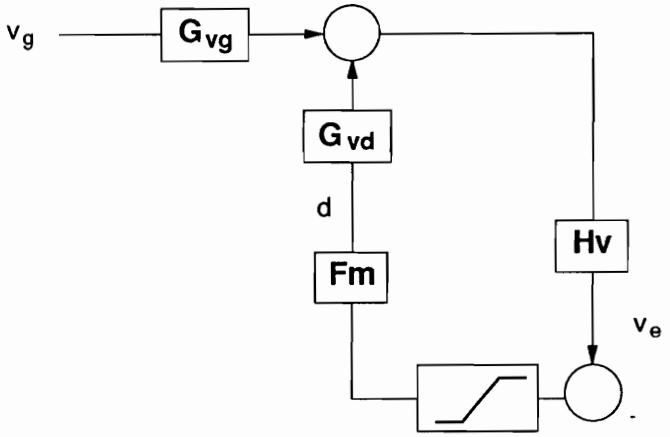

(a)

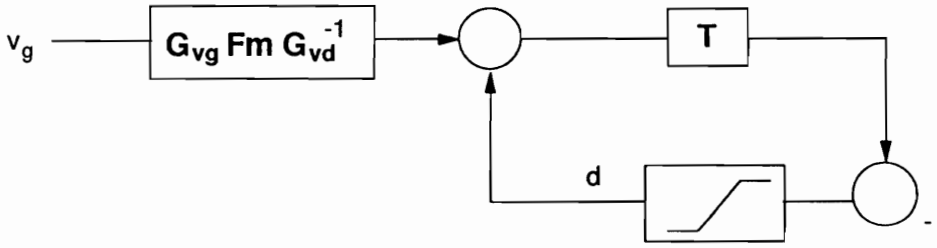

(b)

Fig. 3.7: Block Diagram Representations of the Closed-Loop Buck Converter With Inclusion of the Opamp Saturation Nonlinearity
(a) Equivalent Block Diagram Representation
(b) Reduced Block Diagram Representation

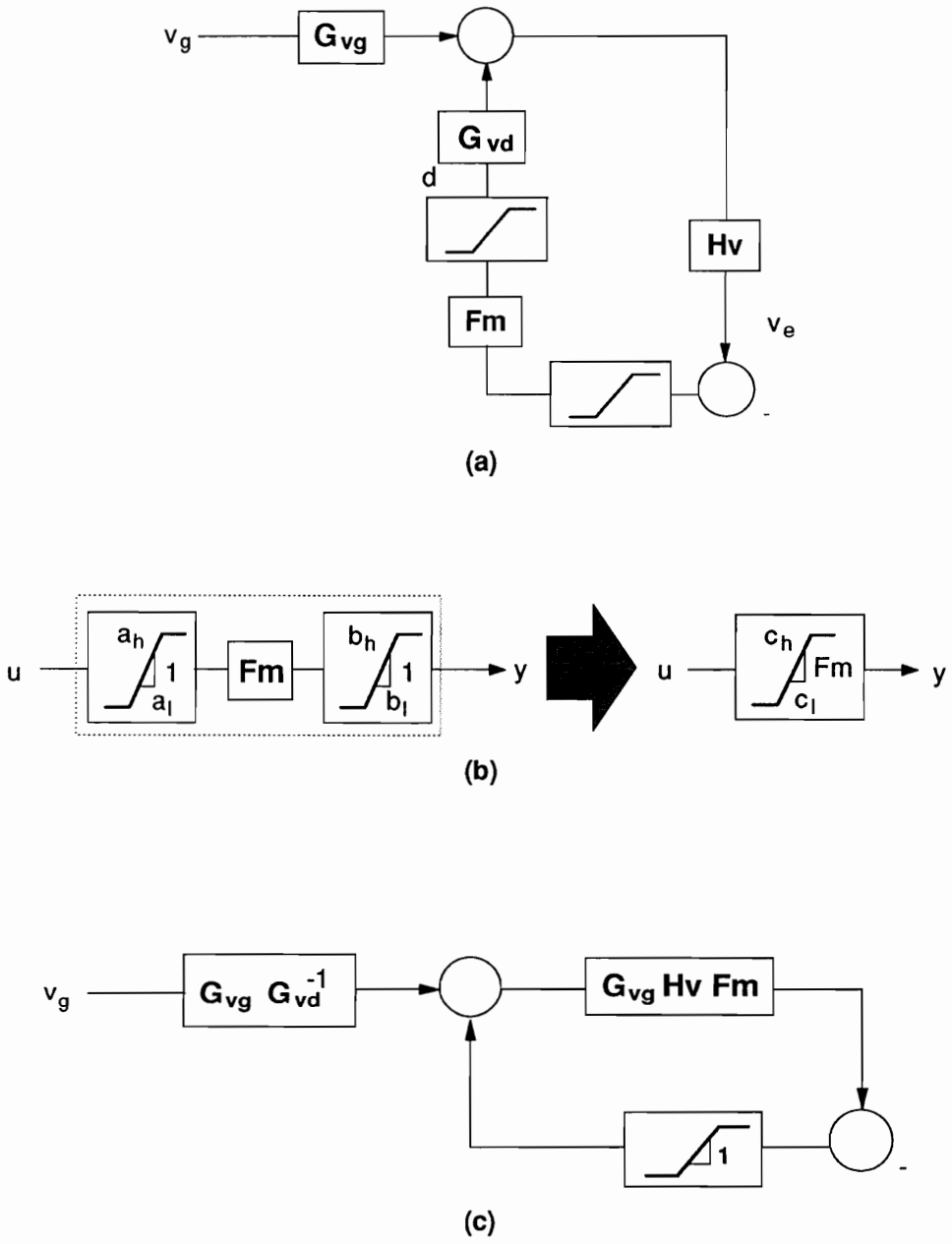

Fig. 3.8: Block Diagram Representations of the Closed-Loop Buck Converter With Inclusion of the Duty Cycle Saturation and the Opamp Saturation

(a) Equivalent Block Diagram Representation
(b) Combined Memoryless Nonlinearities
(c) Reduced Block Diagram Representation

With this particular design, the phase of the loop gain T is boosted up, and conditional stability disappears, as illustrated in Fig. 3.6(a). Also, Fig. 3.6(b) shows that under the same type of input perturbation, the system remains stable.

3.2.2 Effect of Saturation in the Feedback Loop on the Converter Stability

Saturation in the voltage feedback loop can assume a form of actual saturation of the opamp in the compensation circuit or current limiting feature implemented by the designer. Such nonlinearity can be represented by a saturation nonlinearity block, as illustrated in Fig. 3.7(a). Observe that this case is very similar to duty cycle saturation case, and Fig. 3.7(a) can be rearranged as shown in Fig. 3.7(b). Consequently, the same conclusion as in the previous section can be drawn for this voltage-mode-controlled buck converter. In order to achieve global stability, it is sufficient that the Nyquist plot of the loop gain T must not intersect the negative real axis within the segment $(-\infty, -1]$; that is the system must not be conditionally stable.

3.2.3 Combined Saturation Nonlinearities

The block diagram in Fig. 3.8(a) illustrates the equivalent large-signal model of the closed-loop buck converter with the presence of the duty cycle saturation and the opamp saturation. Since both nonlinearities are memoryless and are cascaded next to each other with a constant gain Fm in between, it is possible to combine the effect into a single saturation nonlinearity. As shown in Fig. 3.8(b), if the pair $\{a_l, a_h\}$ denotes the saturation limits of the opamp saturation, and the pair $\{b_l, b_h\}$ represents the saturation limits of the duty cycle saturation, then the resulting saturation nonlinearity will have a gain of Fm in the linear region and saturation limits $\{c_l, c_h\}$, where $c_l = \min(a_l \times Fm, b_l)$ and $c_h = \max(a_h \times Fm, b_h)$. Figure 3.8(c) illustrates the simplified block diagram

representation of the system and implies that global stability can be achieved if the Nyquist plot of the loop gain $T(s) = G_{vd}(s)Hv(s)Fm$ does not intersect the negative real axis within the segment $(-\infty, -1]$. Thus, for a voltage-mode-controlled buck converter, the large-signal stability property of the buck converter is controlled by the loop gain T, and the system is globally stable if the system is not conditionally stable in the small-signal sense– a sufficient condition that is not conservative.

3.3 Large-Signal Stability Analysis in Current-Injection Control

This section addresses the issue of large-signal stability of the buck converter in current injection control. Unlike the voltage mode control, the current injection control is a two-loop feedback control which senses the inductor current and the output voltage, as illustrated in Fig. 3.9(a) where Ri is a constant gain. According to Eq. 3.7, the open-loop large-signal model of the buck converter can be represented by a block diagram shown in Fig. 3.9(b) where G_{id} is the duty-cycle-to-inductor-current transfer function,

$$G_{id} = \frac{V_g}{R} \frac{1 + sRC}{1 + s\left(\frac{L}{R} + R_c C\right) + s^2 LC}, \tag{3.14}$$

and G_{ig} is the input-voltage-to-inductor-current transfer function,

$$G_{ig} = \frac{D}{R} \frac{1 + sRC}{1 + s\left(\frac{L}{R} + R_c C\right) + s^2 LC}. \tag{3.15}$$

Again, as mentioned in the previous section, boundedness is defined in terms of finite magnitude and absolute integrability; therefore, the nonlinearity v_g/V_g can be neglected.

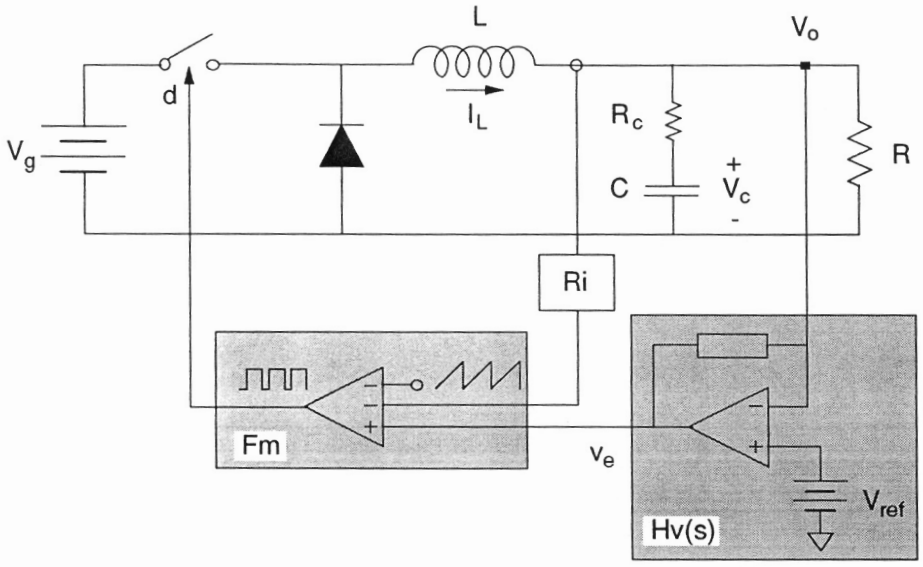

(a)

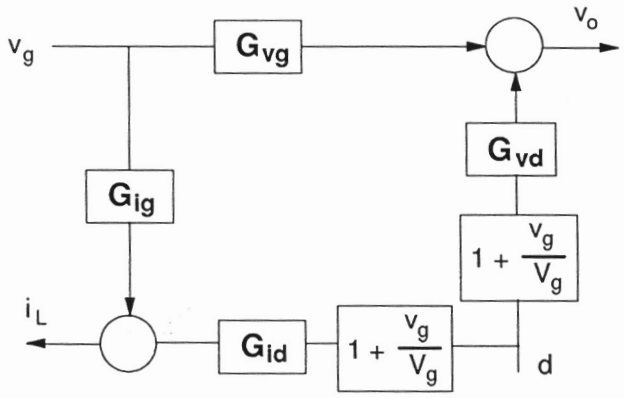

(b)

Fig. 3.9: A Current-Injection-Controlled Buck Converter
(a) Circuit Diagram
(b) Block Diagram Representation of the Open-Loop Buck Converter

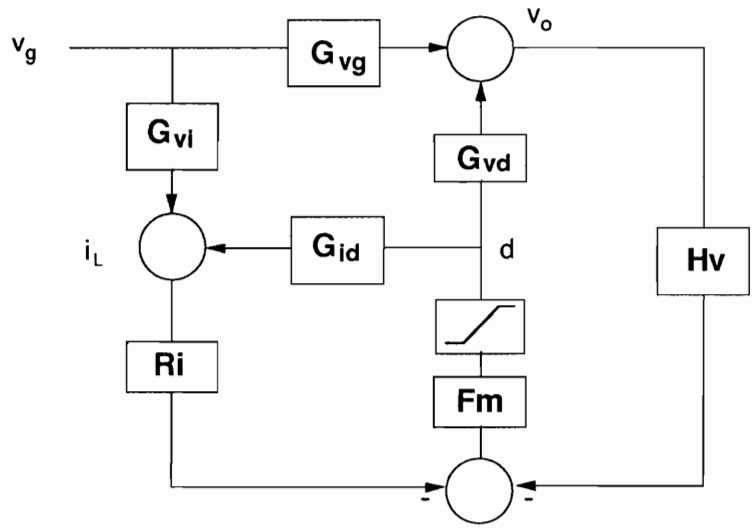

(a)

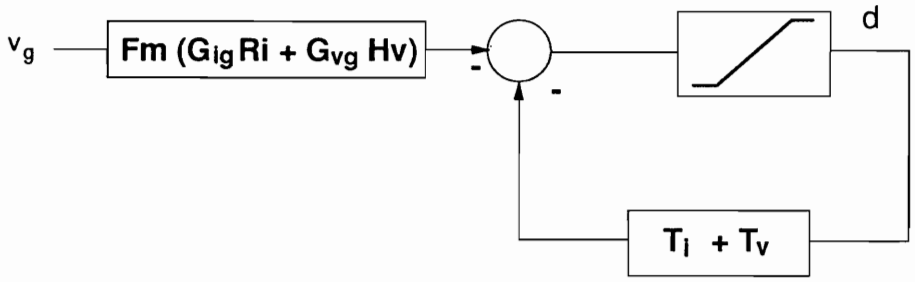

(b)

Fig. 3.10: Block Diagram Representation of the Closed-Loop Buck Converter With Inclusion of the Duty Cycle Saturation Nonlinearity
(a) Inclusion of Duty Cycle Saturation Nonlinearity
(b) Simplified Block Diagram Representation

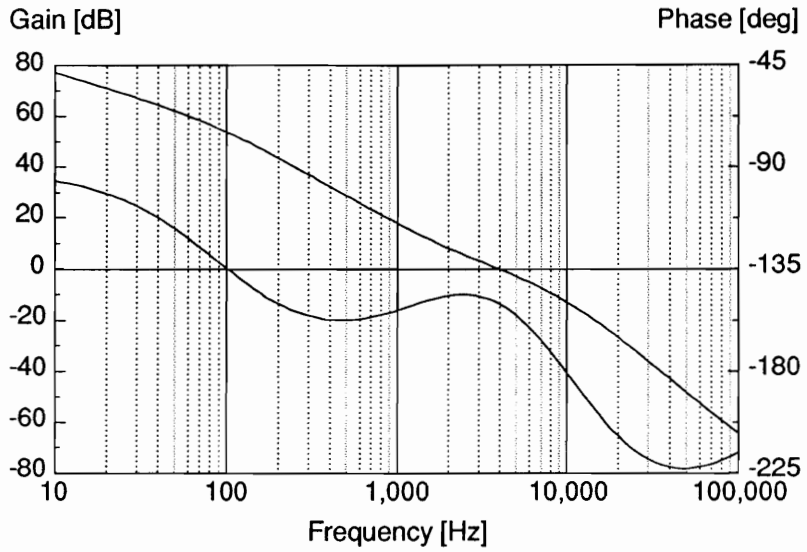

(a)

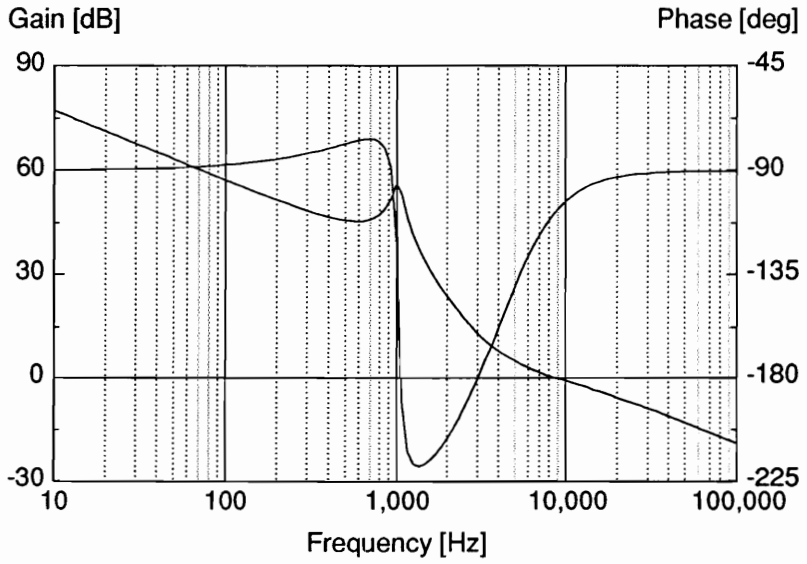

(b)

Fig. 3.11: System Loop Gains
(a) Outer Loop Gain T_2
(b) Loop Gain $T_i + T_v$

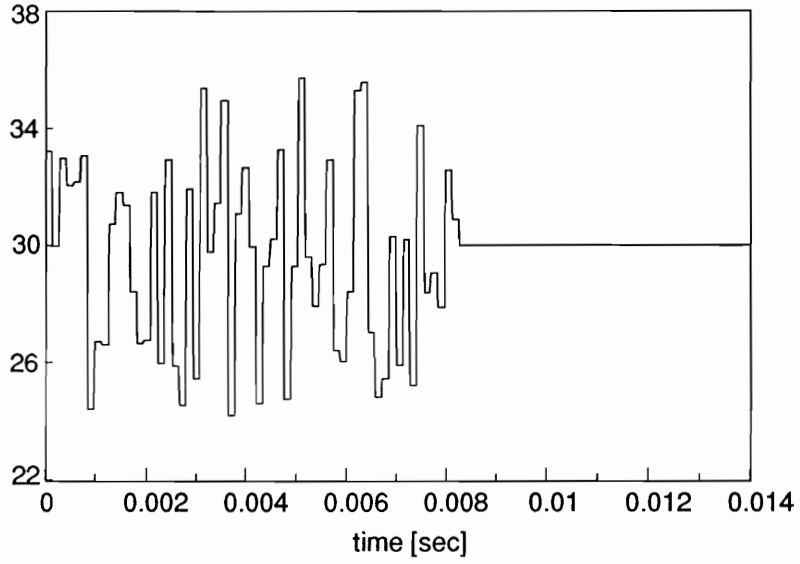

(a)

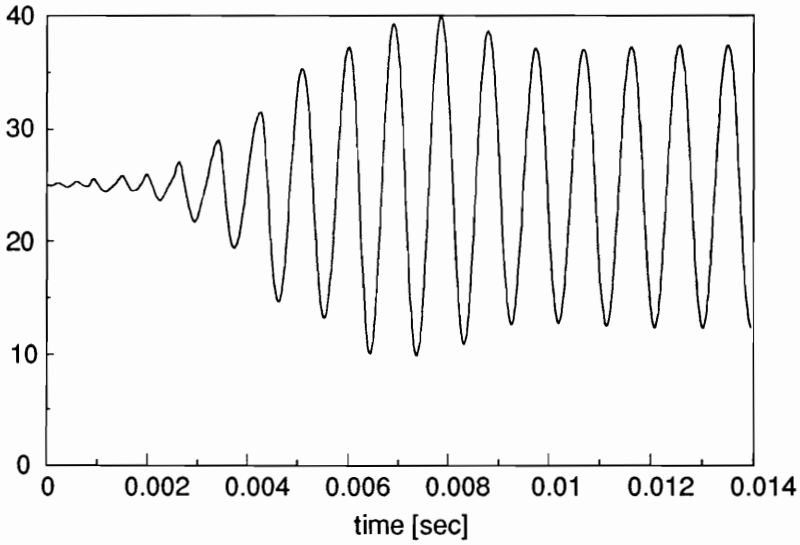

(b)

Fig. 3.12: Simulation Results for an Unstable Closed-Loop Buck Converter
(a) Input Voltage Perturbation, V_g
(b) Oscillation in Output Voltage, V_o

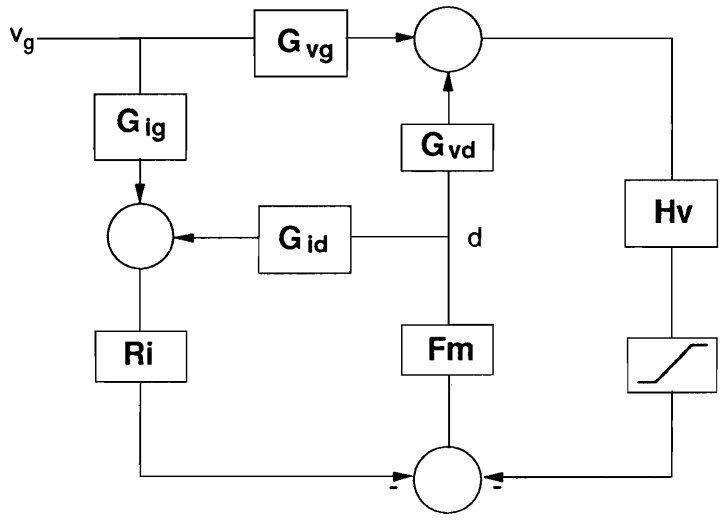

(a)

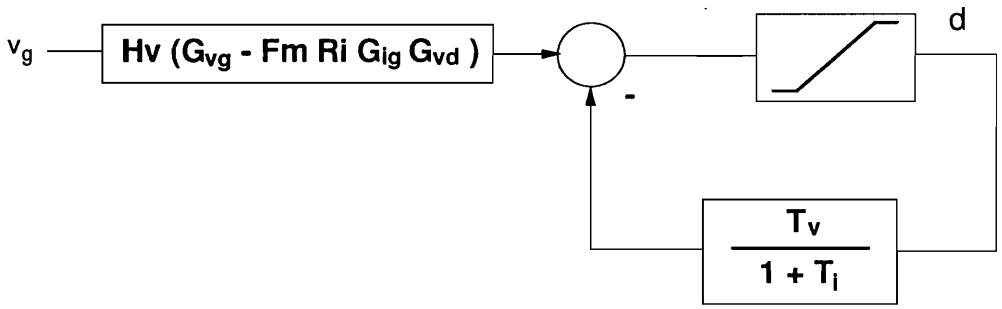

(b)

Fig. 3.13: Block Diagram Representation of the Closed-Loop Buck Converter With Inclusion of the Opamp Saturation Nonlinearity

(a) Inclusion of Opamp Saturation Nonlinearity

(b) Simplified Block Diagram Representation

3.3.1 Effect of Duty Cycle Saturation on the Converter Stability

When the current loop, T_i, and the voltage loop, T_v, are closed upon the open-loop buck converter, one obtains the equivalent block diagram representation of the system as illustrated in Fig. 3.10(a), where the saturation nonlinearity denotes the duty cycle saturation. Figure 3.10(a) can be simplified to yield a single feedback loop with a saturation nonlinearity and a linear part $T_i + T_v$ as shown in Fig. 3.10(b), where

$$T_i = Fm.Ri.G_{id}, \tag{3.16}$$

and

$$T_v = Fm.Hv.G_{vd}. \tag{3.17}$$

Thus, according to the Off-Axis Circle criterion, the system is globally stable if the Nyquist plot of T_v+T_i does not intersect the negative real axis within the segment (-∞, -1]. However, it is a common practice that only the outer loop gain $\frac{T_v}{1+T_i}$ is investigated for the design optimization, and inspection of the loop gain T_v+T_i is often ignored. The above stability analysis makes it clear that the loop gain T_v+T_i is as important as the outer loop gain $\frac{T_v}{1+T_i}$. As an example, a buck converter is designed according to L = 80 μH, C = 300 μF, R_c = 0.05 Ω, R = 6.25 Ω, Fm = 1.9, Ri = 0.1, V_g = 30 V, V_o = 25 V, a switching frequency of 80 KHz, and the upper duty cycle limit set at 0.9. For the outer voltage loop, $Hv(s)$ is selected as

$$Hv(s) = \frac{8000(1+s/10000)}{s(1+s/60000)}. \tag{3.18}$$

Such a design yields the loop gains $\frac{T_v}{1+T_i}$ and T_v+T_i shown in Fig. 3.11. The outer loop gain $\frac{T_v}{1+T_i}$ shows that the system bandwidth is 4 KHz with a phase margin of approximately 35°. This

is an acceptable design, and the system should be stable in the small-signal sense. However, if the loop gain T_v+T_i is measured, it is observed that the phase of T_v+T_i , which dips below -180°, implies that the system is conditionally stable. Then, under some large-signal perturbation of the input, the system exhibits some large-signal oscillations, as illustrated in Fig. 3.12.

3.3.2 Effect of Saturation in the Feedback Loop on the Converter Stability

Saturation in the voltage feedback loop can assume a form of actual saturation of the opamp in the compensation circuit or the current limiting saturation. Such nonlinearity can be represented by a saturation nonlinearity block as illustrated in Fig. 3.13(a). Observe that this case is very similar to the case of duty cycle saturation, and Fig. 3.13(a) can be rearranged as shown in Fig. 3.13(b). Consequently, in order to achieve global stability, the system must not be conditionally stable with respect to the outer loop gain $\frac{T_v}{1+T_i}$.

3.3.3 Combined Saturation Nonlinearities

If both duty cycle saturation and opamp saturation are considered, one obtains the large-signal model of the buck converter as depicted in Fig. 3.14(a). Unlike the voltage mode control for which both saturation nonlinearities can be combined into a single equivalent saturation nonlinearity, the current injection control does not allow a similar simplification due to the presence of the current loop T_i which also has an effect on the duty cycle saturation. In other words, in the mathematical sense, the duty cycle output can be written as $d = N(-Fm.v_i - Fm.v_e)$, where N denotes the duty cycle saturation. Since N is nonlinear, which implies that distributivity property does not apply, $N(-Fm.v_i - Fm.v_e) \neq -N.Fm.v_i - N.Fm.v_e$. Thus, two separate nonlinearities are present in the

system, and analysis techniques for multiple-loop systems must be employed to investigate the large-signal stability properties of the above system.

Since both nonlinearities are memoryless, introduction of the multipliers, M_d and M_o, is permitted (Fig. 3.14(b)). If N_d represents the combined nonlinearity of M_d^{-1} with the duty cycle saturation, and N_o represents the combined nonlinearity of M_o^{-1} with the opamp saturation, then simplification of Fig. 3.14(b) yields the equivalent block diagram representation in Fig. 3.15(a), where the inputs u_1 and u_2 are linear functions of v_g. The nonlinearities N_d and N_o are assumed to have conic sector $\{c_d, r_d\}$ and $\{c_o, r_o\}$, respectively. Therefore, by applying the loop transformation technique, N_d can be factorized into $N_d = c_d + R_d$, where R_d is nonlinear and belongs to the sector $\{-r_d, r_d\}$. Also, $N_o = c_o + R_o$, where R_o is nonlinear and belongs to the sector $\{-r_o, r_o\}$ as depicted in Fig. 3.15(b). Then, according to Fig. 3.15(b)

$$\begin{aligned} e_1 &= -T_i' c_d e_1 - Fmc_o e_2 - T_i' z_1 - Fmz_2 - u_1 \\ e_2 &= \frac{c_d T_v'}{Fm} e_1 + \frac{T_v'}{Fm} z_1 + u_2 \end{aligned} \quad , \tag{3.19}$$

where $T_i' = M_d T_i$, and $T_v' = M_d T_v M_o$. By collecting the terms containing e_1 and e_2 to the left hand side, Eq. 3.19 becomes

$$\begin{bmatrix} 1+T_i' c_d & Fmc_o \\ \frac{-c_d T_v'}{Fm} & 1 \end{bmatrix} \begin{bmatrix} e_1 \\ e_2 \end{bmatrix} = \begin{bmatrix} -T_i' & -Fm \\ \frac{T_v'}{Fm} & 0 \end{bmatrix} \begin{bmatrix} z_1 \\ z_2 \end{bmatrix} + \begin{bmatrix} -1 & 0 \\ 0 & 1 \end{bmatrix} \begin{bmatrix} u_1 \\ u_2 \end{bmatrix}. \tag{3.20}$$

Therefore,

$$\begin{bmatrix} e_1 \\ e_2 \end{bmatrix} = \begin{bmatrix} \frac{-T_i' - c_o T_v'}{\Delta} & \frac{-Fm}{\Delta} \\ \frac{T_v'}{Fm\Delta} & \frac{c_d T_v'}{\Delta} \end{bmatrix} \begin{bmatrix} z_1 \\ z_2 \end{bmatrix} + \begin{bmatrix} \frac{-1}{\Delta} & \frac{-Fmc_o}{\Delta} \\ \frac{-c_d T_v'}{Fm\Delta} & \frac{1+T_i' c_d}{\Delta} \end{bmatrix} \begin{bmatrix} u_1 \\ u_2 \end{bmatrix}, \tag{3.21}$$

where $\Delta = 1 + c_d T_i' + + c_d c_o T_v'$. Since $z_1 = R_d e_1$, and $z_2 = R_o z_2$,

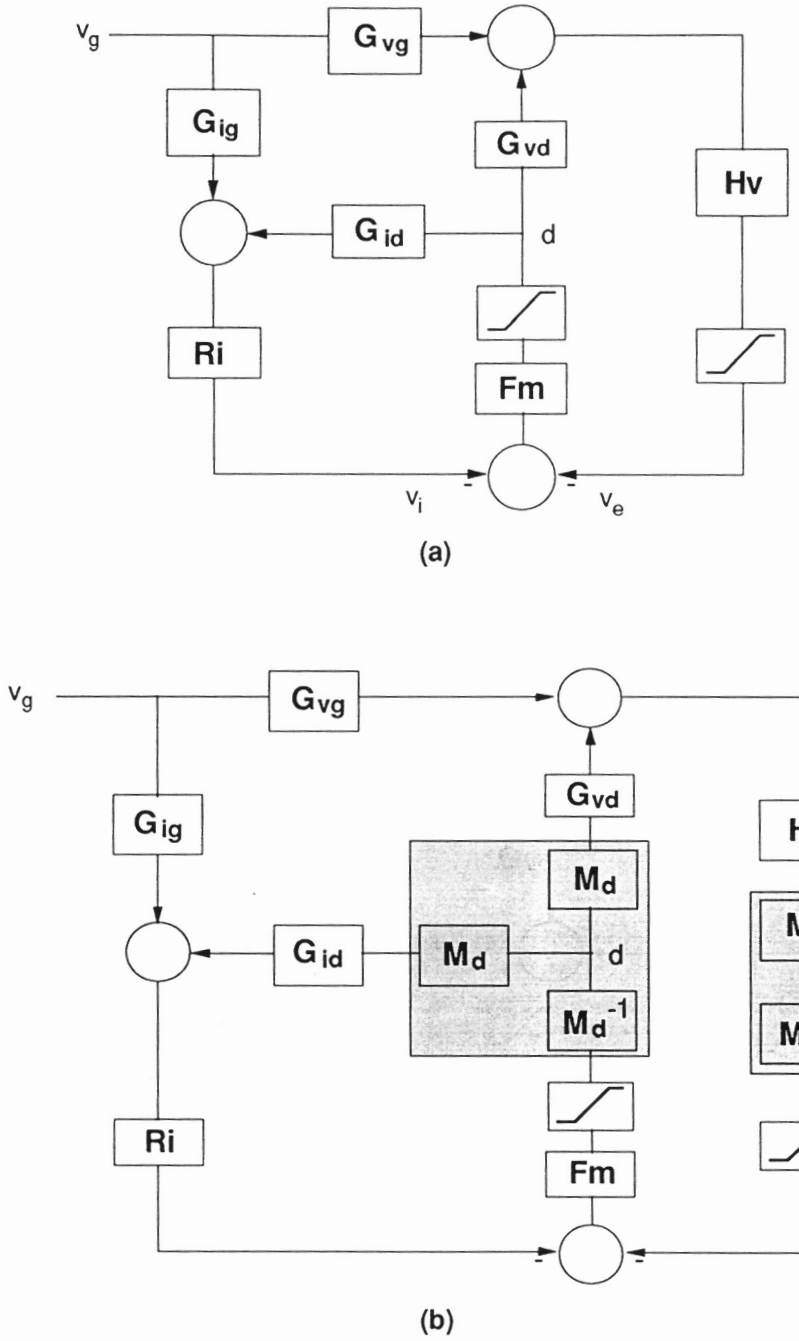

Fig. 3.14: Block Diagram Representation of the Closed-Loop Buck Converter With Inclusion of the Duty Cycle Saturation and the Opamp Saturation

(a) Inclusion of the Opamp and the Duty Cycle Saturation Nonlinearities

(b) Introduction of Multipliers

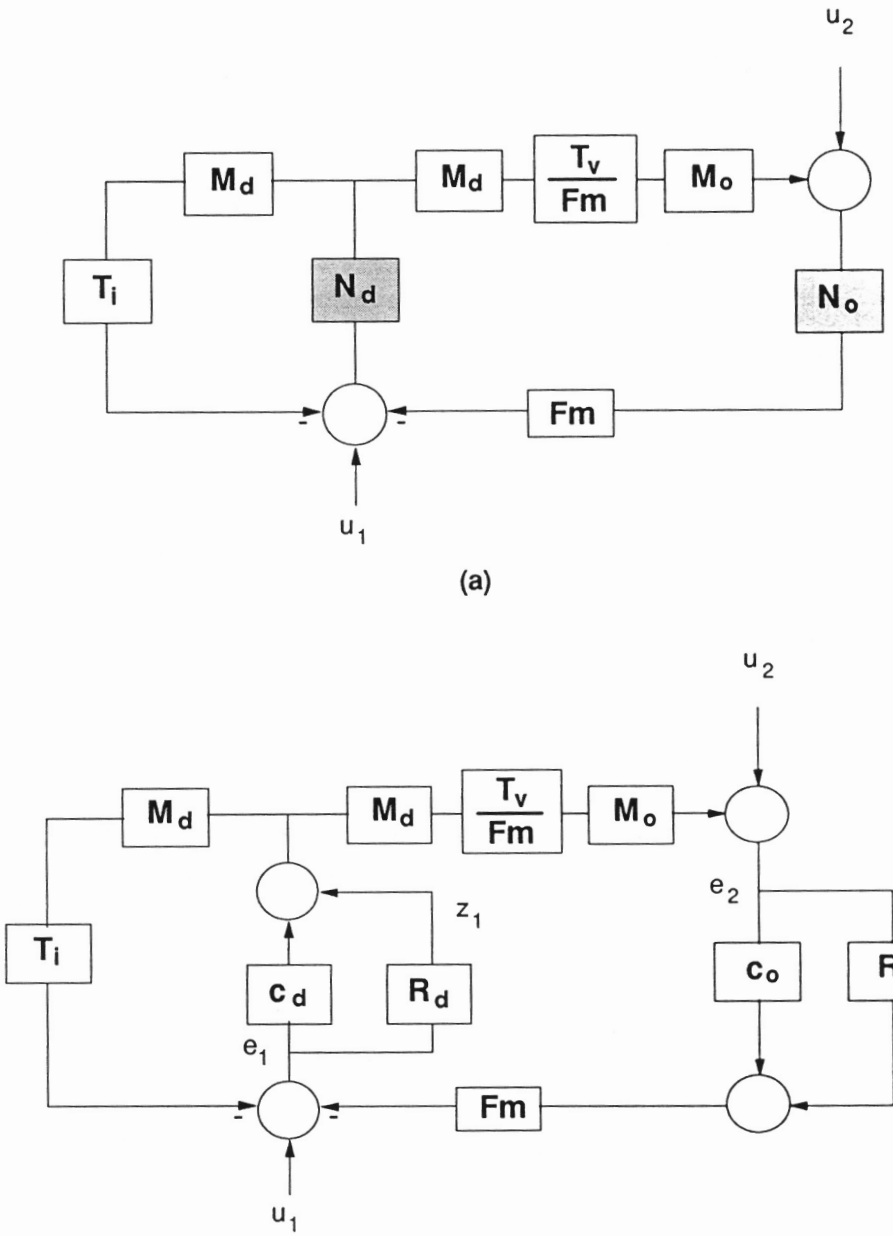

Fig. 3.15: Simplified Block Diagram Representation of the Buck Converter
(a) Simplified Block Diagram Representation
(b) Nonlinearity Conic Sector Expansion

$$\begin{bmatrix} e_1 \\ e_2 \end{bmatrix} = \begin{bmatrix} \dfrac{-T_i' - c_o T_v'}{\Delta} R_d & \dfrac{-Fm}{\Delta} R_o \\ \dfrac{T_v'}{Fm\Delta} R_d & \dfrac{c_d T_v'}{\Delta} R_o \end{bmatrix} \begin{bmatrix} e_1 \\ e_2 \end{bmatrix} + \begin{bmatrix} \dfrac{-1}{\Delta} & \dfrac{-Fmc_o}{\Delta} \\ \dfrac{-c_d T_v'}{Fm\Delta} & \dfrac{1+T_i' c_d}{\Delta} \end{bmatrix} \begin{bmatrix} u_1 \\ u_2 \end{bmatrix}. \tag{3.22}$$

Applying the norm and the triangular inequality yields,

$$\begin{bmatrix} \|e_1\| \\ \|e_2\| \end{bmatrix} \le \begin{bmatrix} g\left(\dfrac{T_i' + c_o T_v'}{\Delta}\right) r_d & g\left(\dfrac{Fm}{\Delta}\right) r_o \\ g\left(\dfrac{T_v'}{Fm\Delta}\right) r_d & g\left(\dfrac{c_d T_v'}{\Delta}\right) r_o \end{bmatrix} \begin{bmatrix} \|e_1\| \\ \|e_2\| \end{bmatrix} + \begin{bmatrix} g\left(\dfrac{1}{\Delta}\right) & g\left(\dfrac{Fmc_o}{\Delta}\right) \\ g\left(\dfrac{c_d T_v'}{Fm\Delta}\right) & g\left(\dfrac{1+T_i' c_d}{\Delta}\right) \end{bmatrix} \begin{bmatrix} \|u_1\| \\ \|u_2\| \end{bmatrix}, \tag{3.23}$$

which becomes

$$\begin{bmatrix} 1 - g\left(\dfrac{T_i' + c_o T_v'}{\Delta}\right) r_d & -g\left(\dfrac{Fm}{\Delta}\right) r_o \\ -g\left(\dfrac{T_v'}{Fm\Delta}\right) r_d & 1 - g\left(\dfrac{c_d T_v'}{\Delta}\right) r_o \end{bmatrix} \begin{bmatrix} \|e_1\| \\ \|e_2\| \end{bmatrix} \le \begin{bmatrix} g\left(\dfrac{1}{\Delta}\right) & g\left(\dfrac{Fmc_o}{\Delta}\right) \\ g\left(\dfrac{c_d T_v'}{Fm\Delta}\right) & g\left(\dfrac{1+T_i' c_d}{\Delta}\right) \end{bmatrix} \begin{bmatrix} \|u_1\| \\ \|u_2\| \end{bmatrix}. \tag{3.24}$$

where $g(.)$ denotes the gain of (.). Equation 3.24 has the following representation

$$\mathbf{R} \begin{bmatrix} \|e_1\| \\ \|e_2\| \end{bmatrix} \le \mathbf{W} \begin{bmatrix} \|u_1\| \\ \|u_2\| \end{bmatrix}. \tag{3.25}$$

Therefore, if $\mathbf{R}$ is invertible and all elements of $\mathbf{R}^{-1}$ are positive, which means that $\mathbf{R}$ must be an M-matrix, then

$$\begin{bmatrix} \|e_1\| \\ \|e_2\| \end{bmatrix} \le \mathbf{R}^{-1} \mathbf{W} \begin{bmatrix} \|u_1\| \\ \|u_2\| \end{bmatrix}, \tag{3.26}$$

and the system is input-output stable. In order for $\mathbf{R}$ to be an M-matrix, all diagonal elements and all principal minors need to be positive; namely

$$\delta_1 \equiv 1 - g\left(\frac{T_i' + c_o T_v'}{1 + c_d (T_i' + c_o T_v')}\right) r_d > 0, \tag{3.27}$$

$$\delta_2 \equiv 1 - g\left(\frac{\dfrac{c_d T_v'}{1+c_d T_i'}}{1+c_o\dfrac{c_d T_v'}{1+c_d T_i'}}\right) r_o > 0, \tag{3.28}$$

$$\delta_1\delta_2 - g\left(\frac{T_v'}{(1+c_d T_i' + c_d c_o T_v')^2}\right) r_o r_d > 0. \tag{3.29}$$

Without using the multipliers ($M_d = M_o = 1$), both saturation nonlinearities belong to the sector $\{1,0\}$, $c_d = c_o = 0.5$ and $r_o = r_d = 0.5$. Then, the conditions in Eqs. 3.27 and 3.28 require that the Nyquist plots of $c_o T_v + T_i$ and $c_d T_v/(1+c_d T_i)$ must stay to the left of the vertical line passing through the (-1,j0) point (case 2 of the circle criterion); these stability conditions are conservative. However, introduction of the multipliers M_o and M_d can improve the above stability conditions. If one selects $M_d = 1$ and $M_o = (1 + s/w_z)/(1 + s/w_p)$ where w_z is a low frequency zero (much lower than any dynamics in the system) and w_p is a high frequency pole (M_o is an RL multiplier), then both saturation nonlinearities belong also to the sector $\{1,0\}$, and therefore, to the sector $\{2,0\}$, which implies that $c_d = c_o = 1$ and $r_o = r_d = 1$. Consequently, according to Eqs. 3.27 and 3.28, the effect of M_o is to shift the phases of $T_v' + T_i'$ and $T_v'/(1+T_i')$ up by 90°. Therefore, if T_v+T_i and $T_v/(1+T_i)$ are not conditionally stable, the multiplier M_o will cause the phases of $T_v' + T_i'$ and $T_v'/(1+T_i')$ to be confined between 90° and -90° and the Nyquist plot of these transfer functions won't intersect the negative real axis within the segment (-∞, -0.5]. Consequently, the conditions in Eqs. 3.27 and 3.28 are satisfied. The condition in Eq. 3.29 is also satisfied because $g\left(\dfrac{T_v'}{(1+T_i'+T_v')^2}\right) << 1$. Thus, when two saturation nonlinearities are present in the system, global stability requires that T_v+T_i and $T_v/(1+T_i)$ not be conditionally stable.

3.4 Large-Signal Stability Analysis of a Boost Converter

Bilinear systems are often encountered not only in power electronics area, but also in many other fields [Coppel, 1966] and [Koditschek, 1982], and the existing literature offers numerous studies devoted to the subject. Unlike in the case of the buck converter, state-space averaging of the boost converter results in a bilinear system– a nonlinear system characterized by a product of the state and the system input. Under large-signal perturbation, the boost converter is prone to instability.

3.4.1 Stability Analysis of a Boost Converter as a Bilinear System

A current-injection-controlled boost converter is selected as an example to illustrate that the closed-loop boost converter can become unstable under large-signal perturbation, and the input-output stability theory can be employed to estimate the stability bound of the closed-loop boost converter. Figure 3.16 illustrates a standard current-injection-controlled boost converter, and the large-signal average state-space representation (according to Eq. 3.4) of the open-loop boost converter is given by

$$\begin{bmatrix} \dot{i}_l \\ v_c \end{bmatrix} = \begin{bmatrix} -\frac{R_l}{L} & -\frac{D'}{L} \\ \frac{D'}{C} & 0 \end{bmatrix} \begin{bmatrix} i_l \\ v_c \end{bmatrix} + \begin{bmatrix} \frac{V_c}{L} \\ -\frac{I_l}{C} \end{bmatrix} d + \begin{bmatrix} 0 & \frac{1}{L} \\ -\frac{1}{C} & 0 \end{bmatrix} \begin{bmatrix} i_l \\ v_c \end{bmatrix} d, \tag{3.30}$$

where the upper case characters represent the steady-state operating point of the system, the lower case characters denote the perturbation around the system operating point, $[i_l \; v_c]^T$ are the state variables, D is the steady-state duty cycle and $D' = 1 - D$. Note that the input u in Eq. 3.4 denotes external disturbance and is ignored in Eq. 3.30. Equation 3.30 can also be represented by

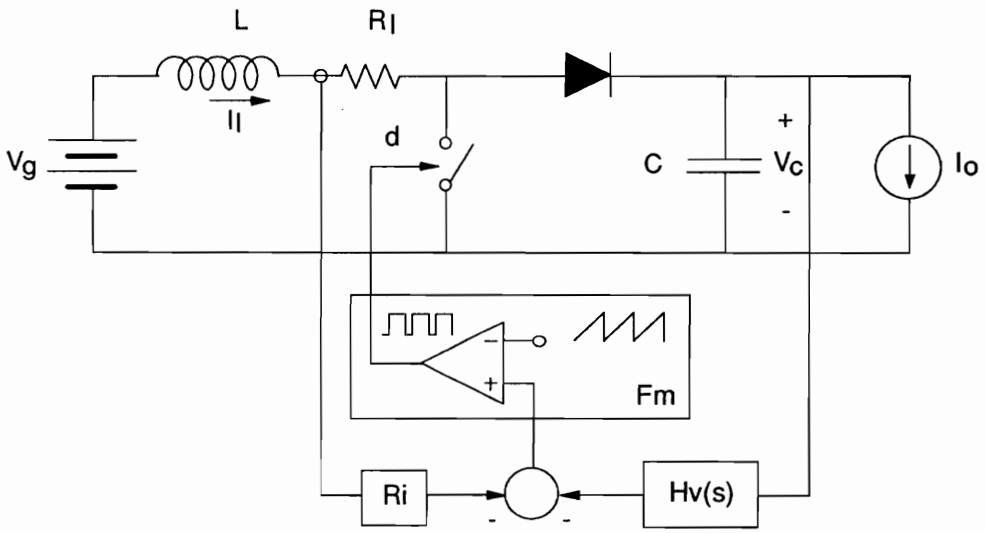

Fig. 3.16: A Current-Injection-Controlled Boost Converter

$$\begin{bmatrix} \dot{i}_l \\ \dot{v}_c \end{bmatrix} = \begin{bmatrix} -\frac{R_l}{L} & -\frac{D'}{L} \\ \frac{D'}{C} & 0 \end{bmatrix} \begin{bmatrix} i_l \\ v_c \end{bmatrix} + \begin{bmatrix} \frac{V_c}{L} & 0 \\ 0 & -\frac{I_l}{C} \end{bmatrix} \begin{bmatrix} 1+\frac{v_c}{V_c} \\ 1+\frac{i_l}{I_l} \end{bmatrix} d. \tag{3.31}$$

If **u** is defined as $\mathbf{u} = \begin{bmatrix} 1+\frac{v_c}{V_c} & 1+\frac{i_l}{I_l} \end{bmatrix}^T d$, then Eq. 3.31 is represented by

$$\begin{bmatrix} \dot{i}_l \\ \dot{v}_c \end{bmatrix} = \mathbf{A} \begin{bmatrix} i_l \\ v_c \end{bmatrix} + \mathbf{Bu}. \tag{3.32}$$

Let G_{id} denote the input-to-inductor current transfer function and G_{vd} denote the input-to-capacitor voltage transfer function (both of which can be found from Eq. 3.32); then, in terms of operator notation, the open-loop boost converter is given by

$$i_l = G_{id}\left(1+\frac{v_c}{V_c}\right) * d, \tag{3.33}$$

$$v_c = G_{vd}\left(1+\frac{i_l}{I_l}\right) * d, \tag{3.34}$$

where * denotes a multiplication in the time domain or a convolution operator in the frequency domain. Also, the feedback loop in Fig. 3.16(a) can be represented by

$$d = -Fm.Ri.i_l - Fm.Hv.v_c + z_o, \tag{3.35}$$

where z_o denotes the input disturbance, which can represent the initial condition of the states in the voltage feedback loop, Hv. Notice from Eqs. 3.33 and 3.34 that if the perturbation is small compared to the steady-state value ($v_c << V_c$, and $i_l << I_l$), the open-loop boost converter can be approximated by a linear small-signal model. However, under large perturbation of the states i_l and v_c, the terms v_c/V_c and i_l/I_l can have considerable effects on the system behavior, and therefore, cannot be neglected. At this point, $\frac{v_c}{V_c}$ and $\frac{i_l}{I_l}$ can be considered two separate nonlinearities with

memory, and Eqs. 3.33, 3.34, and 3.35 represent the average large-signal model of the closed-loop boost converter.

To analyze the stability of the closed-loop boost converter, Eqs. 3.33 and 3.34 are substituted into Eq. 3.35, which yields

$$d = -T_i\left(1+\frac{v_c}{V_c}\right) * d - T_v\left(1+\frac{i_l}{I_l}\right) * d + z_o, \tag{3.36}$$

where $T_i = Fm.Ri.G_{id}$ and $T_v = Fm.Hv.G_{vd}$. Therefore,

$$d = \frac{-T_i}{1+T_i+T_v}\frac{v_c}{V_c} * d + \frac{-T_v}{1+T_i+T_v}\frac{i_l}{I_l} * d + \frac{1}{1+T_i+T_v} z_o. \tag{3.37}$$

Application of the norm and the triangular inequality yields

$$\|d\| \le g\left(\frac{T_i}{1+T_i+T_v}\right)\frac{|v_{c\max}|}{V_c}\|d\| + g\left(\frac{T_v}{1+T_i+T_v}\right)\frac{|i_{l\max}|}{I_l}\|d\| + g\left(\frac{1}{1+T_i+T_v}\right)\|z_o\|. \tag{3.38}$$

where $g(.)$ denotes the gain of (.). Since

$$\|v_c(t)d(t)\|^2 = \int_0^\infty v_c(t)^2 d(t)^2 dt \le |v_{c\max}|^2 \int_0^\infty d(t)^2 dt = |v_{c\max}|^2 \|d(t)\|^2, \tag{3.39}$$

$$\|d\| \le \frac{g\left(\frac{1}{1+T_i+T_v}\right)\|z_o\|}{1 - g\left(\frac{T_i}{1+T_i+T_v}\right)\frac{|v_{c\max}|}{V_c} - g\left(\frac{T_v}{1+T_i+T_v}\right)\frac{|i_{l\max}|}{I_l}}, \tag{3.40}$$

and from Eqs. 3.33 and 3.34, the closed-loop boost is input-output stable if $\|d\|$ is bounded, which requires that

$$1 - g\left(\frac{T_i}{1+T_i+T_v}\right)\frac{|v_{c\max}|}{V_c} - g\left(\frac{T_v}{1+T_i+T_v}\right)\frac{|i_{l\max}|}{I_l} > 0, \tag{3.41}$$

or in the frequency domain

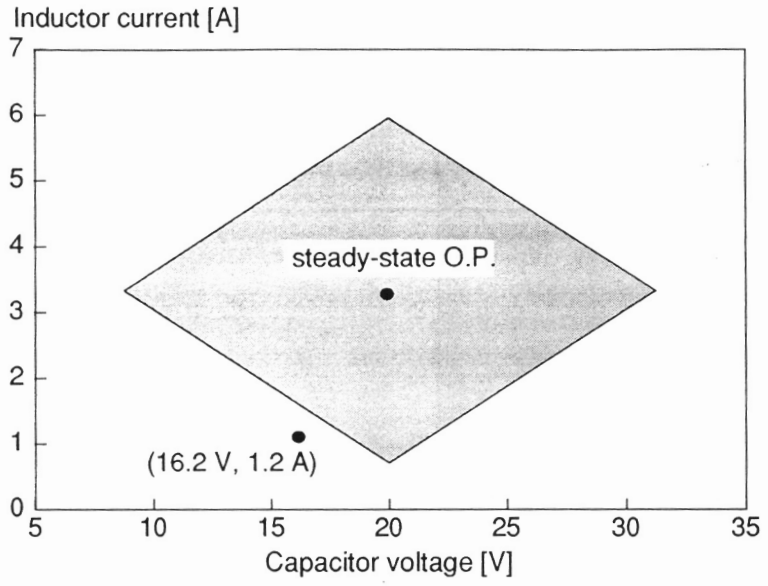

(a)

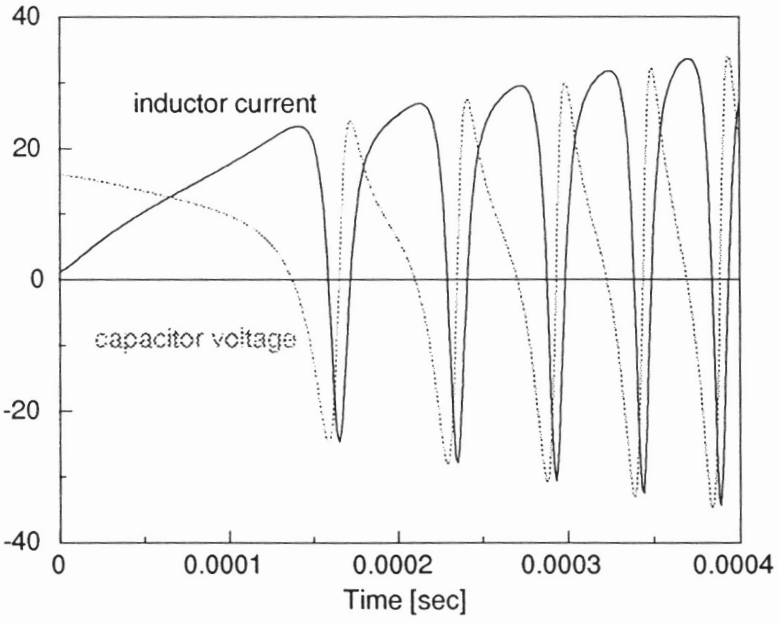

(b)

Fig. 3.17: Stability Conditions for a Closed-Loop Boost Converter
(a) Stability Region
(b) Simulation Results for an Unstable Case

$$1-\left|\frac{T_i(s)}{1+T_i(s)+T_v(s)}\right|\frac{|v_{c\max}|}{V_c}-\left|\frac{T_v(s)}{1+T_i(s)+T_v(s)}\right|\frac{|i_{l\max}|}{I_l}>0. \tag{3.42}$$

Thus, based on selecting appropriate $v_{c\ max}$ and $i_{l\ max}$ such that Eq. 3.42 is satisfied, it is possible obtain a sufficient condition of stability for the closed-loop boost converter, as illustrated in Fig. 3.17(a). For example, the following parameters are selected for a closed-loop boost converter: L = 150 μ H, $R_l = 0.05\ \Omega$, C = 150 μ F, V_g = 15 V, V_c = 20 V, I_o = 2.5 A, Fm = 0.5, Ri = 1, and

$$Hv(s)=\frac{796Hz\left(1+\frac{s}{477Hz}\right)}{1+\frac{s}{9549Hz}}. \tag{3.43}$$

It follows that $\left|\frac{T_i(s)}{1+T_i(s)+T_v(s)}\right|=1.78$, $\left|\frac{T_v(s)}{1+T_i(s)+T_v(s)}\right|=1.27$, and the region of stability is shown in Fig. 3.17(a). The meaning of the region of stability for the closed-loop boost is that as long as the initial condition of the states in $Hv(s)$, or any other disturbance, does not cause (i_l, v_c) to leave the stability region, system stability is preserved. Furthermore, the estimate of the stability region is not too conservative because if one selects (i_l, v_c) = (1.2 A, 16 V) as in Fig. 3.17(a), the boost– as a bilinear system– can exhibit unstable behavior as shown in Fig. 3.17(b).

The instability of the boost converter under large-signal perturbation can be alleviated by properly designing the loop gains $T_1=\frac{T_i}{1+T_v}$ and $T_2=\frac{T_v}{1+T_i}$. Indeed, if one defines

$$\delta_1 \equiv 1-\left|\frac{T_1(s)}{1+T_1(s)}\right|\frac{|v_{c\max}|}{V_c}>0, \tag{3.44}$$

$$\delta_2 \equiv 1-\left|\frac{T_2(s)}{1+T_2(s)}\right|\frac{|i_{l\max}|}{I_l}>0, \tag{3.45}$$

then the sufficient condition in Eq. 3.42 becomes

$$\delta_1 + \delta_2 > 1. \tag{3.46}$$

Equations 3.44 and 3.45 bring to mind the Circle criterion from Appendix A. For Eq. 3.44, the stability can be checked by plotting the Nyquist plot of $T_1(s)$, which must avoid the forbidden region defined by the pair of conic parameters $c = 1$, and $r = |v_{c\,\max}| / V_c$. Also, the condition in Eq. 3.45 requires that the Nyquist plot of $T_2(s)$ must avoid the forbidden region defined by the conic sector $\{1, |i_{l\,\max}| / I_l\}$. If $|i_{l\,\max}| > I_l$, $r >$ c, and according to Case 3 of the Circle criterion, $T_2(s)$ must stay inside a circle defined by $\{c,r\}$. However, since $T_2(s)$ has infinite gain at dc, it violates the requirement. Therefore, the largest possible stability range for the inductor current is when $|i_{l\max}| = I_l$, and $r = 1$. Then, following Case 2 of the Circle criterion, $T_2(s)$ must stay to the left of the vertical line passing through the point (-0.5, j0). Likewise, to achieve $|v_{c\,\max}| = V_c$, the loop gain $T_1(s)$ must stay to the left of the vertical line passing through the point (-0.5, j0). Also, enough margins of boundedness, δ_1 and δ_2 must be provided so that Eq. 3.46 is satisfied.

3.4.2 Effect of Duty Cycle Saturation on the Boost Converter

The problem becomes more realistic when the effect of the duty cycle saturation is considered. Unlike the buck converter case, the boost converter has three nonlinearities, as illustrated in Fig. 3.18(a), where i_o represents an input distrubance; and therefore, simple application of the Off-Axis Circle criterion is not possible. Nevertheless, the loop transformation technique and the multiplier technique from Appendix A can be applied to investigate the effect of the duty cycle saturation on the boost converter. Let us insert a multiplier M_d in the block diagram of Fig. 3.18(a); M_d is an RL multiplier, which is defined as

$$M_d(s) = \frac{1 + s / w_z}{1 + s / w_p}, \tag{3.47}$$

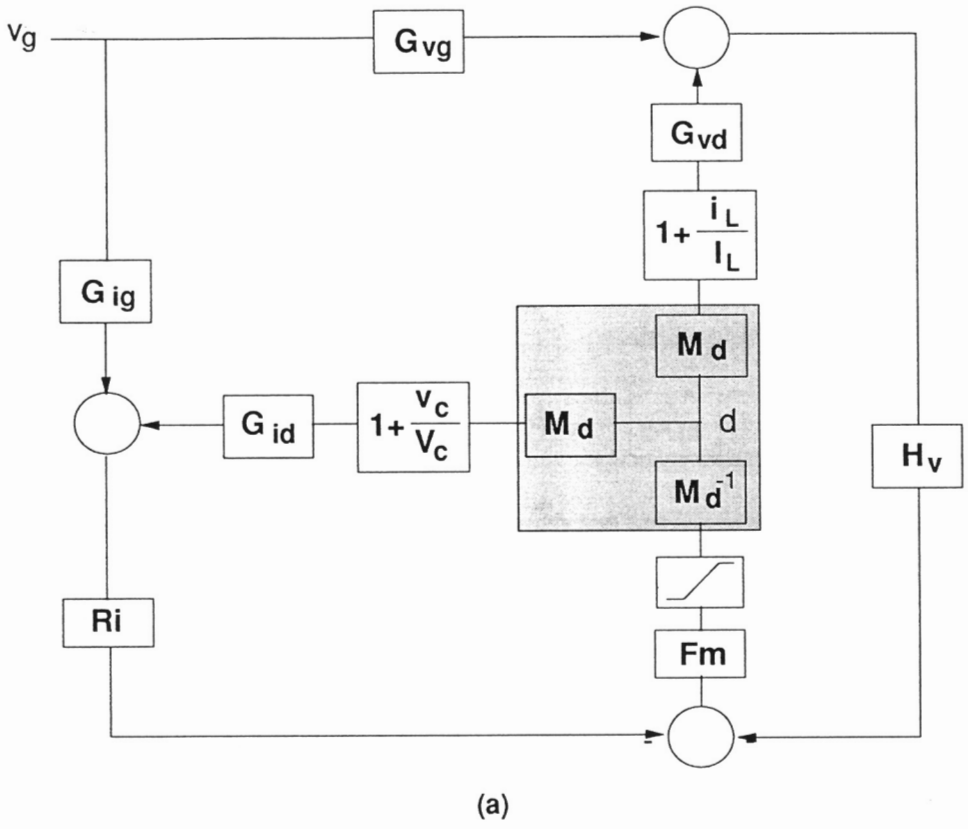

(a)

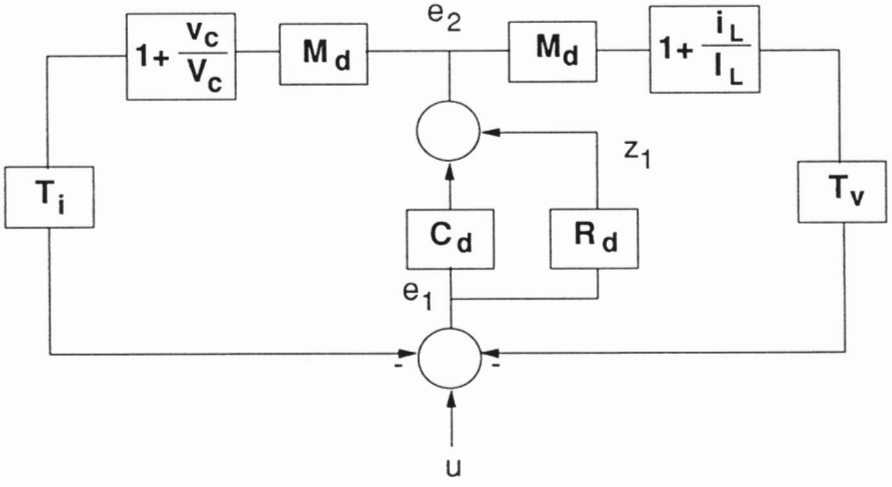

(b)

Fig 3.18: Block Diagram Representation of a Closed-Loop Boost Converter With Inclusion of the Duty Cycle Saturation Nonlinearity

(a) Block Diagram Representation

(b) Simplified Block Diagram

($w_z << w_p$). The block diagram in Fig. 3.18(a) can be simplified to the one shown in Fig. 3.18(b). Note that the duty cycle saturation nonlinearity, combined with M_d^{-1}, has a sector gain of {0,1} and can be expanded into $c_d + R_d$, where c_d is the center conic ($c_d = 0.5$) and R_d is a nonlinearity with gain $r_d = 0.5$. Then, from Fig. 3.18(b)

$$e_2 = c_d e_1 + z_1, \tag{3.48}$$

$$e_1 = -T_i\left(1+\frac{v_c}{V_c}\right) * M_d e_2 - T_v\left(1+\frac{i_l}{I_l}\right) * M_d e_2 + u. \tag{3.49}$$

Eqs. 3.48 and 3.49 can be put in the form

$$\begin{bmatrix} 1 & -c_d \\ M_d(T_i+T_v) & 1 \end{bmatrix}\begin{bmatrix} e_2 \\ e_1 \end{bmatrix} = \begin{bmatrix} z_1 \\ \left(-T_i\dfrac{v_c}{V_c} - T_v\dfrac{i_l}{I_l}\right) * M_d e_2 \end{bmatrix} + \begin{bmatrix} 0 \\ 1 \end{bmatrix} u. \tag{3.50}$$

Solving for $[e_1\ e_2]^T$, and applying the norm yield

$$\begin{bmatrix} \|e_1\| \\ \|e_2\| \end{bmatrix} \le \begin{bmatrix} c_d g\left(\dfrac{M_d T_i}{\Delta}\right)\dfrac{|v_{c\max}|}{V_c} + c_d g\left(\dfrac{M_d T_v}{\Delta}\right)\dfrac{|i_{l\max}|}{I_l} & g\left(\dfrac{1}{\Delta}\right) r_d \\ g\left(\dfrac{T_i}{\Delta}\right)\dfrac{|v_{c\max}|}{V_c} + g\left(\dfrac{T_v}{\Delta}\right)\dfrac{|i_{l\max}|}{I_l} & g\left(\dfrac{M_d(T_i+T_v)}{\Delta}\right) r_d \end{bmatrix}\begin{bmatrix} \|e_1\| \\ \|e_2\| \end{bmatrix} + \begin{bmatrix} g\left(\dfrac{c}{\Delta}\right) \\ g\left(\dfrac{1}{\Delta}\right) \end{bmatrix}\|u\|, \tag{3.51}$$

or

$$\begin{bmatrix} 1 - c_d g\left(\dfrac{M_d T_i}{\Delta}\right)\dfrac{|v_{c\max}|}{V_c} - c_d g\left(\dfrac{M_d T_v}{\Delta}\right)\dfrac{|i_{l\max}|}{I_l} & -g\left(\dfrac{1}{\Delta}\right) r_d \\ -g\left(\dfrac{T_i}{\Delta}\right)\dfrac{|v_{c\max}|}{V_c} + g\left(\dfrac{T_v}{\Delta}\right)\dfrac{|i_{l\max}|}{I_l} & 1 - g\left(\dfrac{M_d(T_i+T_v)}{\Delta}\right) r_d \end{bmatrix}\begin{bmatrix} \|e_1\| \\ \|e_2\| \end{bmatrix} \le \begin{bmatrix} g\left(\dfrac{c}{\Delta}\right) \\ g\left(\dfrac{1}{\Delta}\right) \end{bmatrix}\|u\|, \tag{3.52}$$

where $\Delta = 1 + c_d M_d(T_i + T_v)$. Thus, $\left[\|e_1\| \|e_2\|\right]^T$ is bounded if the matrix on the left hand side of Eq. 3.52 is an M-matrix; that is

$$\delta_1 \equiv 1 - c_d g\left(\frac{M_d T_i}{\Delta}\right)\frac{|v_{c\max}|}{V_c} - c_d g\left(\frac{M_d T_v}{\Delta}\right)\frac{|i_{l\max}|}{I_l} > 0, \tag{3.53}$$

$$\delta_2 \equiv 1 - g\left(\frac{M_d(T_i + T_v)}{\Delta}\right) r_d > 0, \tag{3.54}$$

$$\delta_1\delta_2 - \left(g\left(\frac{T_i}{\Delta}\right)\frac{|v_{c\max}|}{V_c} + g\left(\frac{T_v}{\Delta}\right)\frac{|i_{l\max}|}{I_l}\right) g\left(\frac{1}{\Delta}\right) r_d > 0. \tag{3.55}$$

Equation 3.53 is similar to Eq. 3.42 and defines a stability region as in Fig. 3.17(a) ; Eq. 3.54 indicates the effect of the duty cycle saturation on the stability of the boost converter; and Eq. 3.55 takes into account the interaction between both nonlinearities, the bilinear structure and the duty cycle saturation. It follows from Eq. 3.54 that, since $c_d = 0.5$ and $r_d = 0.5$, Case 2 of the Circle criterion requires that the Nyquist plot of $M_d(T_i + T_v)$ must stay on the right of the vertical line passing through the (-1, j0) point . Consequently, in order to alleviate the effect of the duty cycle saturation on the stability of the boost converter, $T_i + T_v$ must not show a conditionally stable system. The reason is that introduction of M_d can shift the phase of $M_d(T_i + T_v)$ up by 90° and force it to stay in the RHP, thus satisfying Eq. 3.54. It is observed that this requirement is very similar to the one used in the buck converter case.

To illustrate the effect of the duty cycle saturation on the boost converter, the following design parameters are selected: $L = 50\ \mu H$, $R_l = 0.05\ \Omega$, $C = 300\ \mu F$, $R_c = 0.05\ \Omega$, $Ri = 0.1$, $Fm = 1$, $F_s = 80\ KHz$, $V_{in} = 15\ V$, $V_o = 20\ V$, $I_o = 5$ A. If the following $Hv(s)$ is selected,

$$Hv(s) = \frac{6000(1 + s/10000)}{1 + s/10^5}, \tag{3.56}$$

which results in the loop gain T_2 and $T_i + T_v$ shown in Fig. 3.19, the system can exhibit instability under output current perturbation as illustrated in Fig. 3.20 when the duty cycle is limited at [0.2, 1]. Observe that the system does not oscillate as in the buck converter case, but becomes unbounded due to the inherent nonlinearity in the boost converter.

However, if $Hv(s)$ is redesigned so that conditional stability can be avoided, that is the zero of $Hv(s)$ is moved toward the low frequency with adjustment of the integrator gain,

$$Hv(s)=\frac{3000(1+s/5700)}{1+s/10^5}, \tag{3.57}$$

as illustrated in Fig. 3.21, then instability can be avoided as shown by the simulations in Fig. 3.22.

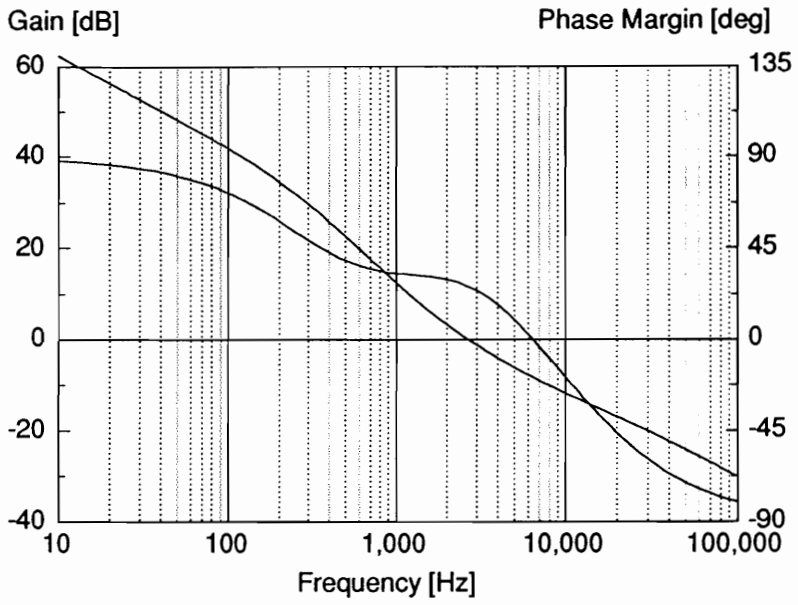

(a)

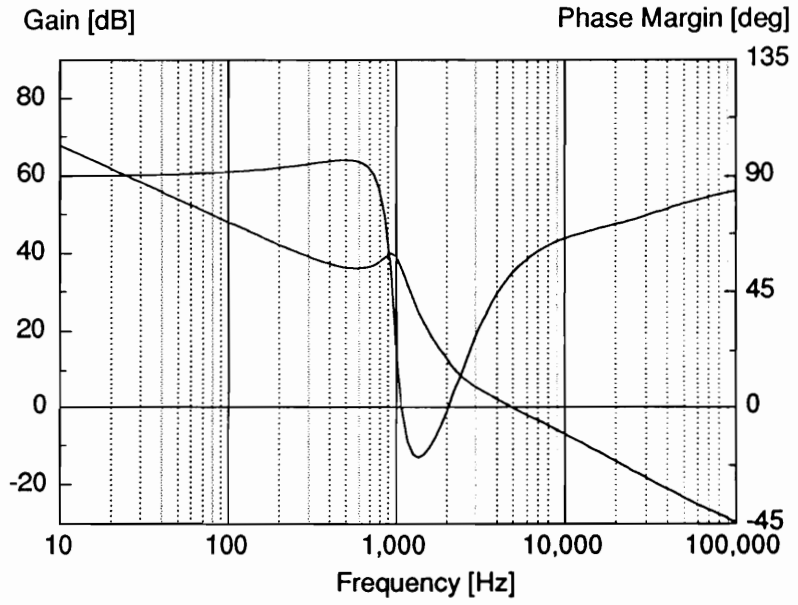

(b)

Fig 3.19: Loop Gains of the Closed-Loop Boost Converter
(a) Loop Gain T_2
(b) Loop Gain $T_i + T_v$

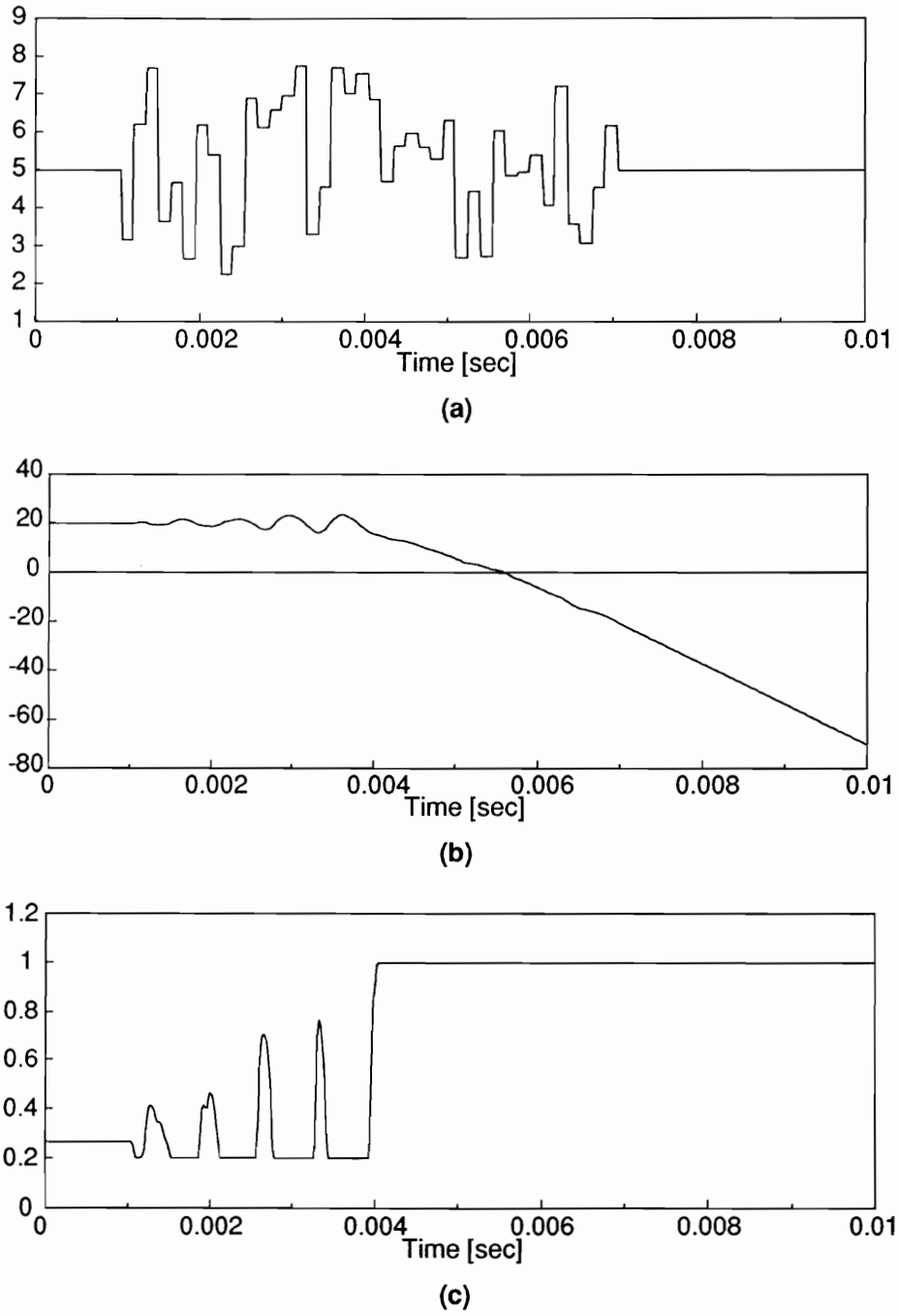

Fig. 3.20: Simulation Results For an Unstable Boost Converter
(a) Output Perturbation Current
(b) Output Voltage
(c) Duty Cycle

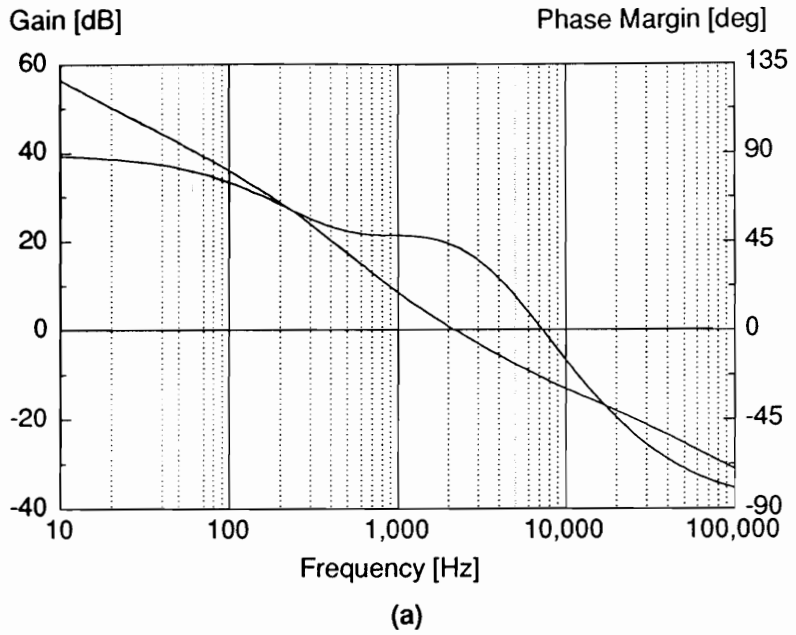

(a)

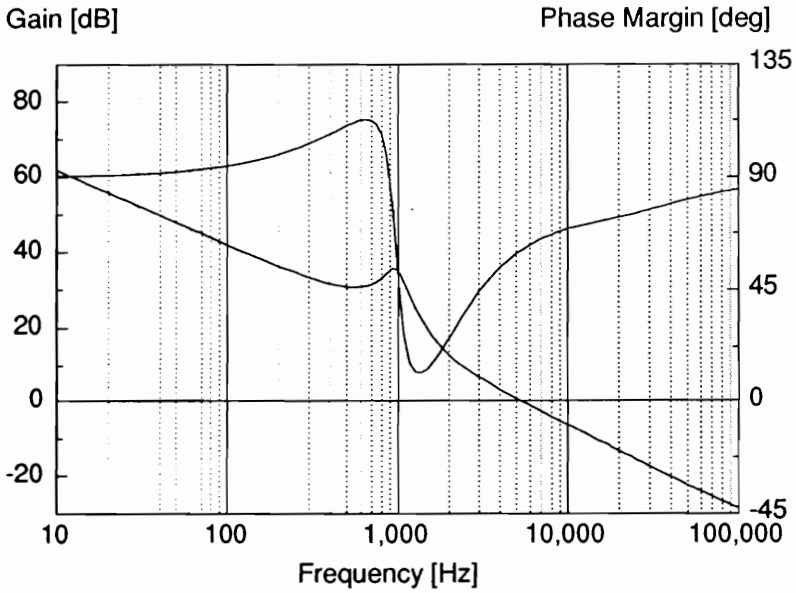

(b)

Fig 3.21: Loop Gains of the Closed-Loop Boost Converter
(a) Loop Gain T_2
(b) Loop Gain $T_i + T_v$

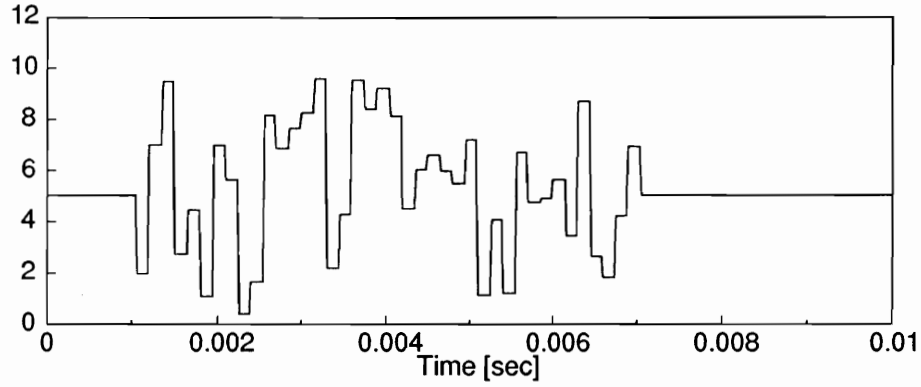

(a)

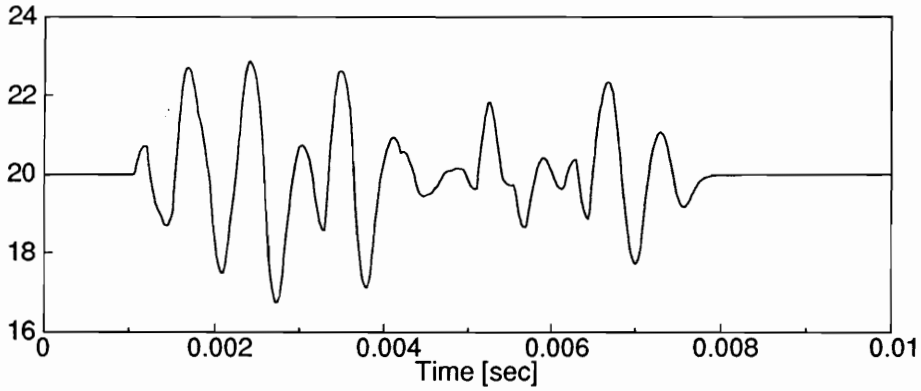

(b)

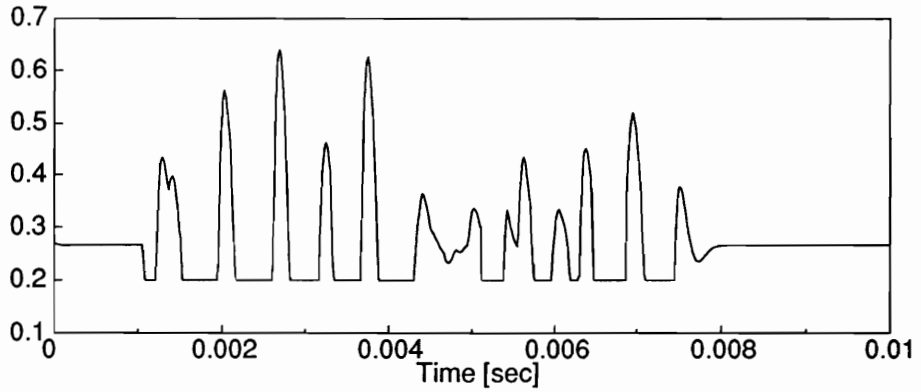

(c)

Fig. 3.22: Simulation Results For a Stable Boost Converter
(a) Output Perturbation Current
(b) Output Voltage
(c) Duty Cycle

3.5 Summary

Applicability of the input-output theory in the large-signal stability analysis of PWM converters is investigated in this chapter. It has been shown that the input-output stability theory is able to predict large-signal instability due to the nonlinearities that exist in PWM converters: the bilinear structure, the duty cycle saturation, and the opamp saturation.

Large-signal stability analysis of a buck converter in voltage-mode control is conducted first, and the closed-loop buck converter is globally stable if the small-signal loop gain defined at the steady-state operating point does not show a conditionally stable characteristic.

For current-injection control, the buck converter is globally stable if both loop gains T_v+T_i and $\frac{T_v}{1+T_i}$ do not show conditionally stable characteristics.

Unlike in the buck converter case, the bilinear structure of the boost converter can considerably affect its stability, even when the saturation nonlinearities are not taken into account. Under current-injection control, it has been shown that the closed-loop boost converter is not globally stable. A sufficient condition is derived, which allows to approximate a stability boundary for the closed-loop boost. In order to alleviate the instability of the boost converter due to its bilinear structure, ways of designing the loop gains $\frac{T_v}{1+T_i}$ and $\frac{T_i}{1+T_v}$ are discussed. Furthermore, when the duty cycle saturation nonlinearity is included in the boost model, it can worsen the boost converter stability if the loop gain $T_i + T_v$ is not properly designed. Instability can be alleviated (but global stability cannot be achieved anyhow) if $T_i + T_v$ does not show conditionally stable characteristic.

Chapter 4

Stability Analysis of a Large-Scale Power Electronics System

In Chapter 2, a methodology for the stability analysis of large-scale power electronics systems has been proposed. The procedure consists of decoupling the entire system into a source subsystem and a load subsystem. The stability of the system can then be investigated based on the characteristic of the feedback loop formed by the interconnection of the source and the load. This chapter focuses on the applicability aspect and practical consideration of the proposed methodology.

The objective of this chapter is threefold. First, guidelines and various steps, starting from the identification process of the source and load subsystems to the application of the stability criterion, are discussed in more detail. Practical considerations, such as selection of sampling intervals for recording input/output data, generation of perturbing input signals, and computation techniques for the approximation of the linear part and the sector gain, are illustrated. Also, it has been pointed out in Chapter 2 that any stability criterion derived from the input-output stability theory yields only a sufficient condition and not a necessary condition. The degree of conservativeness depends upon the system being dealt with. Therefore, it is necessary to quantify, if possible, this level of conservativeness of the derived stability criterion in Chapter 2 as applied to power electronics

systems. The goal at this point is to assure that the derived stability criterion can yield results that are near necessary conditions as well. Lastly, the results in this chapter can illustrate also that small-signal design guidelines can be established to ensure not only small-signal stability, but large-signal stability as well, since the large-signal stability criterion derived in Chapter 2 utilizes small-signal loop gains.

A subsystem of the Space Station power system, which consists of a Direct Dc-to-dc Converter Unit (DDCU) and a load subsystem, is selected to illustrate the proposed methodology. Emphasis is placed on the nonlinearities present in the DDCU and on large-signal interaction of an arbitrary load converter with the DDCU.

4.1 DDCU and a Load Subsystem

In this section, interaction between the DDCU and a particular load subsystem is analyzed based on the proposed methodology. The objective is to investigate the large-signal stability properties of the interconnected system, where the source is the DDCU and the load subsystem is an arbitrary load converter with an input filter. Also, conservativeness of the developed stability criterion is quantified.

A simulation model of the entire system is built for the analysis purpose, and Fig. 4.1 illustrates the key points of the interconnected system. The DDCU input voltage is set at 115 V (worst case stability condition for the DDCU), and the DDCU output is regulated at 124 V. Also, it is designed to handle load power from no load to 6.25 K Watts. The load converter input filter is selected so that large-signal instability occurs under perturbation, while small-signal analysis predicts the system stability around the steady-state operating point. A uniformly distributed CSRS, I_p, with an amplitude of 50 A, and a perturbation period of 200 μsec, is injected into the

system at three different loading conditions: (1) 6.25 KW load with R_d = 0.06 Ω, (2) 3.125 KW load with R_d = 0.02 Ω, and (3) 240 W load with R_d = 0.03 Ω, and Fig. 4.2 illustrates the DDCU output voltage response. For the full load and half load cases, the system exhibits limit cycle oscillations due to the duty cycle saturation in the DDCU. In fact, the damping resistor, R_d, is selected based on trials and errors such that the system is almost exactly on the borderline between large-signal instability and stability. For case 3, even though the oscillation damps out eventually, such abnormal behavior predicts that the system is on the verge of becoming unstable if the damping resistor R_d is set at a smaller value.

Because of the nonlinear interaction (duty cycle saturation in the DDCU) between the DDCU and the load, small-signal analysis based on the impedance comparison technique fails to predict the system stability. Investigation of the system large-signal stability can be performed based on the methodology developed in Chapter 2, and is to be discussed in the following sections. The methodology requires identification of the source and the load, followed by the application of the stability criterion developed in Chapter 2. The source and load identification will result in two block structure models, which consist of a linear part in series with a nonlinear part, representing the source and the load subsystems.

The identification process begins with approximation of the linear part (small-signal model) of both source and load subsystems, as discussed in the next section.

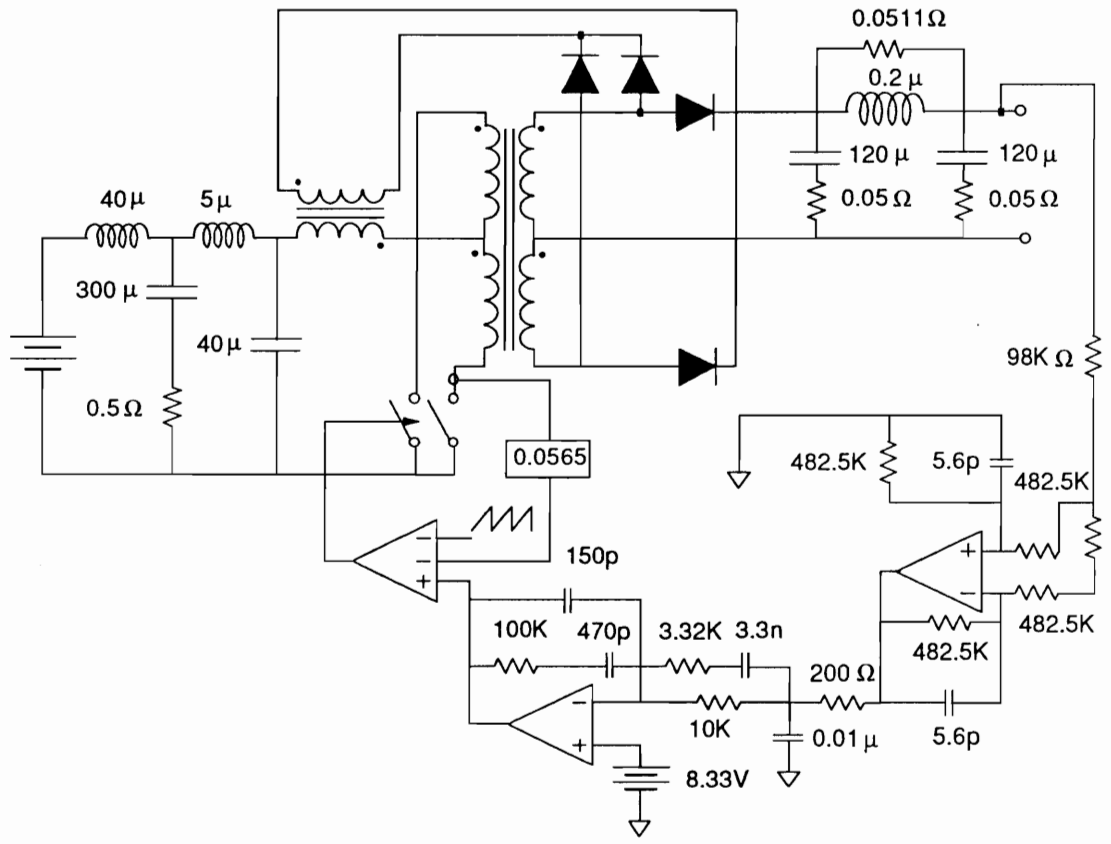

Fig. 4.1: Circuit Diagram of the DDCU and a Load Converter
(a) Circuit Diagram of the DDCU
(b) System Interconnection

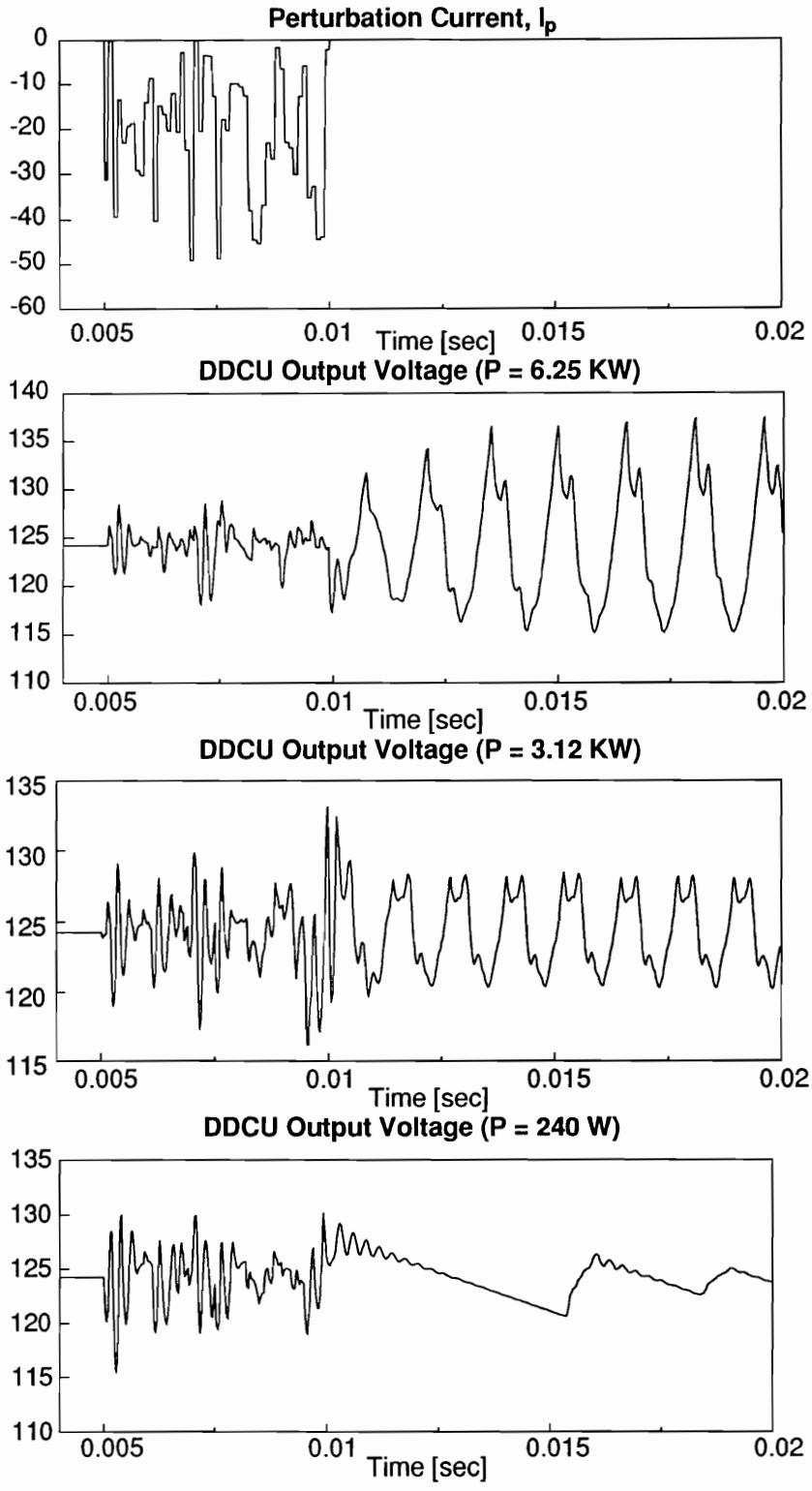

Fig. 4.2: Large-Signal Instability Results for the Interconnected System

4.1.1 Small-Signal Identification of the DDCU and the Load Subsystem

As discussed in Chapter 2, nonlinear identification of either the source or the load requires identification of the linear part first, which represents the linear dynamic of the system around a small neighborhood of the steady-state operating point (small-signal model). Therefore, the linear identification of the system requires injection of a small-signal perturbation into the system, measurement of the input/output data, and application of the least-square-fit algorithm discussed in Chapter 2 to identify an equivalent ARMA model for the unknown system.

To identify the DDCU's small-signal model, a CSRS, which is uniformly distributed with a zero mean and an amplitude of 0.5 A, is injected on top of the dc output current of the DDCU. A sampling frequency of 80 KHz (which is the same as the switching frequency of the DDCU) and a perturbing frequency of 20 KHz for the CSRS are selected. Selecting the perturbing period four times slower than the sampling period helps to avoid the aliasing effect when sampling the DDCU current and output voltage. Also, 500 data points are recorded for the small-signal identification.

Given the sample data points, the least-square-fit algorithm can be applied to identify the small-signal model of the DDCU. A MATLAB program (Appendix D) is written to approximate the parameters of the ARMA model for the system. Since the order of the DDCU is assumed to be unknown, ARMA models of various orders (from 2^{nd} order to 7^{th} order) are selected, and the corresponding RMS error between the exact output voltage response of the DDCU and the output response of the ARMA model is computed. Table 4.1 illustrates the LOG (RMS error) for various orders and different load powers. It is observed that the larger the order of the ARMA model is, the smaller the LOG(RMS error) becomes, and the more accurately the corresponding ARMA model identifies the system. However, for orders larger than the 5^{th} order, the RMS errors tend to level down, indicating that ARMA models of orders larger than 5 do not yield much more improvement in terms of accuracy. Consequently, an ARMA model of order 5 should yield accurate prediction of the DDCU.

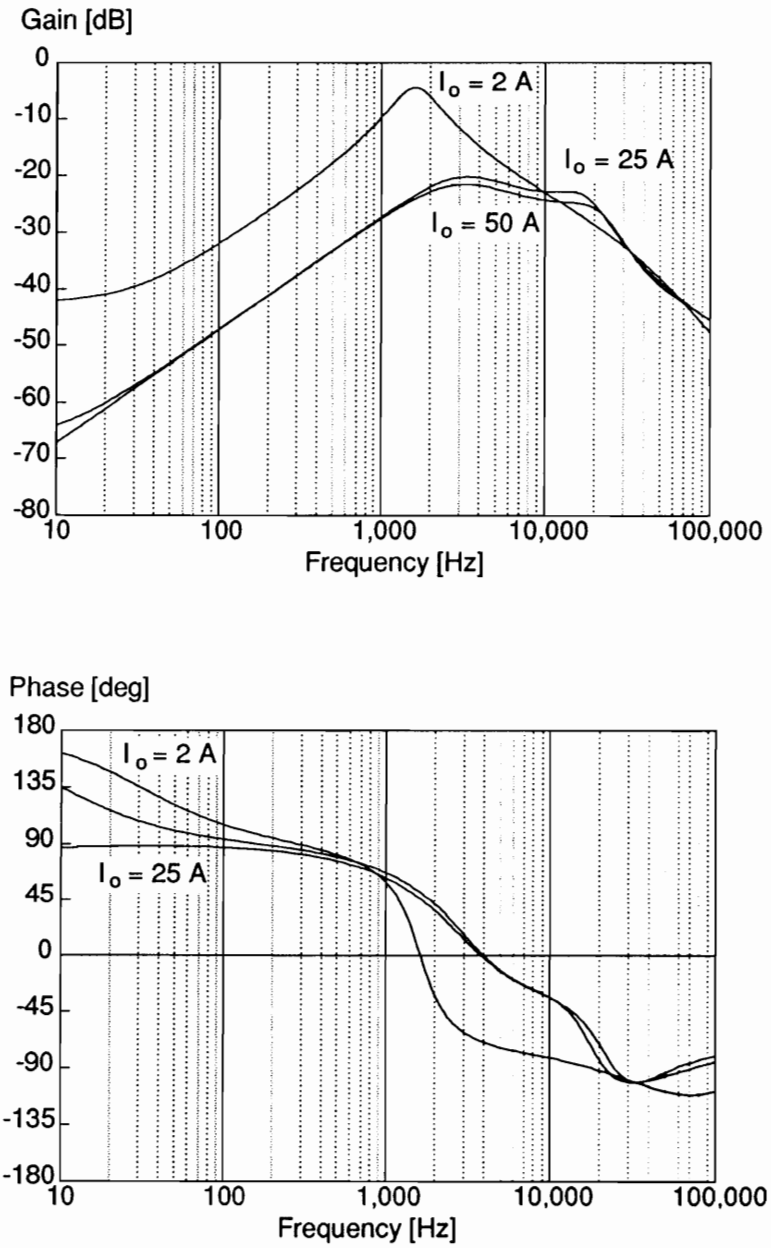

Fig. 4.3: DDCU Output Impedance

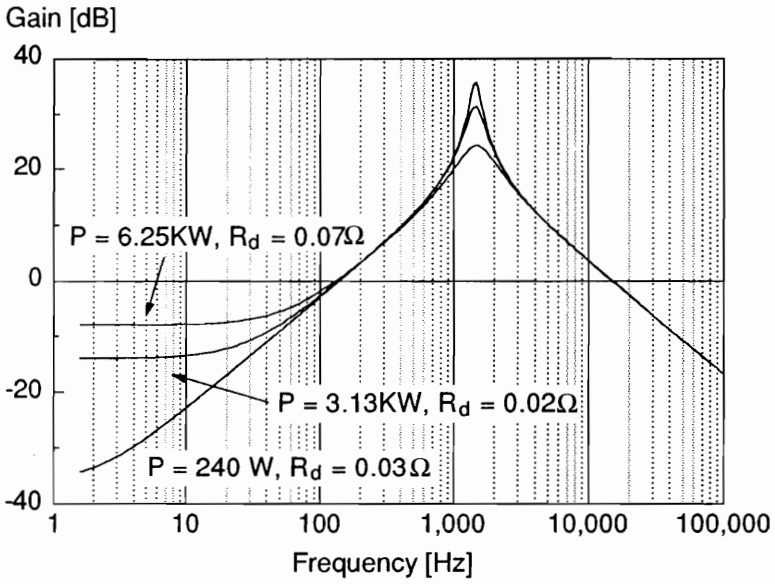

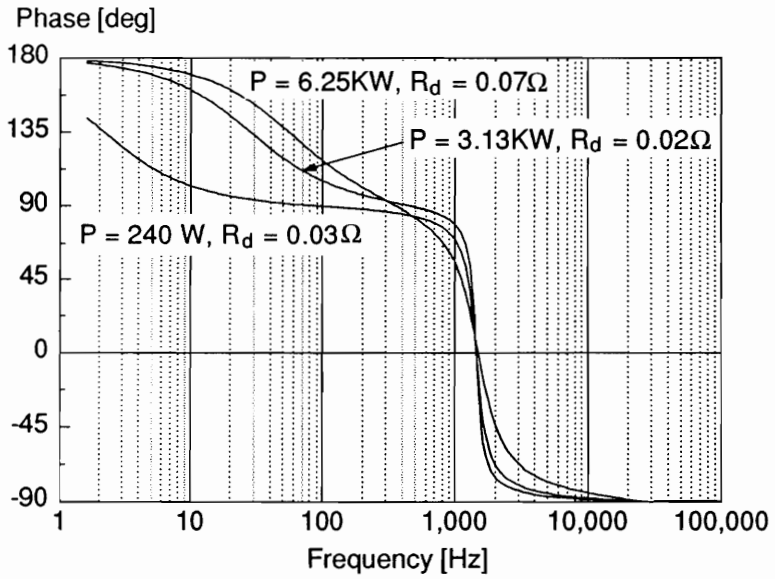

Fig. 4.4: Load Output Admittance

Table. 4.1: Log (RMS error) for Different System Orders

	Output Power (V_{in} = 115 V)		
System Order	I_o = 50 A	I_o = 25 A	I_o = 2 A
2	-2.43	-2.47	-3.35
3	-3.00	-3.00	-4.01
4	-3.44	-3.33	-4.22
5	**-4.26**	**-4.22**	**-4.81**
6	-4.34	-4.27	-4.84
7	-4.36	-4.32	-4.86

For instance, Eq. 4.1 represents the ARMA model of the system at $I_o = 50$ A:

$$\begin{aligned} y(k) \;=\; & 7.5056 + .0010u(k) + .0430u(k-1) - .0497u(k-2) \\ & + .0026u(k-3) + .0003u(k-4) + .0028u(k-5) + 1.5495y(k-1) \\ & - .7735y(k-2) + .3043y(k-3) - .1277y(k-4) - .0130y(k-5) \end{aligned} \tag{4.1}$$

Figure 4.3 depicts the identified output impedance of the DDCU at three different loading conditions. The same procedure is performed on the load, and Fig. 4.4 illustrates the identified load output admittance.

4.1.2 Sector Gain Identification of the DDCU and the Load Subsystem

Once the linear part is identified, the nonlinear part sector gain can be approximated next. A large-signal input disturbance, u, is injected into the system to excite all the existing nonlinearities, and both u and the output response, y_e, are recorded. As has been discussed in Chapter 2, since the nonlinear block is in series with the linear block, sector gain identification of the nonlinear block requires knowledge of the output of the linear part, y_a, when u is introduced into the system. Since

the linear block is already identified , y_a, can be approximated from the identified ARMA model given the input disturbance u, and therefore, the data set $\{y_a, y_e\}$ represents the input/output data of the nonlinear block and can be used to approximate the nonlinear block sector gain.

4.1.2.1 Selection of a CSRS for Large-Signal Perturbation

The first step in the sector gain identification of the nonlinear block is generation of a CSRS appropriate for large-signal perturbation. An appropriate CSRS should cover the entire region of operation of the system and at the same time transfer maximum perturbation power to excite the existing nonlinearities in the system. As is discussed in Appendix D, properties of a CSRS depend upon the variance of the random signal (amplitude of the signal) and the perturbation period, Δt. Therefore, an amplitude of excitation should be chosen in such a way as to cover the entire region of operation. For instance, since the DDCU should be able to handle loads from 0 to 6.25 KW, or 0 to 50-A load current respectively, a perturbation current of 25 A amplitude around a 25-A dc load current should be adequate. This makes sure that the entire region of operation of the DDCU, including both DCM and CCM, is covered. Likewise, a perturbation voltage around 124 V dc (which should be the regulated output voltage of the DDCU) should be used for the load subsystem. Selection of the perturbation voltage amplitude for the load subsystem depends on the output voltage response of the DDCU under the above current disturbance, since the DDCU output voltage will become the input to the load subsystem when the DDCU and the load subsystem are interconnected.

Selection of the perturbation period, Δt, depends on which range of frequencies excites the nonlinearity in the system the most. However, since it is not known beforehand what frequency range the nonlinearity in the system occupies, a preliminary investigation of the system is

necessary. As defined in Chapter 2, if the system is linear, then the system transfer function is given by

$$|H(j2\pi f)| = \sqrt{\frac{\wp_y(f)}{\wp_u(f)}}. \tag{4.2}$$

On the other hand, if the system is nonlinear, it is expected that the nonlinear gains in higher-order kernels of the Volterra series would add up to the linear transfer function, therefore revealing the exciting frequencies of the nonlinearity in the system. Thus, detection of nonlinearities can be performed based on injecting large-signal perturbation into the system, recording the system response, and applying Eq. 4.2 using any existing FFT algorithm (Appendix D) to obtain the approximated system transfer function. Figure 4.5 illustrates the comparison between the transfer functions computed from Eq. 4.2 and the small-signal identification from the previous section for DDCU output impedance and the load input admittance. The approximation using Eq. 4.2 is performed based on injecting a CSRS with $1/\Delta t$ = 20 KHz (four times slower than the sampling period), an amplitude of 25 A for the DDCU, and an amplitude of 80 V for the load subsystem. Thus, the signal power can span the whole range of frequencies of interest and detect existing nonlinearities in the subsystems. The number of data points is 8200, which is required to observe the system dynamic accurately from approximately 50 Hz up to half of the sampling frequency. For the DDCU case, the discrepancy between the transfer function computed from Eq. 4.2 and the ARMA small-signal model indicates that the DDCU contains a nonlinearity, which has a considerable effect at about 1.5 KHz. In fact, this nonlinearity is due to the duty cycle saturation in the DDCU. As far as the load subsystem is concerned, Fig. 4.5(b) indicates that, dynamically, the load subsystem behaves very much linearly under large-signal perturbation. The above procedure permits determining whether a nonlinearity exists in the system and identifying its exciting frequency.

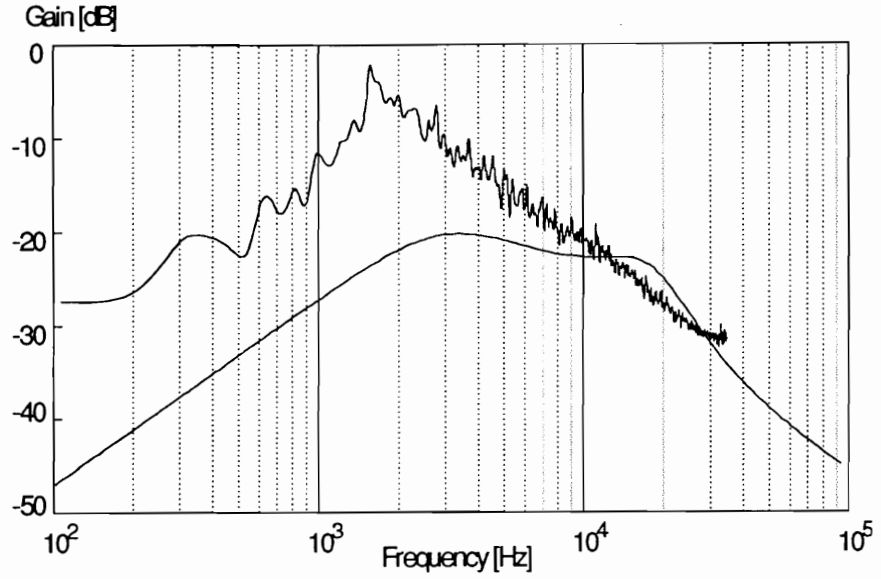

(a)

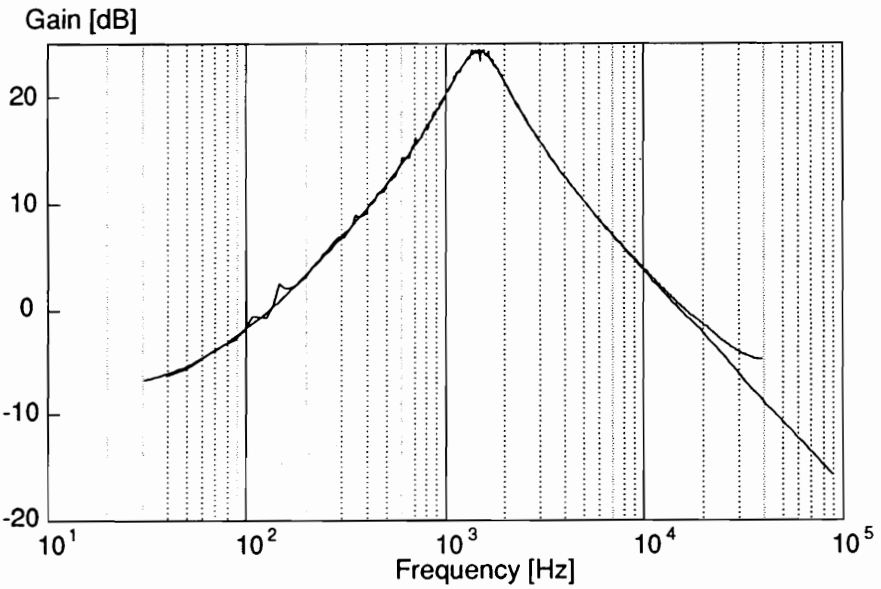

(b)

Fig. 4.5: Nonlinearity Detection
(a) DDCU
(b) Load Subsystem

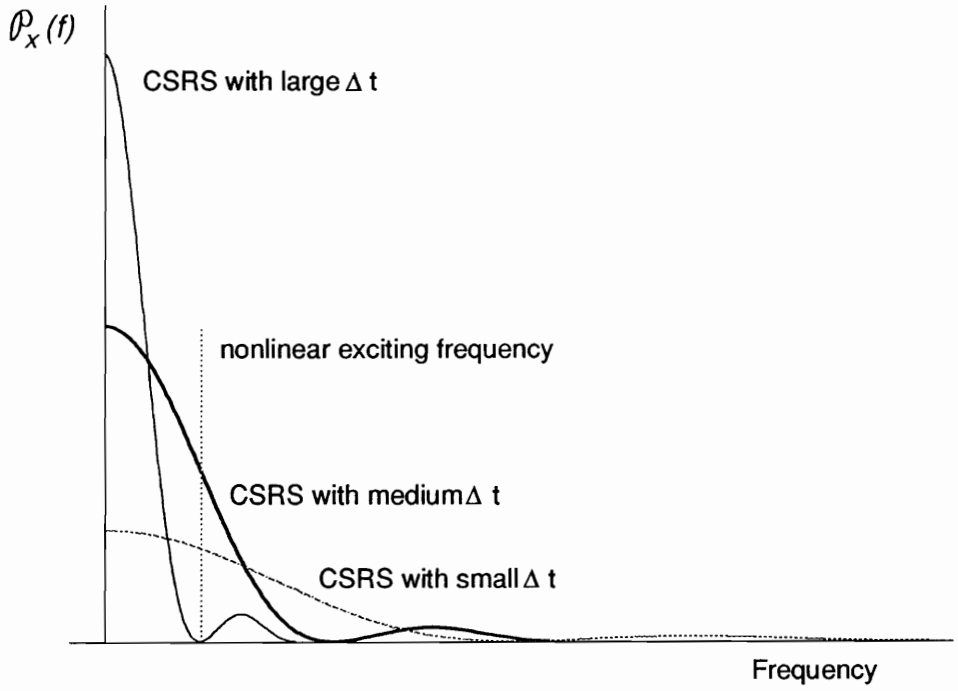

Fig. 4.6: Power Spectra of CSRSs with Different Δts

Once the exciting frequency of the nonlinearity is identified, the perturbation period Δt of the CSRS can be selected so that the perturbing random signal can excite the nonlinearity as much as possible. Intuitively, if the nonlinearity appears at the midband frequency, then a too large Δt implies that most of the signal power will concentrate at the low frequency range, and therefore, not enough signal power is present at the midband frequency to excite the nonlinearity, as illustrated in Fig. 4.6. On the other hand, if Δt is near the sampling period, the total signal power will spread equally from the low frequency to the high frequency range and result in less than adequate power at the midband to excite the nonlinearity. It follows that Δt should be chosen such that the power bandwidth of the random signal is approximately close to the exciting frequency of the system.

4.1.2.2 Sector Gain Identification

The criteria discussed in the previous section allow designing an appropriate CSRS for large-signal perturbation. For the DDCU, a perturbation output current with a mean of 25 A dc, an amplitude of 50 A, and a Δt of 500 μsec is injected at the output port, and 8200 samples of the output perturbation current and the DDCU output voltage are recorded. Likewise, a random input voltage with a mean of 124 V dc, an amplitude of 50 V, and a Δt of 500 μsec is used to perturb the load subsystem at three different loading conditions, 6250 W, 3125 W, and 240 W. These signal properties ensure that the entire operating region is covered. Figures 4.7(a) and 4.7(b) illustrates the data generation process for the source and the load converter at full load, respectively.

Once the data are sampled, they can be processed, along with the identified ARMA models (small-signal linear models), by a MATLAB program (Appendix D) to approximate the conic sectors of the nonlinear parts. The algorithm consists of two distinct functions:

1) Given the measured input perturbation signal, u, and the ARMA model, compute the

output of the linear part (ARMA model), y_a.

2) Given y_a and the measure output response of the system, y_e, compute the conic sector.

Figure 4.8 illustrates the approximated radius, r, as a function of center conic, c, for the load subsystem and the DDCU. Notice that the sector gains of the load subsystem for all the three loading conditions are very small, indicating that the load subsystem is nearly linear. These results are well expected, since, even though the load subsystem is a constant power load, the operating region is confined within the linear range of the constant power curve (100 V– 150 V). However, for the DDCU, the sector gains are quite large due to the duty cycle saturation effect.

4.1.2.3 Multiplier Insertion and Identification of a New Sector Gain for the DDCU

At this point, properties of the DDCU and the load subsystem are properly characterized, and the next step should be application of the stability criterion for the analysis of the interconnected system. However, it is possible to proceed one step further, that is to insert a multiplier, M, in between the linear part and the nonlinear part of the DDCU, to reduce the conservativeness of the stability result. The reason is that the stability criterion developed in Chapter 2 requires the loop gain, $T = L_z L_y$, to avoid a certain forbidden region defined by the sets $\{r_z,c_z\}$ and $\{r_y,c_y\}$, and inspection of the stability criterion indicates that shrinking T to the origin as much as possible will make it easier to meet the requirements set by the three conditions stated by the stability criterion. In fact, this is the optimum condition for achieving global stability because such T would avoid the forbidden regions defined by $\{r_z,c_z\}$ and $\{r_y,c_y\}$ the most. Notice that the point of insertion of the multiplier, whether within the DDCU block structure or the load subsystem block structure, is arbitrary. However, application of the stability criterion indicates that insertion of M in between the DDCU linear and nonlinear parts can yield a less conservative result.

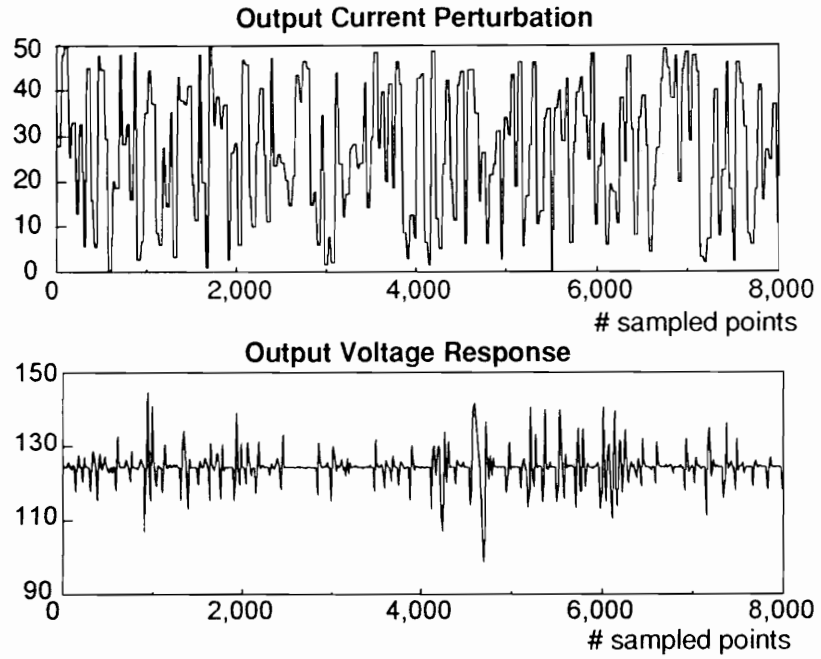

(a)

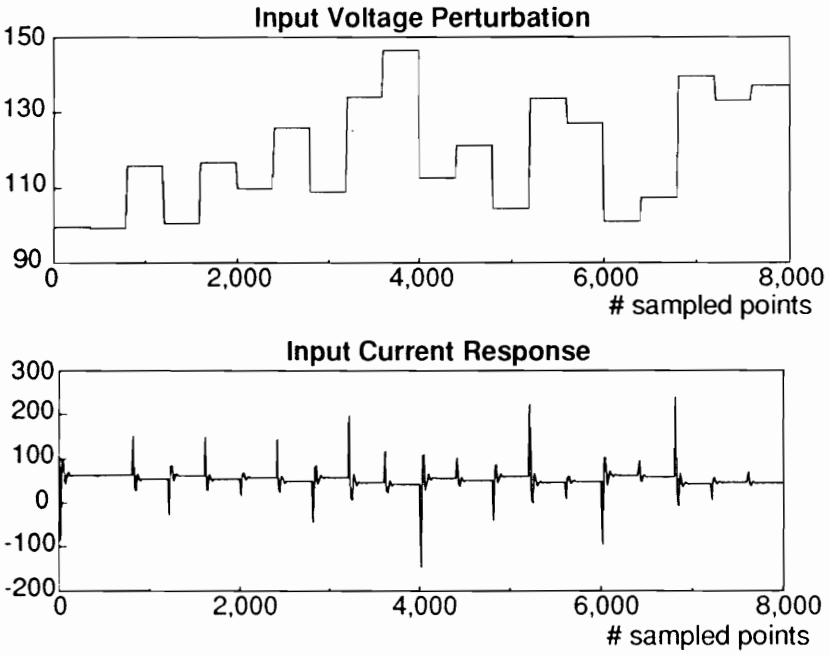

(b)

Fig. 4.7: Data Generation for Sector Gain Identification
(a) DDCU
(b) Load Converter

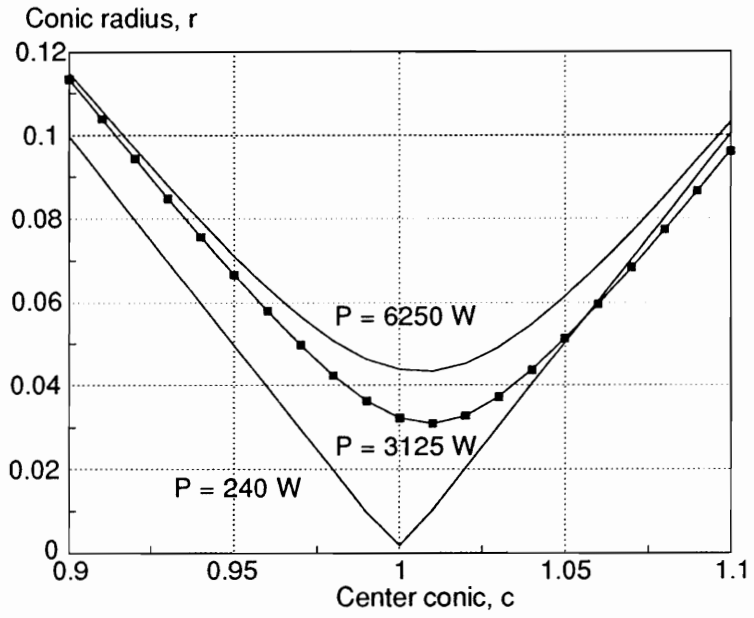

(a)

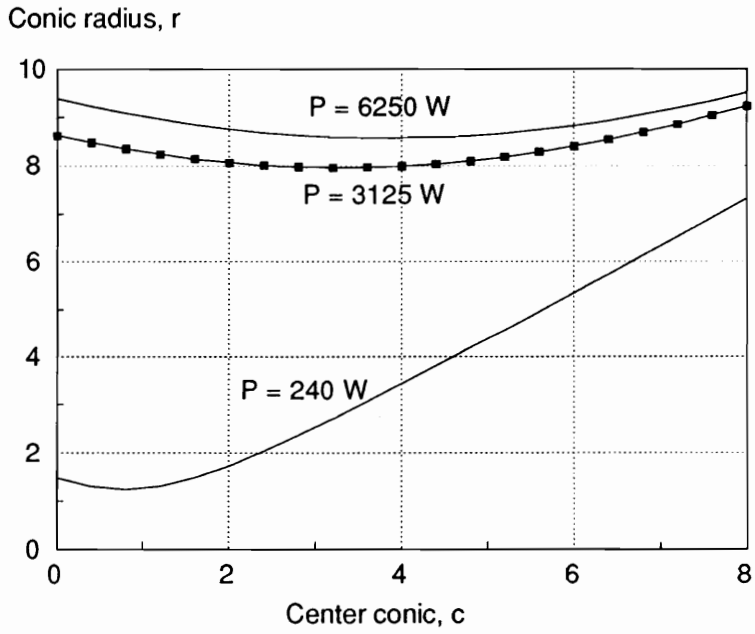

(b)

Fig. 4.8: Conic Radius-Center Conic Relationship
(a) Load Subsystem
(b) DDCU

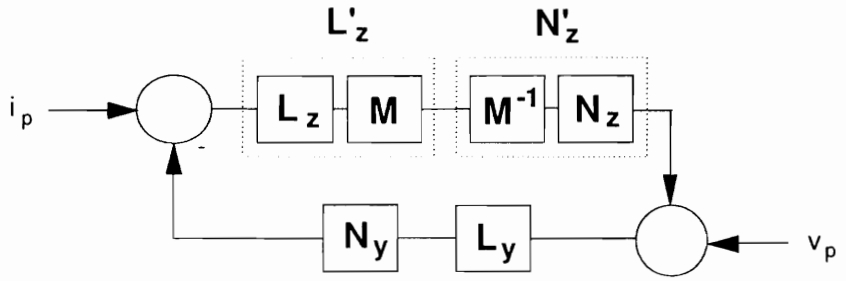

(a)

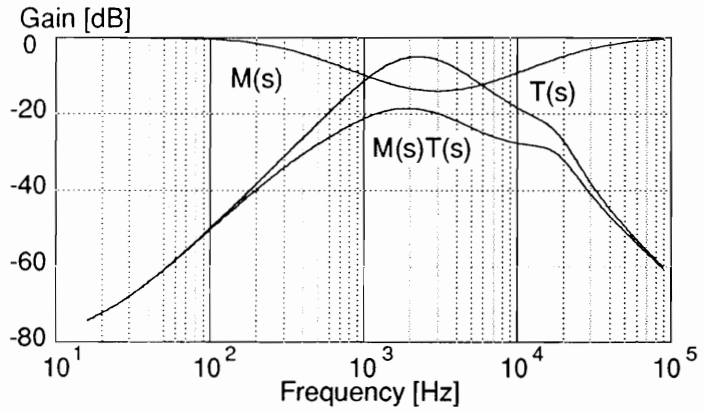

(b)

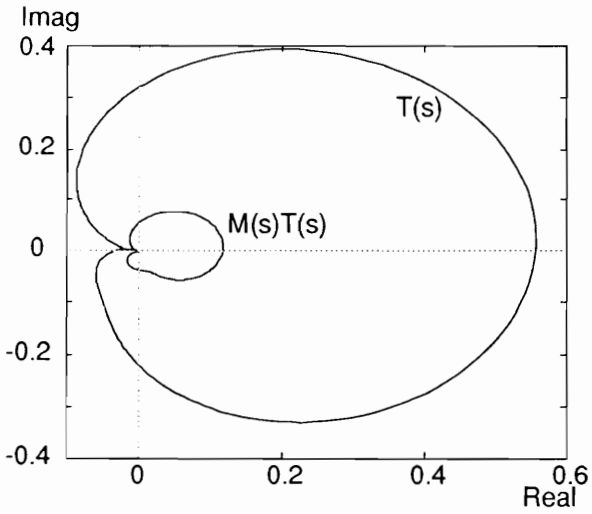

(c)

Fig. 4.9: Insertion of a Multiplier
(a) Interconnected System with Multiplier Insertion
(b) Bode Plots of M(s), T(s), and M(s)T(s)
(c) Nyquist Plots of T(s) and M(s)T(s)

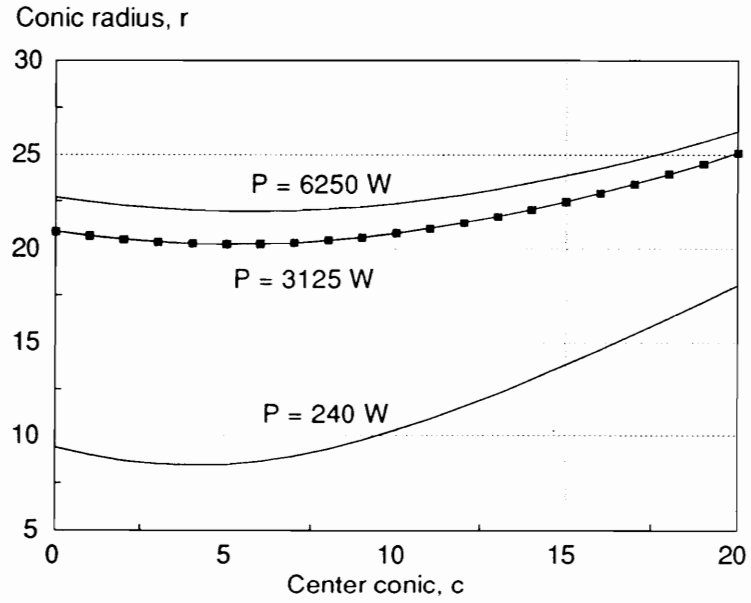

Fig. 4.10: New Sector Gain for the DDCU

The next complication is selection of the multiplier, M. According to the bode plot of the loop gain, T, as illustrated in Fig. 4.9(b), an appropriate multiplier must be

$$M(s)=\frac{(1+\frac{s}{w_{z1}})(1+\frac{s}{w_{z2}})}{(1+\frac{s}{w_{p1}})(1+\frac{s}{w_{p2}})}, \tag{4.3}$$

where $w_{p1} < w_{z1} < w_{z2} < w_{p2}$, as depicted in Fig. 4.9(b). Such a multiplier will result in a new loop gain, MT, with $|M(s)T(s)| < |T(s)|$. Illustration of the new loop gain, MT, in Fig. 4.9(b) suggests that w_{p1} should be chosen as small as possible and w_{p2} should be chosen as large as possible in order to shrink T as much as possible. However, recall that insertion of M will result in a larger sector gain, $M^{-1}N_z$, (Fig. 4.9(a)) because of the reciprocal properties of M^{-1} as compared to M. Furthermore, as stated in the stability criterion, a larger sector gain will result in a larger forbidden region in the Nyquist plot that MT must avoid. Thus, insertion of M will result in shrinking the loop gain, T, but at the same time, enlarging the forbidden region. Currently, there is no guideline for selecting an optimum multiplier M for a given system. However, for the DDCU case, it is observed that setting $w_{z1} = w_{z2}$ near the peak of $T(s)$, and w_{p1} and w_{p2} about one decade lower and higher than the peak of $T(s)$, respectively, can yield a satisfactory (near optimum) stability result– it is less conservative than without applying M when performing the stability test.

The amount of increase of the sector gain in $M^{-1}N_z$ depends on systems, and there is no analytical technique available to approximate the sector gain, since N_z is a nonlinear system with memory. However, determination of the sector gain of $M^{-1}N_z$ can be performed numerically based on Eq. 4.2 where the input to the block $M^{-1}N_z$ is $y_a = ML_zu$ (L_z is the linear part of the DDCU) and the output of $M^{-1}N_z$ is the measured output response of the DDCU, y_e. Therefore, approximation of the sector gain of $M^{-1}N_z$ consists of three steps

1) Given the measured input perturbation signal, u, and the ARMA model of L_z, compute

the output, $y_b = L_z u$.

2) Given M, compute $y_a = M y_b$.

3) Given y_a and the measure output response of the system, y_e, compute the conic sector.

Figure 4.10 illustrates a new r-c relationship for the DDCU after the multiplier M is inserted. For the full load and the half load case, M was set at

$$M(s) = \frac{(1+\frac{s}{18800})(1+\frac{s}{18800})}{(1+\frac{s}{1880})(1+\frac{s}{188000})}, \tag{4.4}$$

and

$$M(s) = \frac{(1+\frac{s}{10000})(1+\frac{s}{10000})}{(1+\frac{s}{1000})(1+\frac{s}{10^5})} \tag{4.5}$$

for the DCM loading condition. Observe that the overall sector gain is increased by a factor of 2.5, while the size of MT (Fig. 4.9(c)) is decreased by a factor of 4. Intuitively, this suggests that one should obtain a less conservative stability result.

4.1.3 Stability Analysis of the Interconnected DDCU and Load Subsystem

The block structures of both the DDCU and the load subsystem are identified. The next step is application of the stability criterion developed in Chapter 2 to the stability analysis of the interconnected DDCU and load subsystem. Recall that the key identification results are the DDCU output impedance and the load subsystem input admittance, as illustrated in Fig. 4.3 and Fig. 4.4, respectively, and the r-c plots in Fig. 4.8(a) (load subsystem's sector gain) and in Fig. 4.10 (DDCU's sector gain). Let $T(s)$ represent the small-signal loop gain of the interconnected system, $\{r_z, c_z\}$ denote the conic sector of the DDCU, and $\{r_y, c_y\}$ denote the conic sector of the load

subsystem; then, from Chapter 2, the interconnection system is stable in the large-signal sense if the following three conditions are satisfied:

$$\delta_z \equiv 1 - \left| \frac{T(s)c_y}{1 + c_z T(s) c_y} \right| r_z > 0, \tag{4.6}$$

$$\delta_y \equiv 1 - \left| \frac{T(s)c_z}{1 + c_y T(s) c_z} \right| r_y > 0, \tag{4.7}$$

$$G(f) \equiv \left| \frac{T(s)}{[1 + c_z c_y T(s)]^2} \right| < \frac{\delta_z \delta_y}{r_y r_z}, \tag{4.8}$$

where δ_z and δ_y are the margins of boundedness and are to be determined from Eqs. 4.6 and 4.7, respectively. Recall also that Eqs. 4.6 and 4.7 have a graphical interpretation as described in Chapter 2 (Circle criterion), from which δ_z and δ_y can be determined easily. Since a sector gain defines the shape of the forbidden region in the Nyquist plot, and since each subsystem has different sector gains depending on where the center conic, c, is set, it is a matter of selecting c_z and c_y appropriately so that the Nyquist plots of $T(s)c_y$ and $T(s)c_z$ can avoid, if possible, the forbidden regions. Also, some margins of boundedness from Eqs. 4.6 and 4.7 must be set aside so that Eq. 4.8 is satisfied.

The least conservative results are obtained when c_y = 1, and the remaining parameters are selected according to the following table:

Table 4.2: Key Parameters for the Stability Analysis

	6250 W	3125 W	240W
r_y	0.04	0.035	0.0017
c_z	16	16	11
r_z	23.8	22.5	10.9
δ_z	0.035	0.035	0.003
δ_y	0.975	0.975	0.9982
R_{da}	0.07Ω	0.02Ω	0.03Ω
R_{db}	0.16Ω	0.16Ω	0.09Ω

where R_{da} denotes the damping resistor values for the interconnected system to be on the borderline of instability, and R_{db} denotes the damping resistor values for the interconnected system to meet the stability test. Knowing $\{r_z,c_z\}$, $\{r_y,c_y\}$, and the small-signal loop gain $T(s)$ makes it possible to proceed to the stability analysis. The graphical results of Eqs. 4.6, 4.7, and 4.8 for the load power of 6.25 KW case are illustrated in Figs. 4.11(a), (b), and (c), respectively. Figures 4.12 and 4.13 illustrate the stability conditions for the load powers of 3.25 KW and 240 W, respectively. The transfer functions T_a(s) and $G_a(s)$ result from selecting the damping resistor R_{da}, whereas $T_b(s)$ and $G_b(s)$ result from selecting R_{db}. Notice that selecting R_{da} fails to meet the stability test. Only when the values of the damping resitor is increased to R_{db} that $T_b(s)$ and $G_b(s)$ avoid the forbidden regions and satisfy the stability conditions. Furthermore, these sufficient conditions do not seem to be far from the necessary conditions. Figures 4.11(d), 4.12(d), and 4.13(d) depict the impedance comparison between the DDCU and the load subsystem for the three loading conditions, where $Z_a(s) = 1/Y_a(s)$ denotes the load impedance curve for which the system is actually on the verge of instability, and $Z_b(s) = 1/Y_b(s)$ denotes the load impedance required by the stability test to meet the large-signal stability conditions. The conservativeness of the stability test results in a more

damped resonant frequency of the load input filter. However, these requirements set by the stability test are not too difficult to meet.

To further investigate the conservativeness of the stability test, two single-stage input filters are selected as shown in Figs. 4.14(a), and 4.15(a). The filter resonant frequencies are set at 200 Hz and 10 KHz. System identification is performed on both load subsystems, and the stability criterion is applied with inclusion of the multipliers as shown in Figs. 4.14(b), and 4.15(b). For the interconnected system to be stable, the requirements set by the stability test for the load impedance are illustrated in Figs. 4.14(c), and 4.15(c). Observe that the system can tolerate very high damping factor, Q, for both filters, even higher than the one from the load subsystem analyzed previously. These results means simply that the resonant frequencies of both input filters, 200 Hz and 10 KHz, do not coincide with the exciting frequency of the nonlinearity in the DDCU, which is approximately 1.6 KHz; therefore, interaction between the source and the load is not as pronounced as in the case where the input filter resonant frequency is 2 KHz (first case).

Thus, the outcome of this investigation suggests that even though the stability criterion developed in Chapter 2 yields only a sufficient condition regarding the stability property of the interconnected system, it is not conservative in terms of design criteria and realizability of the load subsystems.

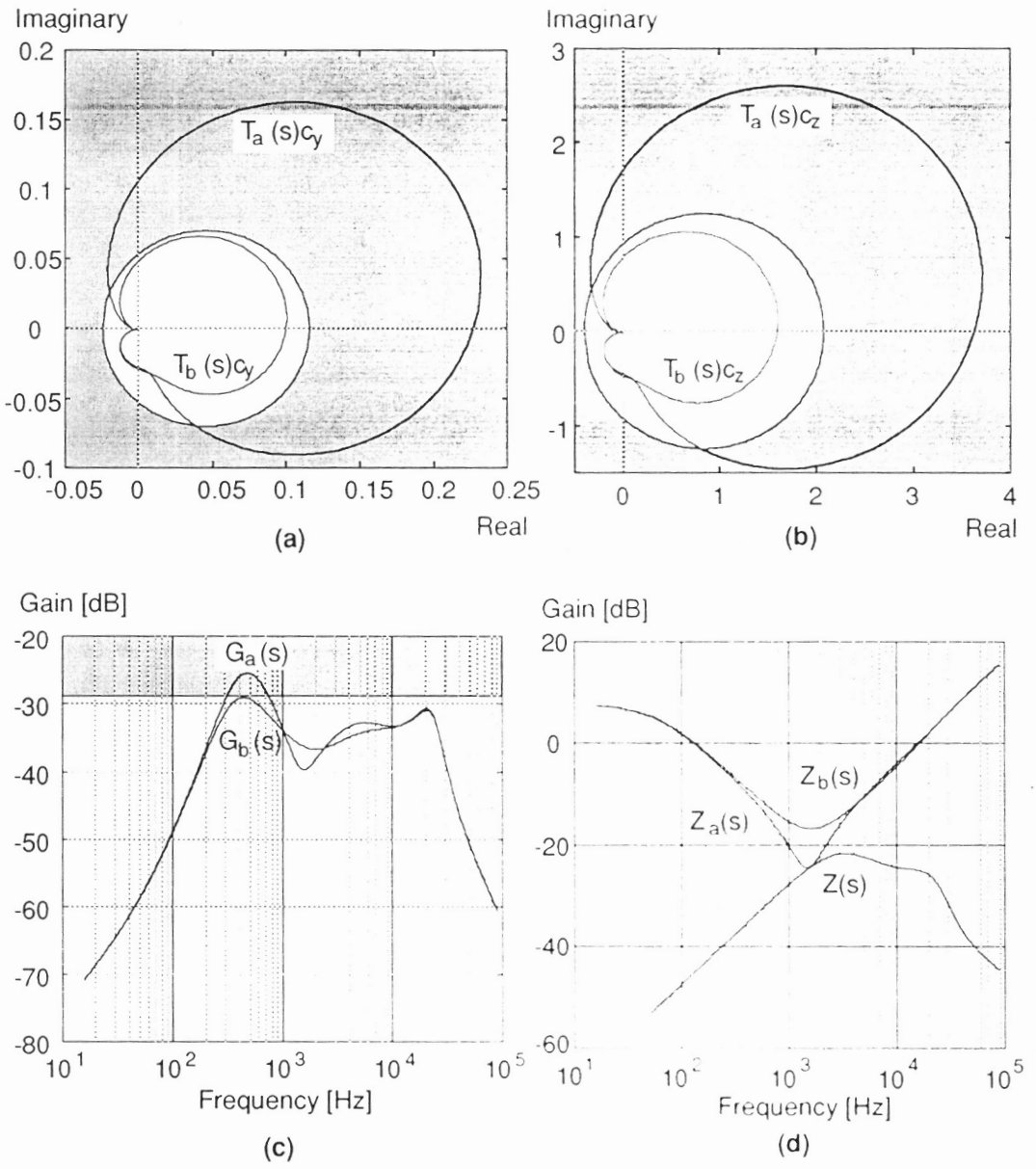

Fig. 4.11: Stability Results for Load Power = 6250 W

(a) First Stability Condition
(b) Second Stability Condition
(c) Third Stability Condition
(d) Impedance Comparison

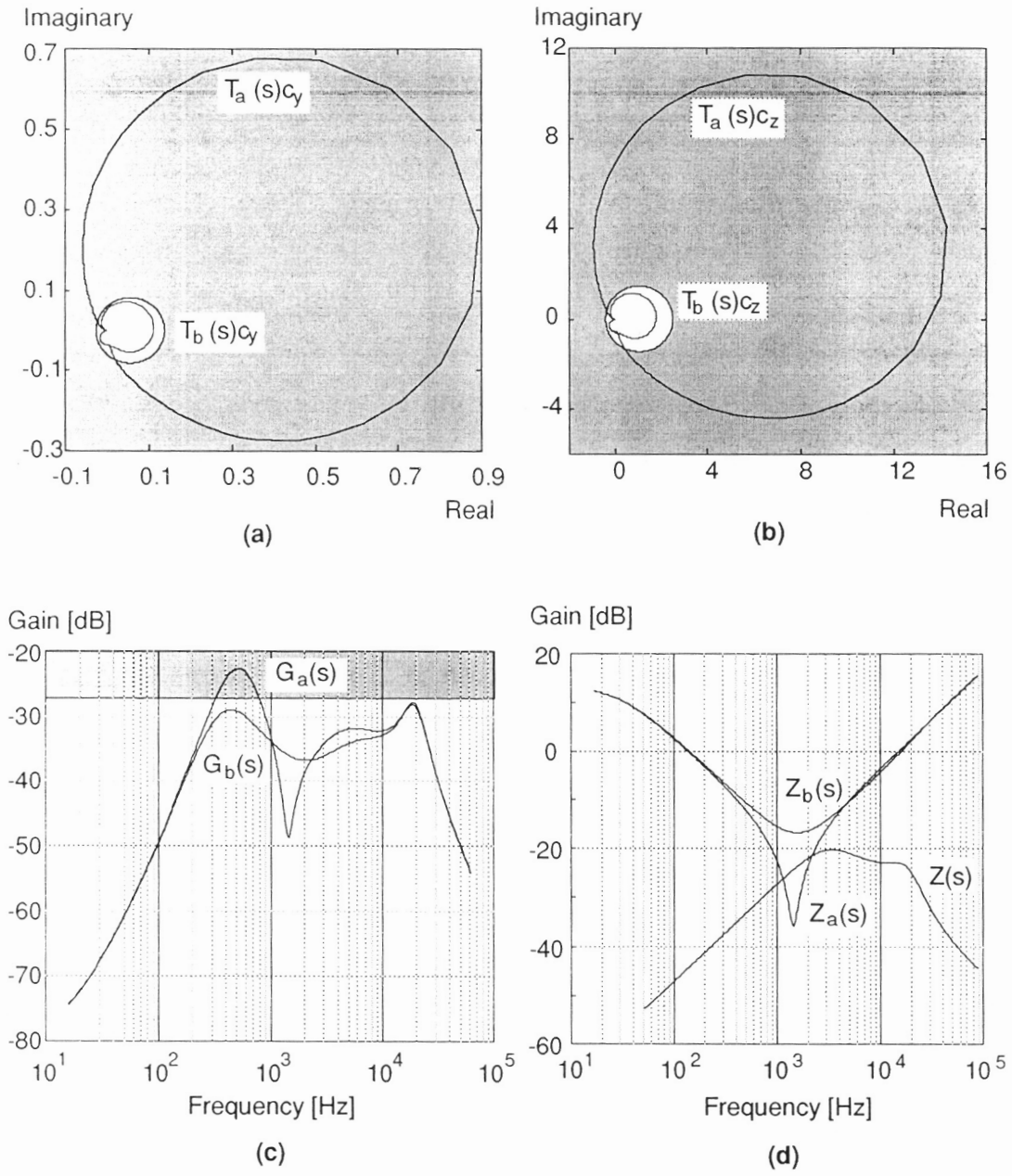

Fig. 4.12: Stability Results for Load Power = 3125 W

(a) First Stability Condition
(b) Second Stability Condition
(c) Third Stability Condition
(d) Impedance Comparison

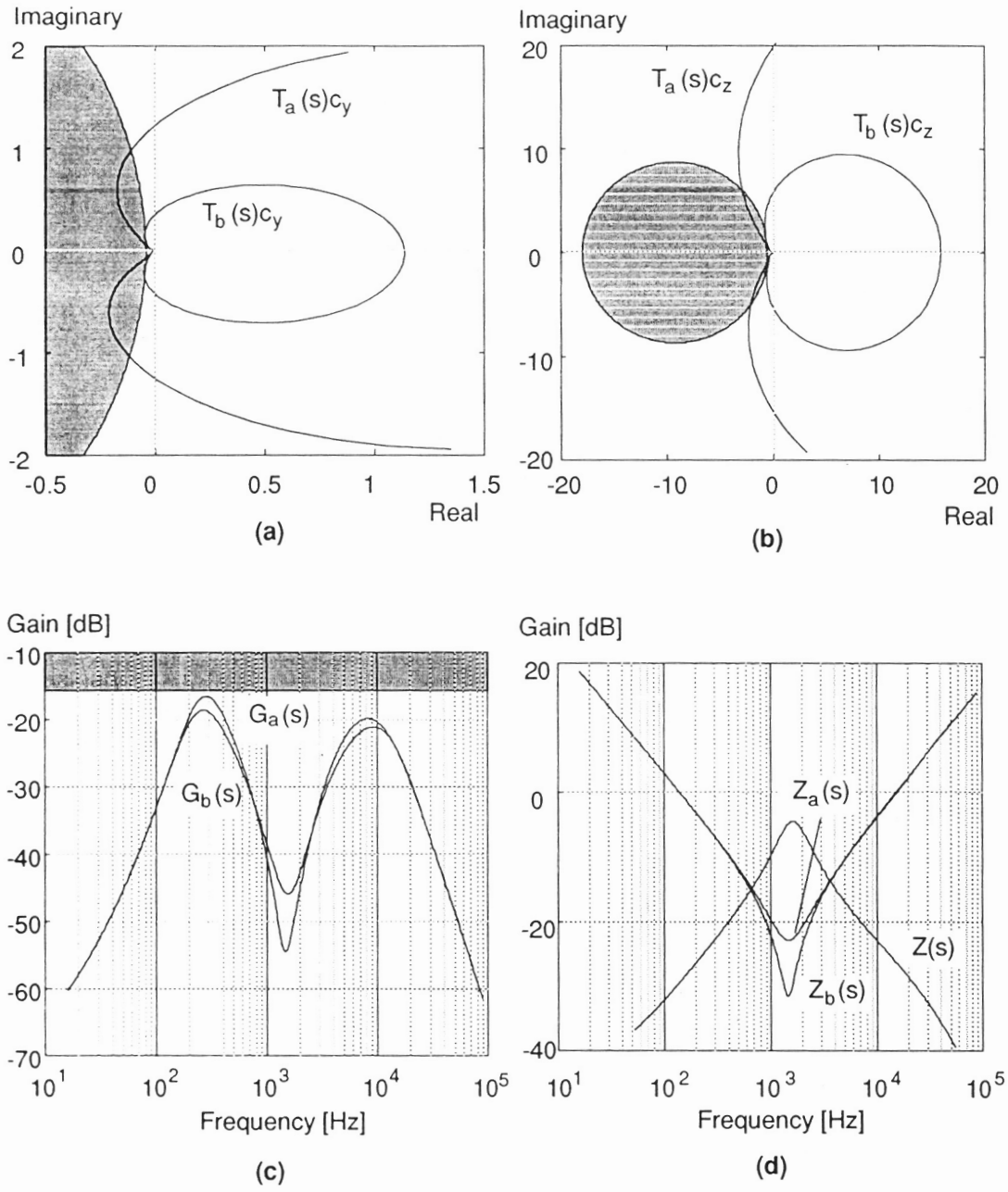

Fig. 4.13: Stability Results for Load Power = 240 W
(a) First Stability Condition
(b) Second Stability Condition
(c) Third Stability Condition
(d) Impedance Comparison

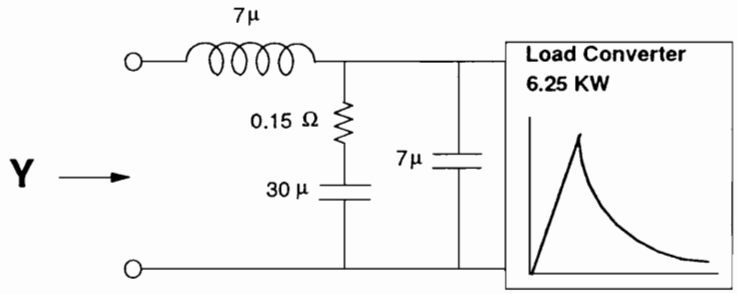

(a)

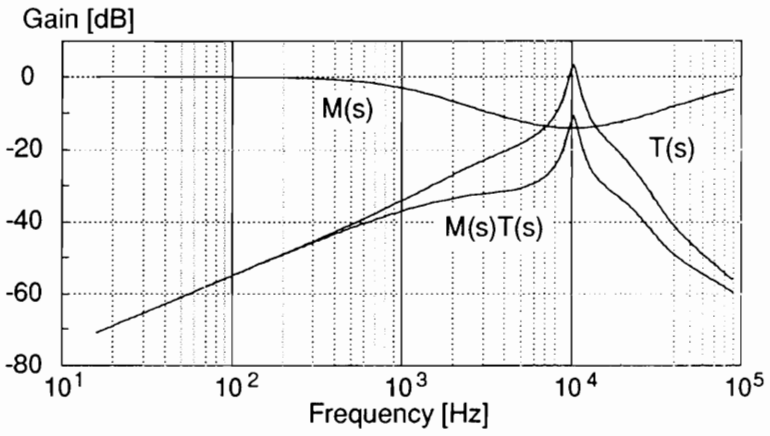

(b)

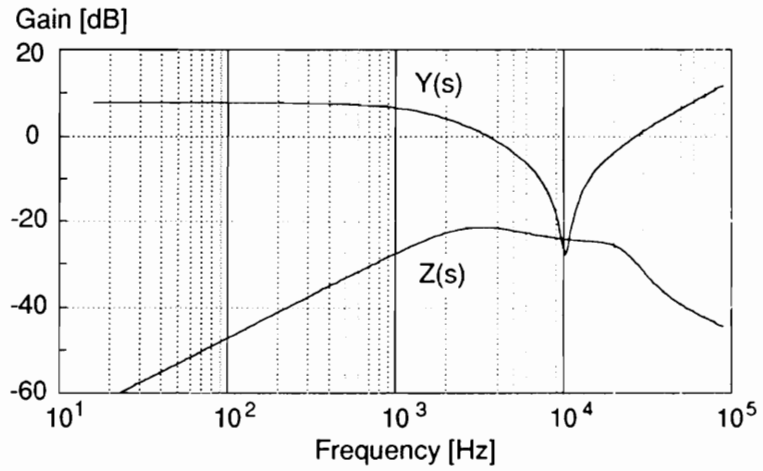

(c)

Fig. 4.14: Case 1 - New Load Subsystem Characteristics and Stability Results
(a) Input Filter Characteristics
(b) Selection of Multiplier
(c) Impedance Comparison

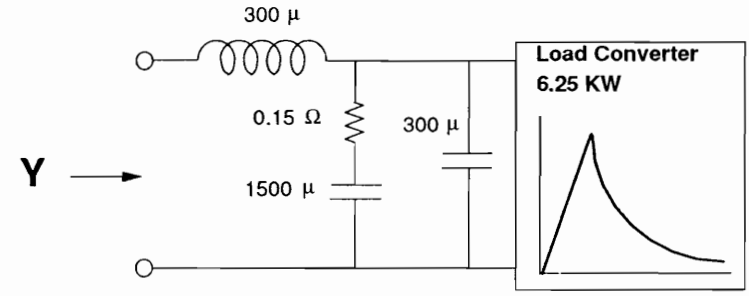

(a)

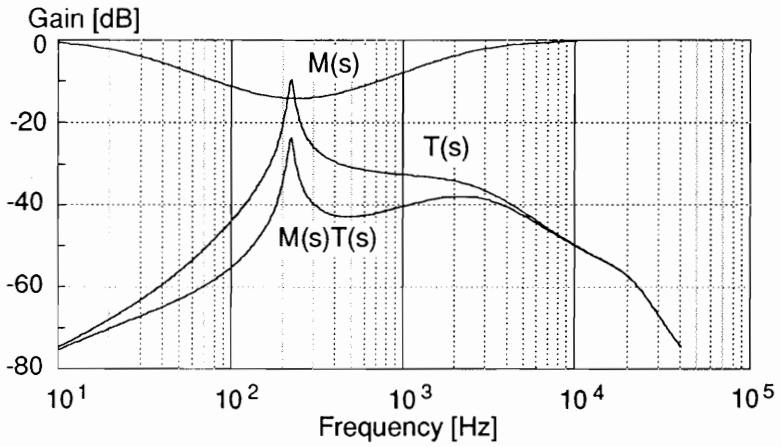

(b)

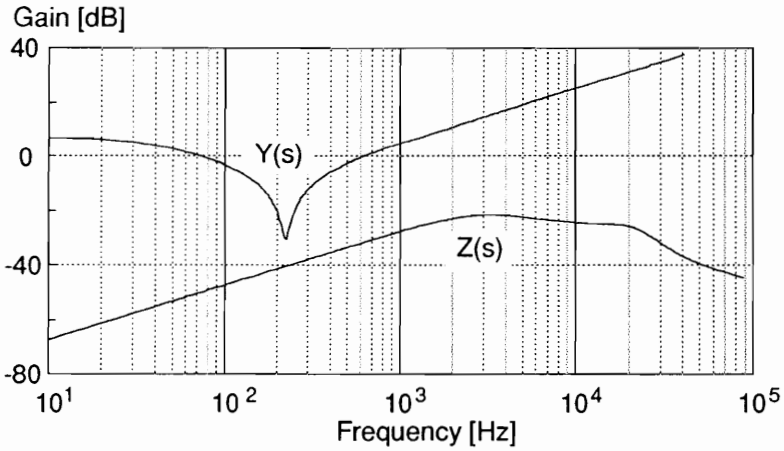

(c)

Fig. 4.15: Case 2 - New Load Subsystem Characteristics and Stability Results
(a) Input Filter Characteristics
(b) Selection of Multiplier
(c) Impedance Comparison

4.2 Graphical Design Insights of the Small-Signal Loop Gain Leading to Large-Signal Stability

The previous section illustrates that development of this new methodology provides a significant understanding in the know-how of designing the small-signal loop gain to achieve large-signal stability for the interconnected system. Indeed, one can select $c_z = c_y = 1$, and in order to meet the stability conditions in Eqs. 4.6 and 4.7, the Nyquist plot of the small-signal loop gain $T(s)$ must avoid the forbidden regions defined by the sector gains of the nonlinear parts, N_z and N_y. It is known that a small sector gain translates into a small circle that contains the $(-1,j0)$ point in the Nyquist plane, as illustrated in Fig. 4.16(a). However, when the sector gain becomes larger, the forbidden region expands and occupies the entire left half plane, when $r = c = 1$. Furthermore, when the system is very nonlinear, which results in a large sector gain ($r > c$), the forbidden region wraps around the right half plane.

Consequently, assume that during the preliminary design stage, when only the information regarding the linear dynamics of the source and the load about the steady-state operating point is available, it is possible to shape the small-signal loop gain $T = L_z L_y$ in such a way as to alleviate the large-signal instability of the interconnected system. According to Fig. 4.16(a), in order to avoid as much as possible the forbidden region defined by an unknown sector gain, the small-signal loop gain T must stay as near the origin of the Nyquist plane as possible. Since the loop gain T is the product of the source impedance and the load admittance, a loop gain having small magnitudes at all frequencies requires that there is no overlap between the source impedance and the load admittance; in other words, there must be no interaction between the source and the load (Fig. 4.16(b)). On the other hand, if the condition requiring no overlap between the source impedance and the load impedance is too stringent for the design process to meet, then the overlap (Fig. 4.16(c)), should it exist, must result in the loop gain T expanding outward in the right-half Nyquist plane. The reason is that under less severe nonlinearities in both source and load, which result in

smaller sector gains and smaller forbidden regions, the loop gain T expading outward in the right-half plane can avoid the forbidden regions more adequately. This implies that the phase of the loop gain T must not exceed the [-90°,90°] range within the frequency range where overlapping occurs.

4.3 Summary

Stability of an interconnected system, which consists of a DDCU and arbitrary load converters, is investigated based on the proposed methodology. Practical guidelines and considerations in the application of the method are illustrated thoroughly.

The results indicate that the small-signal stability analysis does not guarantee large-signal stability and that the new methodology is quite effective for the large-signal stability analysis. Even though the stability test is only a set of sufficient conditions, it does not yield conservative results in terms of subsystem design and realizability.

Also, the results provide a valuable insight into shaping the small-signal loop gain to achieve large-signal stability, a fact which can only be proved through the development of this new methodology.

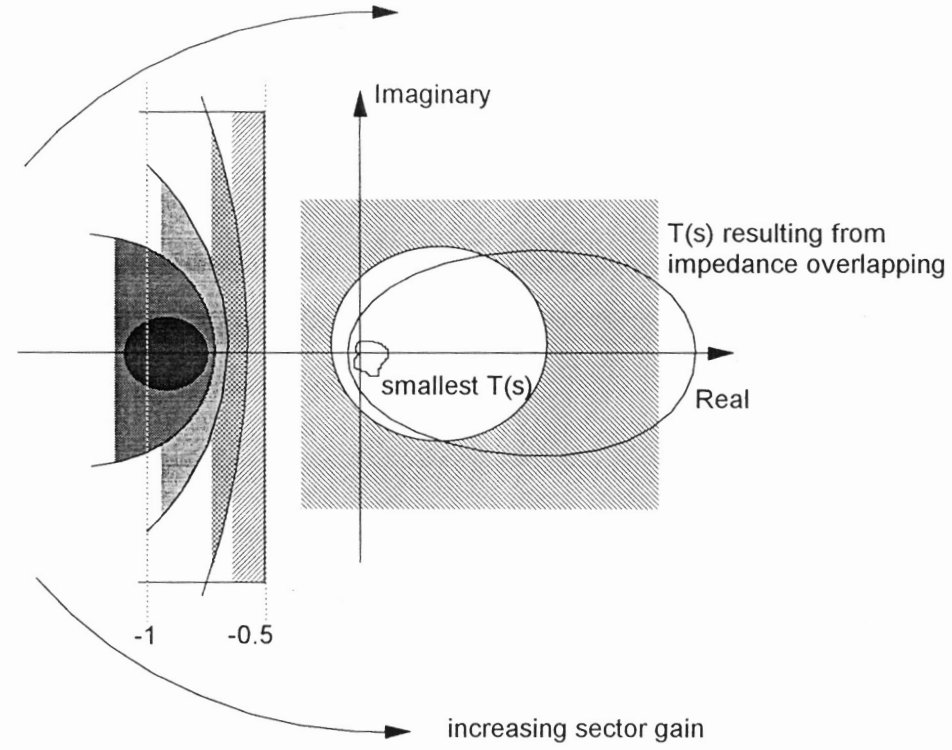

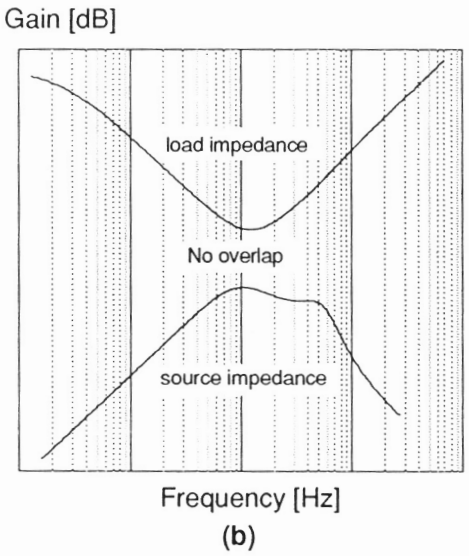

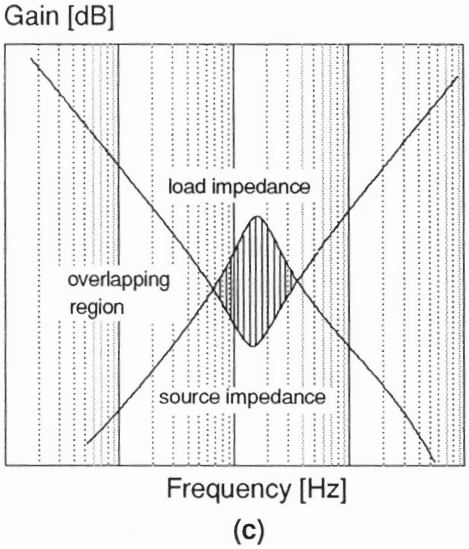

Fig 4.16: Graphical Interpretation of Designing the Small-Signal Loop-Gain Leading to Large-Signal Stability

(a) Forbidden Regions and Shapes of the Small-Signal Loop Gain
(b) Condition for Small Loop Gain
(c) Impedance Overlapping

Chapter 5

Conclusions

Presently, the common method in designing and analyzing stability of power electronics systems is based on the small-signal linear characteristics of the system around the steady-state operating point. However, such a method can only predict small-signal stability and fail in predicting the system large-signal stability, given that power electronics systems are nonlinear. Consequently, the principal objective of this dissertation is to develop a new methodology for the large-signal stability analysis of large-scale power electronics systems.

The input-output stability theory and system identification theory, which are relatively new to power electronics applications, are adopted to develop a new methodology for the stability analysis of power electronics systems. This methodology proposes to decouple the system into a source that comprises all the upstream modules and a load that comprises all the downstream modules at any interface point. Then, stability of the system can be analyzed based on investigating the feedback loop formed by interconnection of the source and the load.

Since both source and load are nonlinear, a characterization of both subsystems– a particular structure that can be used for the stability analysis– is defined. It consists of factorizing each subsystem into a series combination of a linear part, which represents the small-signal dynamic around the steady-state operating point, and a nonlinear part, which represents the large-signal

dynamic. Identification of the linear part results in an equivalent ARMA model, whereas identification of the nonlinear part consists of approximating the nonlinear part sector gain.

Knowledge of the source and the load as above permits to investigate the stability of the interconnected system. Since the feedback loop formed by the interconnection contains two nonlinear blocks, the Nyquist criterion is not applicable; therefore, a new stability criterion suitable for this particular interconnection structure is developed based on the input-output stability theory.

The input-output stability theory is a powerful technique suitable for the large-signal stability analysis of power electronics systems. To illustrate the power of this theory in dealing with nonlinear systems, PWM converters are selected, and effects of inherent nonlinearity in PWM converters (bilinear structure) and of saturation such as duty cycle saturation and opamp saturation on the stability of PWM converters are investigated. The theory predicts that in order to avoid large-signal instability due to the saturation nonlinearities, no loop gain transfer function can show conditional stability characteristic. Also, the theory indicates that the closed-loop boost converter, under conventional feedback linear closed-loop design, is not globally stable.

Finally, to illustrate the effectiveness of the proposed methodology, a subsystem of the Space Station system, which consists of a DDCU and an arbitrary load converter, is investigated. Practical guidelines and considerations in the application of the method are illustrated thoroughly. Furthermore, this new methodology has shown how to overcome the deficiency of the small-signal analysis in analyzing stability of nonlinear interconnected systems. The outcome indicates that the new methodology is an effective tool in the large-signal nonlinear stability analysis and design of power electronics systems. It also provides a valuable insight into ways of performing small-signal design of the loop gain leading to large-signal stability for the interconnected system, which can only be proved through the development of this new methodology.

References

[1] M. Araki, "Stability of Large-Scale Nonlinear Systems- Quadratic-Order Theory of Composite-System Method Using M-Matrices," IEEE Trans. Auto. Control, Vol. AC-23, No. 2, pp. 129-141, 1978.

[2] J. A. Ball, J. W. Helton, "Interconnection of Nonlinear Causal Systems, " IEEE Trans. Auto. Control, Vol. 34, No. 11, pp. 1132-1140, 1989.

[3] J. S. Bendat, "Nonlinear System Analysis and Identification from Random Data, " John Wiley & Sons, New York, 1990.

[4] J. S. Bendat, A. Piersol, "Engineering Applications of Correlation and Spectral Analysis," John Wiley & Sons, New York, 1980.

[5] A. R. Bergen, R. P. Iwens, and A. J. Rault, "On Input-Output Stability of Nonlinear Feedback Systems, " IEEE Trans. Auto. Control, pp. 742-744, 1966a.

[6] A. R. Bergen, R. P. Iwens, "Zero Steady-State Error Operation of Feedback Systems with a Time-Varying Nonlinear Element, " IEEE Trans. Auto. Control, pp. 746-748, 1966b.

[7] S. A. Billings, K. M. Tsang, "Spectral Analysis for Non-linear Systems, Part I: Parametric Non-linear Spectral Analysis," Mech. Syst. & Sig. Proc., pp. 319-339, 1989a.

[8] S. A. Billings, K. M. Tsang, "Spectral Analysis for Non-linear Systems, Part II: Interpretation of Non-linear Frequency Response Function," Mech. Syst. & Sig. Proc., pp. 341-359, 1989b.

[9] S. A. Billings, K. M. Tsang, "Spectral Analysis of Block Structured Non-linear Systems, " Mech. Syst. & Sig. Proc., pp. 117-130, 1990.

[10] R. W. Brockett, H. B. Lee, "Frequency-Domain Instability Criteria for Time-Varying and Nonlinear Systems, " Proc. IEEE, Vol. 55, No. 5, pp. 604-618, 1967.

[11] R. W. Brockett, J. L. Willems, "Frequency Domain Stability Criteria - Part I, " IEEE Trans. Auto. Control, pp. 255-261, 1965a.

[12] R. W. Brockett, J. L. Willems, "Frequency Domain Stability Criteria - Part II, " IEEE Trans. Auto. Control, pp. 407-413, 1965b.

[13] B. S. Chen, S. S. Wang, "The Stability of Feedback Control with Nonlinear Saturating Actuator: Time Domain Approach, " IEEE Trans. Auto. Control, Vol. 33, No. 5, pp. 483-387, 1988.

[14] C. T. Chen, "Linear System Theory and Design, " Holt, Rinehart and Winston, New York, 1984.

[15] C. T. Chen, "L_n Stability of Linear Time-Varying Feedback Systems, " SIAM J. Control, Vol. 6, No. 2, 1968.

[16] F. Chen, X. S. Cai, "Design of Feedback Control Laws for Switching Regulators Based on the Bilinear Large Signal Model, " IEEE Trans. Power Electronics, Vol. 5, No. 2, pp. 236-240, 1990.

[17] L. K. Chen, X. Yang, R. R. Mohler, "Stability Analysis of Bilinear Systems, " IEEE Trans. Auto. Control, Vol. 36, No. 11, pp. 1310-1315, 1991.

[18] B. H. Cho and J. R. Lee, "Design, Analysis and Simulation of the Main Bus Dynamics of Spacecraft Power Systems, " IECEC 1988.

[19] B. H. Cho and F. C. Lee, "Modeling and Analysis of Spacecraft Power Systems, " IEEE Trans. Power Electronics, 1988.

[20] Y. S. Cho, K. S. Narendra, "Stability of Nonlinear Time-Varying Feedback Systems, " Automatica, Vol. 4, pp. 309-322, 1968a.

[21] Y. S. Cho, K. S, Narendra, "On Off-Axis Circle Criterion for the Stability of Feedback Systems with a Monotonic Nonlinearity, " IEEE. Trans. Auto. Control, pp. 413-416, 1968b.

[22] P. A. Cook, "On the Behaviour of Dynamical Systems Subject to Bounded Disturbances, " Int. J. Systems Sci., Vol. 11, No. 2, pp. 159-170, 1980.

[23] P. A. Cook, "On the Stability of Interconnected Systems, " Int. Journ. Control, Vol. 20, No. 3, pp. 407-415, 1974.

[24] W. A. Coppel, "A Survey of Quadratic Systems, " Journal of Diff. Equ., Vol. 2, pp. 293-304, 1966.

[25] L. W. Couch II, "Digital and Analog Communication Systems," Macmillan, Inc., New York, 1993.

[26] C. A. Desoer, K. K. Wong, "Small-Signal Behavior of Nonlinear Lumped Networks, " Proc. IEEE, Vol. 56, No. 1, pp. 14-22, 1968a.

[27] C. A. Desoer, "An Extension to the Circle Criterion, " IEEE Trans. Auto. Control, pp. 587-588, 1968b.

[28] C. A. Desoer, M. Vidyasagar, "Feedback Systems: Input-Output Properties, Academic Press, New York, 1975.

[29] C. A. Desoer, "Stability of Linear Time-Invariant Systems, " IEEE Trans. Auto. Control, Vol. 15, No. 3, pp. 245-250, 1968.

[30] R. J. Dickson, L. M. Perko, "Bounded Quadratic Systems in the Plan, " Journal of Diff. Equ., Vol. 7, pp. 251-273, 1970.

[31] R. Fante, "Signal Analysis and Estimation," John Wiley & Sons, New York, 1988.

[32] K. Godfrey, "Perturbation Signals for System Identification, " Prentice Hall, New York, 1993.

[33] D. J. Hill, "On the Stability of Nonlinear Networks, " IEEE Trans. on Circuits and Systems, Vol. CAS-25, No. 11, pp. 941-943, 1978.

[34] D. J. Hill, P. J. Moylan, "Connections Between Finite Gain and Asymptotic Stability, " IEEE Trans. Auto. Control, Vol. AC-25, No. 5, pp. 931-935, 1980.

[35] J. M. Holtzman, "Nonlinear System Theory: A Functional Analysis Approach, " Prentice-Hall, Englewood Cliffs, N.J., 1970.

[36] J. M. Holtzman, "A Local Bounded-Input Bounded-Output Condition for Nonlinear Feedback Systems, " IEEE Trans. Auto. Control, pp. 585-586, 1968.

[37] Phuong Huynh and Bo H. Cho, "Small-Signal Modeling of Switching Regulators Using Pspice, " Project Report, Blacksburg, Virginia.

[38] R. Iwens, "Bounds on the Responses of Nonlinear Control Systems, " Journ. Franklin Inst., Vol. 285, pp. 261-274, 1968.

[39] D. E. Koditschek, K. Narendra, "The Stability of Second-Order Quadratic Differential Equations, " IEEE Trans. Auto. Control, Vol. AC-27, No. 4, pp. 783-798, 1982.

[40] R. L. Kosut, "Design of Linear Systems with Saturating Linear Control and Bounded States, " IEEE Trans. Auto. Control, Vol AC-28, No. 1, pp. 121-124, 1983.

[41] B. C. Kuo, "Automatic Control Systems, " Prentice-Hall, Englewood Cliffs, N. J., 1987.

[42] E. L. Lasley, "The Qualitative Analysis of Composite System, " Ph. D. Dissertation, Dept. of electrical Engineering, Iowa State Univ., Ames, Iowa, 1975.

[43] L. P. Lecoq, A. M. Hopkin, "A Functional Analysis Approach to L_∞ Stability and Its Applications to Systems with Hysteresis, " IEEE Trans. Auto. Control, Vol. 17, No. 3, pp. 328-338, 1972.

[44] Lennart Ljung, "System Identification: Theory For the User," Prentice-Hall, Englewood Cliffs, New Jersey, 1987.

[45] L. R. Lewis, B. H. Cho, F. C. Lee, "Modeling and Analysis of Distributed Power Systems, " IEEE PESC, 1989.

[46] J. Liu, S. Schulz, B. H. Cho, and F. C. Lee, "Design Considerations for Distributed Power Systems, " VPEC Seminar, Blacksburg, Virginia, 1989.

[47] K. Liu, R. L. Lewis, "An Improved Result on the Stability Analysis of Nonlinear Systems, " IEEE Trans. Auto. Control, Vol. 37, No. 9, pp. 1425-1430, 1992.

[48] R. Longchamp, "Stable Feedback Control of Bilinear Systems, " IEEE Trans. Auto. Control, Vol. AC-25, No. 2, pp. 302-306, 1980.

[49] P. Z. Marmarelis, V. Z. Marmarelis, "Analysis of Physiological Systems, " Plenum Press, New York, 1978.

[50] A. N. Michel, "On the Status of Stability of Interconnected Systems, " IEEE Trans. Auto. Control, Vol. AC-28, No. 6, pp. 639-653, 1983.

[51] A. N. Michel, R. K. Miller, "Qualitative Analysis of Large-Scale Dynamical Systems, " Academia Press, New York, 1977.

[52] J. B. Moore, "A Circle Criterion Generalization for Relative Stability, " IEEE Trans. Auto. Control, pp. 127-128, 1968.

[53] R. D. Middlebrook, "Input Filter Considerations in Design and Application of Switching Regulators, " IEEE Industry Applications Society Annual Meeting, 1976 Record, pp. 366-382.

[54] M. S. Mousa, R. K. Miller, and A. N. Michel, " Stability Analysis of Hybrid Composite Dynamical Systems: Descriptions Involving Operators and Differential Equations, " IEEE Trans. Auto. Control, Vol. AC-31, No. 3, pp. 216-225, 1986.

[55] P. Moylan, D. Hill, "Stability Criteria for Large-Scale Systems," IEEE Trans. Auto Control, Vol. AC-23, No. 2, pp. 143-149, 1978.

[56] N. E. Nahi, S. Partovi, "On the Absolute Stability of a Dynamic System with a Nonlinear Element Function of Two State Variables, " IEEE Trans. Auto. Control, pp. 573-575, 1968.

[57] J. P. Norton, "An Introduction to Identification, " Academic Press, New York, 1986.

[58] D. W. Porter, "Stability of Multiple-Loop Nonlinear Time-Varying Systems, " Ph.D. Dissertation, Iowa State Univ., Ames, Iowa, 1972.

[59] D. W. Porter, A. N. Michel, "Input-Output Stability of Time-Varying Nonlinear Multiloop Feedback Systems, " IEEE Trans. Auto. Control, pp. 422-427, 1974.

[60] Z. V. Rekasius, J. R. Rowland, "A Stability Criterion for Feedback Systems Containing a Single Time-Varying Nonlinear Element, " IEEE Trans. Auto. Control, pp. 352-354, 1965.

[61] Z. V. Rekasius, "A Stability Criterion for Feedback Systems with One Nonlinear Element, " IEEE Trans. Auto. Control, pp. 46-50, 1964.

[62] I. W. Sandberg, "On the L_2 Boundedness of Solutions of Nonlinear Functional Equations, " Bell Syst. Tech. Journal, pp. 1581-1598, July 1964.

[63] I. W. Sandberg, "Some Stability Results Related to Those of V. M. Popov, " Bell Syst. Tech. Journal, pp. 2133-2148, November 1965a.

[64] I. W. Sandberg, "A Condition for the L_∞ Stability of Feedback Systems Containing a Single Time-Varying Nonlinear Element, " Bell Syst. Tech. Journal, pp. 1815-1817, July 1965b.

[65] I. W. Sandberg, "An Observation Concerning the Applications of the Contraction-Mapping Fixed-Point Theorem, and a Result Concerning the Norm-Boundedness of Solutions of Nonlinear Functional Equations, " Bell Syst. Tech. Journal, pp. 1809-1812, October 1965c.

[66] I. W. Sandberg, "A Frequency-Domain Condition for the Stability of Feedback Systems Containing a Single Time-Varying Nonlinear Element, " Bell Syst. Tech. Journal, pp. 1601-1608, July 1965.

[67] N. Satyanarayana, M. A. L. Thathachar, M. D. Srinath, "Stability of a Class of Multiplicative Nonlinear Systems, " IEEE Trans. Auto. Control, pp. 647-649, 1970.

[68] M. Schetzen, "The Volterra and Wiener Theories of Nonlinear Systems", John Wiley & Sons, New York, 1980.

[69] S. Schulz, B. H. Cho, and F. C. Lee, "Design Considerations for a Distributed Power Systems, " PESC 1990.

[70] K. S. Shanmugan, A. M. Breipohl, "Random Signals: Detection, Estimation, and Data Analysis, " John Wiley & Sons, New York, 1988.

[71] S. J. Skar, R. K. Miller, A. N. Michel, "On Nonexistence of Limit Cycles in Interconnected Systems, " IEEE Trans. Auto. Control, Vol. AC-26, No. 3, pp. 669-676, 1981.

[72] J. J. Slotine, W. Li, "Applied Nonlinear Control, " Prentice-Hall, Englewood Cliffs, N.J., 1991.

[73] M. K. Sundareshan, M. Vidyasagar, "L_2-Stability of Large-Scale Dynamical Systems: Criteria Via Positive Operator Theory, " IEEE Trans. Auto. Control, pp. 396-399, 1977.

[74] H. Tamura, T. Yoshikawa, "Large-Scale Systems Control and Decision Making, " Marcel Dekker Inc., New York, 1990.

[75] M. Vidyasagar, "L_2-Stability of Interconnected System Using a Reformulation of the Passivity Theorem, " IEEE Trans. Auto. Control, Vol. CAS-24, No. 11, pp. 637-645, 1977.

[76] M. Vidyasagar, "Nonlinear Systems Analysis, " Prentice Hall, Englewood Cliffs, N.J., 1993.

[77] M. Vidyasagar, "New Passivity-Type Criteria for Large-Scale Interconnected Systems, " IEEE trans. Auto. Control, Vol. AC-24, No. 4, pp. 575-579, 1979.

[78] J. A. Walker, N. H. McClamroch, "Finite Regions of Attraction for Feedback Systems Containing a Single Time-Varying Nonlinearity, " IEEE Trans. Auto. Control, pp. 587-587, 1968.

[79] J. A. Walker, "Finite Regions of Attraction for the Problem of Lur'e, " Int. J. Control, Vol. 6, No. 4, pp. 331-336, 1967.

[80] D. Weiner, J. Spina, "Sinusoidal Analysis and Modeling of Weakly Nonlinear Circuits, " Van Nostrand Reinhold Company, New York, 1980.

[81] S. Weissenberger, "Application of Results from the Absolute Stability Problem to the computation of Finite Stability Domains, " IEEE Trans. Auto. Control, pp. 124-125, 1968.

[82] J. C. Willems, "Dissipative Dynamical Systems - Part I: General Theory, " Arch. Ration. Mech. Anal., Vol. 45, No. 5, pp. 321-351, 1972.

[83] J. C. Willems, "The generation of Lyapunov Functions for Input-Output Stable Systems, " J. SIAM Control, Vol. 9, pp. 105-134, 1971a.

[84] J. C. Willems, "The Analysis of Feedback Systems, " The M.I.T. Press, Cambridge, Massachusetts, 1971b.

[85] M. Y. Wu, C. A. Desoer, "L_p Stability ($1 \leq p \leq \infty$) of Nonlinear Time-Varying Feedback Systems, " SIAM J. Control, Vol. 7, No. 2, pp. 356-364, 1969.

[86] J. L. Wyatt, et al., "Energy Concepts in the State-Space Theory of Nonlinear n-Ports - Part I: Passivity, " IEEE Trans. on Circuits and Systems, Vol. CAS-28, No. 1, pp. 48-60, 1981.

[87] J. L. Wyatt, et al., "Energy Concepts in the State-Space Theory of Nonlinear n-Ports - Part I: Losslessness, " IEEE Trans. on Circuits and Systems, Vol. CAS-29, No. 7, pp. 417-430, 1982.

[88] G. Zames, P. L. Falb, "Stability Conditions for Systems with Monotone and Slope-Restricted Nonlinearities, " SIAM J. Control, Vol. 6, No. 1, pp. 89-108, 1968a.

[89] G. Zames, "Stability of Systems with Sector Nonlinearities: A Comparison of Various Inequalities, " IEEE Trans. Auto. Control, pp. 709-711, 1968b.

[90] G. Zames, P. L. Falb, "On the Stability of Systems with Monotone and Odd Monotone Nonlinearities, " IEEE Trans. Auto. Control, pp. 221-223, 1967.

[91] G. Zames, "Functional Analysis Applied to Nonlinear Feedback Systems, " IEEE Trans. Circuit Theory, Vol. C-T 10, pp. 392-404, 1963.

[92] G. Zames, "On the Input-Output Stability of Time-Varying Nonlinear Feedback Systems - Part I: Conditions Derived Using Concepts of Loop Gain, Conicity, and Positivity, " IEEE Trans. Auto. Control, Vol. AC-11, No. 2, pp. 228-238, 1966a.

[93] G. Zames, "On the Input-Output Stability of Time-Varying Nonlinear Feedback Systems - Part II: Conditions Involving Circles in the Frequency Plane and Sector Nonlinearities, " IEEE Trans. Auto. Control, Vol. AC-11, No. 3, pp. 465-475, 1966b.

[94] G. Zames, "Nonlinear Time Varying Feedback Systems - Conditions for L_∞ Boundedness Derived Using Conic Operators on Exponentially Weighted Space, " Proc. Allerton Conf., pp. 460-471, 1965.

Appendix A

Input-Output Stability Theory for Nonlinear Systems

The input-output stability theory, which has been pioneered by Sandberg and Zames in the early 60's, was first developed for a single-loop feedback system and quickly reached its maturity at the end of the 60's. In the 70's, the input-output stability theory geared toward multi-input and multi-output systems, and major developments of the theory have been contributed by Michel, Araki, Vidyasagar, and Moylan.

In this appendix, basic results of the input-output stability theory are presented. The objective of this appendix is not to overcome the readers with the level of abstractness and mathematical complexities of the theory, but to convey the basic results in a concise and understandable manner and to aim at the applicability of the theory in the stability analysis of power electronics systems. Most of the results are stated without proofs, except for a few important theorems for which proofs are necessary in order to provide insights and techniques that can be used to derive new stability criteria. A more detailed theory can be found in [Desoer, 1975], [Vidyasagar, 1993], [Michel, 1977], and [Holtzman, 1971].

Various basic concepts and definitions are introduced first, and the input-output stability theory is presented subsequently. Single-loop feedback systems are considered, and a general input-output stability criterion– the small-gain theorem– for single-loop feedback systems is

established. However, the small-gain theorem provides a conservative stability condition; therefore, less conservative stability criteria are developed subsequently based on the loop transformation theorem and the multiplier technique. Lastly, the input-output stability theory for a single-loop system is extended to multiple-loop systems by applying the properties of M-matrices.

A.1 Signals and Systems

In the theory of input-output stability, the terminologies often encountered are ***signals*** and ***systems***. A signal, $x(t)$, is a real-valued function of the time variable t; that is for any fixed value of the time variable t, the value of the signal at time t is a real number. On the other hand, a system can be termed as a relation that maps an input signal to an output signal.

A.1.1 Norms

The norm of a signal x (the argument (t) is dropped to simplify the notation), which is written as $\|x\|$, describes in a sense the size of the signal x. If α is a real number, a norm must have the following four properties:

(i) $\|x\| \le 0$, (A.1a)

(ii) $\|x\| = 0 \iff x(t) = 0$, (A.1b)

(iii) $\|\alpha x\| = |\alpha| \|x\|$, (A.1c)

(iv) $\|x + y\| \le \|x\| + \|y\|$ (triangular inequality). (A.1d)

Several different norms are defined as follows:

1-norm: $\|x\|_1 \equiv \int_0^\infty |x(t)| dt$, (A.2)

2-norm: $\|x\|_2 \equiv \sqrt{\int_0^\infty x(t)^2 dt}$, (A.3)

∞-norm: $\|x\|_\infty \equiv \sup_t |x(t)|$. (A.4)

From the definition, the 2-norm is related to the concept of signal energy. In fact, all the development of the stability theory will be based on the 2-norm because, due to Parseval's theorem, there is a closed relationship between the 2-norm of a signal and its frequency domain description. The concept of 1-norm will become clearer later, as convolution representation of linear systems is introduced.

Having defined the concept of norm of a real-valued signal, we can proceed to define L_p (p = 1, 2, or ∞) as a space of signals whose norms have finite values; that is

$$x \in L_p \quad if \quad \|x\|_p < \infty. \tag{A.5}$$

For example, $x(t) = e^{-t}$ has finite 1-norm, 2-norm, and ∞-norm, while $x(t) = e^t$ does not. Therefore, e^{-t} belongs to L_p (for p = 1, 2, ∞).

When studying BIBO stability of a system, it is not presumably known whether the output is bounded or unbounded given that the input is bounded. Therefore, it is also necessary to define another space of signals that contains unbounded signals. Let a truncated signal $x(t)$ be defined as

$$x(t)_T \equiv \begin{cases} x(t) & ,t \le T \\ & ; \\ 0 & ,t > T \end{cases} \tag{A.6}$$

then the extended L_p space, denoted by L_{pe}, is a space of signals which has the following properties: these signals are unbounded in the sense of 1-norm, 2-norm, or ∞-norm as $t \to \infty$, but truncation of time at some finite time T results in finite norms. That is,

$$x \in L_{pe} \quad if \quad x_T \in L_p. \tag{A.7}$$

For instance, the signal $x(t) = e^t$ does belong to L_{pe} (p = 1,2, ∞) since its norms are finite for any finite truncated time T. Consequently, by introducing the concept of L_p and L_{pe}, one excludes all the signals whose values can explode in finite time, such as $x(t) = \frac{1}{t-10}$, in the input-output stability theory.

A.1.2 Systems

As mentioned earlier, a system, in the input-output theory, is a relation that maps an input signal to an output signal. In general, systems are divided into two classes: linear systems and nonlinear systems. However, in the input-output stability theory, no distinction is usually made between the two, and various concepts, which are common to both linear and nonlinear systems, are developed as a foundation for the theory of input-output stability.

A.1.2.1 Gain of a System

A system, in the context of input-output stability, can be termed as a relation, say H, that maps an input signal u to a corresponding output signal, y. The mapping is denoted by

$$y = Hu. \tag{A.8}$$

Let $g(H)$ denote the ***gain of the relation*** H; then $g(H)$ is the maximum ratio of the output norm over the input norm for all time t, namely

$$g(H) \equiv \sup_{u \neq 0, t \geq 0} \frac{\|Hu\|}{\|u\|}, \tag{A.9}$$

and there exist different types of system gains for different norms. Furthermore, it is evident from the definition that

$$\|y\| \leq g(H)\|u\|. \tag{A.10}$$

A.1.2.2 BIBO Stability

The concept of ***bounded-input bounded-output*** (BIBO) stability can be formally introduced as follows: a system is BIBO stable if a bounded input results in a bounded output, that is if whenever an input $u \in L_p$ ($p = 1, 2,$ or ∞), then the output $y \in L_p$ ($p = 1, 2,$ or ∞), and there exists a finite positive constant α such that

$$u \in L_p \Rightarrow \|y\|_p \leq \alpha \|u\|_p . \tag{A.11}$$

Notice that the definition of BIBO stability as in Eq A.11 is analogous to the one provided in Eq. A.10, and therefore BIBO stability of a system H with an input u and an output y requires that the input u be bounded and H have a finite gain, $g(H)$.

A.1.2.3 Sectoricity

In the context of BIBO stability, the two key parameters are the system gain and the norm of a signal. Thus, the concept of system gain disregards any particular characteristics or properties of a system and generalizes to many classes of systems. In fact, to further exploit all the properties of a system in terms of gain from the system input to the system output, the minimum gain of the system– the smallest ratio of the output norm over the input norm– is also needed. A ***sector*** $\{a,b\}$ is a pair of real numbers a and b which characterizes the gain of a relation H. Saying H belongs to the sector $\{a,b\}$ means that there exist constants a and b such that

$$a \leq \frac{\|Hu\|}{\|u\|} \leq b \quad \text{for all } t \geq 0, \tag{A.12}$$

where b is obviously the gain of the system H, $g(H)$, and a the minimum gain of H. For a memoryless system, a graphical interpretation of the above definition is shown in Fig. A.1(a), where the output response y lies between two straight lines of slopes a and b. On the other hand,

if y does not lie between these two straight lines, one says H is outside the sector $\{a,b\}$, as shown in Fig. A.1(b).

A.1.2.4 Conicity

A sector $\{a,b\}$ can also be characterized equivalently by another pair of parameters. Let

$$c = \frac{b+a}{2} \quad \text{and} \quad r = \frac{b-a}{2}; \tag{A.13}$$

then c and r are said to be the ***center*** and the ***conic radius*** of the sector $\{a,b\}$, respectively. The concepts of center and radius are illustrated in Figs. A.1(c) and A.1(d). The meaning of the radius r is that if the output y lies inside the sector $\{a,b\}$, then y - cu will lie inside the sector $\{-r,r\}$. Therefore, saying that H is inside (outside) the sector $\{a,b\}$ is equivalent to saying that H is interior (exterior) conic $\{c,r\}$, and the sector $\{a,b\}$ can be recovered from $\{c,r\}$ by

$$a = c - r \quad \text{and} \quad b = c + r. \tag{A.14}$$

Consequently, the definition of conicity makes it clear that if a relation H is interior conic $\{c,r\}$, then there must exist a relation R, which belongs to the sector $\{-r,r\}$, such that H is factorizable into a parallel combination

$$H = R + c, \tag{A.15}$$

and

$$y = Hu = (R + c)u = Ru + cu. \tag{A.16}$$

A.1.2.5 Linear Systems

The class of linear system is defined by the principle of superposition. If y_1 and y_2 are the outputs of a system H when u_1 and u_2 are the respective inputs, then H is linear if and only if

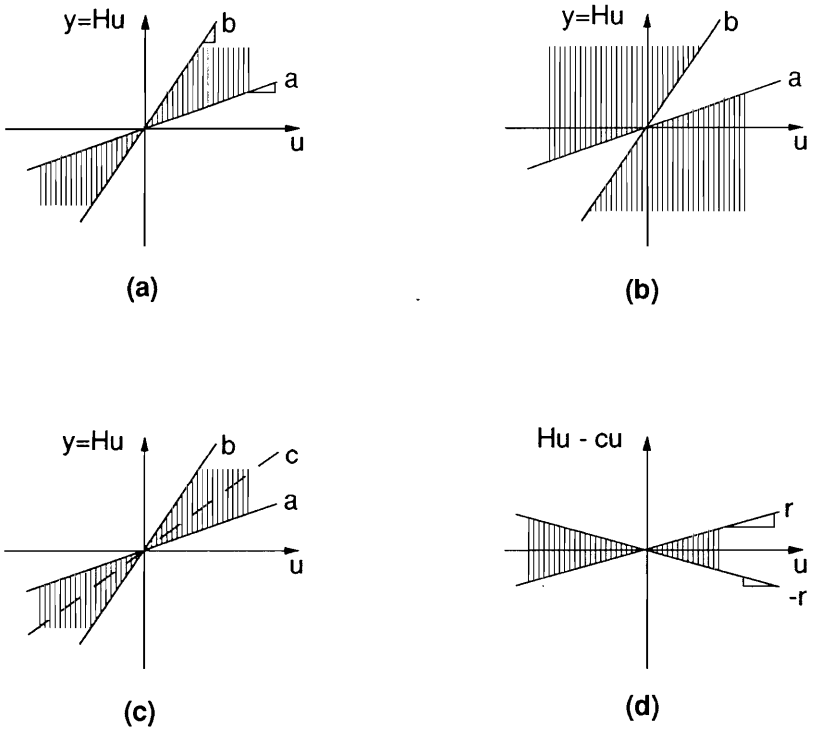

Fig. A.1: Sectoricity and Conicity

$$H(u_1 + u_2) = Hu_1 + Hu_2 = y_1 + y_2, \tag{A.17}$$

and

$$H(au_1) = aHu_1 = ay_1, \tag{A.18}$$

where a is an arbitrary constant. Subsequently, linear systems which are causal and time-invariant are assumed throughout. The input-output relationship for this particular class of linear systems can be represented by a convolution operator as follows:

$$y(t) = h(t) * u(t) = \int_0^t h(t-\tau)u(\tau)d\tau, \tag{A.19}$$

where $h(t)$ is the impulse of the system H. It follows that the concept of 1-norm and ∞-norm can be understood in the context of BIBO stability of a linear convolution system H in the L_∞ space. Let u be an input to the system H, and let it be bounded by $\|u\|_\infty \le k$ for all time $t \in [0,\infty)$. Then

$$\|y(t)\|_\infty = \left\| \int_0^t h(t-\tau)u(\tau)d\tau \right\|_\infty \le \int_0^t |h(t-\tau)| \|u(\tau)\|_\infty d\tau \le k \int_0^t |h(\tau)| d\tau = k\|h(t)\|_1. \tag{A.20}$$

Therefore, $\|y\|_\infty < \infty$ if the gain of the system, $g(H) = \|h(t)\|_1$, is finite.

On the other hand, the concept of 2-norm in the context of BIBO stability in the L_2 space does not involve time-domain analysis, but frequency domain analysis instead. Indeed,

$$\|y(t)\|_2^2 = \int_0^\infty y(t)^2 dt = \int_{-\infty}^\infty |Y(j2\pi f)|^2 df \quad \text{(due to Parseval's theorem)}$$

$$= \int_{-\infty}^\infty |H(j2\pi f)|^2 |U(j2\pi f)|^2 df \le \sup_f |H(j2\pi f)|^2 \int_{-\infty}^\infty |U(j2\pi f)|^2 df$$

$$= \sup_f |H(j2\pi f)|^2 \|u(t)\|_2^2, \tag{A.21}$$

where $U(j2\pi f)$, $H(j2\pi f)$, and $Y(j2\pi f)$ denote the frequency domain descriptions of u, the system H, and y, respectively. Therefore, the system H is BIBO stable in the context of 2-norm if all the poles of $H(s)$ are strictly negative and the output y is bounded by

$$\|y\|_2 \leq \sup_f |H(j2\pi f)| \|u\|_2. \tag{A.22}$$

Thus, the gain of the system H in the context of 2-norm is $g(H) = \sup_f |H(j2\pi f)|$.

Lastly, the concepts of sectoricity and conicity can be applied to linear system as well. Let c and $r \geq 0$ be real constants; then it has been shown in [Zames Part II, 1966] that if

(i) $|H(j2\pi f) - c| \leq r$ for $f \in (-\infty, \infty)$, then H is interior conic $\{c, r\}$.

(ii) $|H(j2\pi f) - c| \geq r$ for $f \in (-\infty, \infty)$ and if the Nyquist plot of $H(s)$ does not encircle the point $(c, 0)$, then H is exterior conic $\{c, r\}$.

A.1.2.6 Nonlinear Systems

A nonlinear system is a system for which the principle of superposition does not hold. Since a nonlinearity can assume many different forms, it is very difficult to generalize some unique set of properties for the class of nonlinear systems. Instead, the use of sectoricity and conicity is well suitable for a nonlinear system. A nonlinear relation N can be said to belong to a sector $\{a,b\}$, and following the definition of the system gain, the gain of a nonlinear relation N is therefore $g(N) = b$. N is said to be memoryless if the value of the output y is only a function of the instantaneous value of the input u, and not of the past values of u. Otherwise, N is said to have memory. Finally, it is important to realize that since the principle of superposition does not hold for nonlinear systems, distributivity and commutativity are not valid for nonlinear operators; namely

$$N(x + y) \neq Nx + Ny, \tag{A.23}$$

and

$$NLx \neq LNx. \tag{A.24}$$

A.2 Input-Output Stability of Single-Loop Systems

The input-output stability results are based on the concepts of norms of signals and gain of a system which are developed in the previous section. The following section will address the issue of BIBO stability of a closed-loop feedback system: *Given two open-loop systems that are BIBO stable, one needs to establish a stability condition for their feedback interconnection.* The stability results will be developed first for a single-loop system in this section and extended to multiple-loop systems in the next section.

A.2.1 A Small-Gain Theorem for Single Loop Systems

Consider a general basic single loop feedback system shown in Fig. A.2, where H_1 and H_2 denote relations from e_1 to y_1 and e_2 to y_2 , respectively. The inputs to the closed-loop system are u_1 and u_2 , which can represent external disturbance or effect of non-zero initial conditions. The above system can be described as

$$y_1 = H_1 e_1, \tag{A.25a}$$

$$e_1 = u_1 - y_2, \tag{A.25b}$$

$$y_2 = H_2 e_2, \tag{A.25c}$$

$$e_2 = u_2 + y_1. \tag{A.25d}$$

The objective is to develop conditions under which the output signals y_1 and y_2 and the error signals e_1 and e_2 are bounded, given that the input signals u_1 and u_2 are bounded, and that H_1 and H_2 are BIBO stable systems

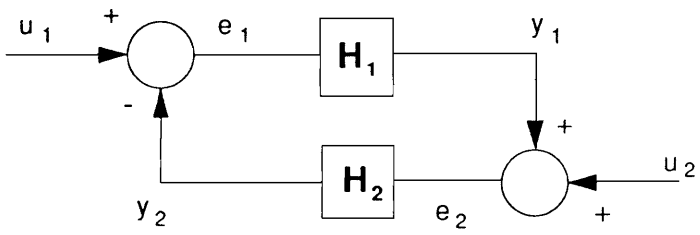

Fig. A.2: A Basic Single Loop System

Theorem (Small-gain theorem):

Consider the system shown in Fig. A.2, and suppose that the open-loop systems H_1 and H_2 are BIBO stable (both can be linear or nonlinear), that is the system gains $g(H_1)$ and $g(H_2)$ are finite so that

$$\|(H_1 e_1)_T\| \le g(H_1)\|e_{1T}\| \quad \forall T > 0, \tag{A.26}$$

$$\|(H_2 e_2)_T\| \le g(H_2)\|e_{2T}\| \quad \forall T > 0, \tag{A.27}$$

where the subscript T denotes the truncation of time at T. Under this condition, if $g(H_1)g(H_2) < 1$, then the closed-loop system is BIBO stable for bounded inputs u_1 and u_2.

Proof: From Eq. A.25,

$$\begin{aligned} e_1 &= u_1 - H_2 e_2; \\ e_2 &= u_2 + H_1 e_1. \end{aligned} \tag{A.28}$$

Applying the triangular inequality and the definition of the system gain yields

$$\begin{aligned} \|e_{1T}\| &\le \|u_{1T}\| + g(H_2)\|e_{2T}\| \\ \|e_{2T}\| &\le \|u_{2T}\| + g(H_1)\|e_{1T}\| \end{aligned} \tag{A.29}$$

Therefore,

$$\begin{bmatrix} 1 & -g(H_2) \\ -g(H_1) & 1 \end{bmatrix} \begin{bmatrix} \|e_{1T}\| \\ \|e_{2T}\| \end{bmatrix} \le \begin{bmatrix} \|u_{1T}\| \\ \|u_{2T}\| \end{bmatrix}, \tag{A.30}$$

where $g(.)$ denotes the gain of $(.)$. Provided that the matrix on the left hand side is invertible

$$\begin{bmatrix} \|e_{1T}\| \\ \|e_{2T}\| \end{bmatrix} \le \frac{1}{1 - g(H_1)g(H_2)} \begin{bmatrix} 1 & g(H_2) \\ g(H_1) & 1 \end{bmatrix} \begin{bmatrix} \|u_{1T}\| \\ \|u_{2T}\| \end{bmatrix}. \tag{A.31}$$

Equation A.31 is valid only if $1 - g(H_1)g(H_2) > 0$, since norm and gain are non-negative real values. If $T \to \infty$, and since u_1 and u_2 are bounded by assumption, Eq. A.31 implies that $\|e_1\|$ and $\|e_2\|$ are also bounded. Similarly, since $\|y_1\| \le g(H_1)\|e_1\|$ and $\|y_2\| \le g(H_2)\|e_2\|$ (Eq. A.25), the outputs y_1 and y_2 are also bounded if e_1 and e_2 are bounded. From the proof, it is clear that the sufficient condition for the closed-loop system to be BIBO stable is

$$1 - g(H_1)g(H_2) > 0. \tag{A.32}$$

Equation A.32 is the cornerstone of all the stability results developed subsequently for single- as well as multiple-loop systems.

A.2.2 Margin of Boundedness

The ***margin of boundedness*** of a closed-loop system, δ, is defined as $\delta \equiv 1 - g(H_1)g(H_2)$, which is somewhat equivalent to the notion of gain and phase margins for linear systems. The margin of boundedness δ will assume values between $0 < \delta < 1$. According to the small-gain theorem, a value of δ near 1 means that the closed-loop system is very stable, whereas a value of δ near 0 suggests that the closed-loop system is not very stable, or even on the verge of instability. Note that since the small-gain theorem yields only a sufficient condition, $\delta = 0$ zero does not necessarily mean that the system is unstable.

A.2.3 Loop Transformation Theorem

The small-gain theorem stated in the previous section provides a conservative stability condition, and the usefulness of the small-gain theorem is limited because the requirement that the open-loop gain product be less than one is seldom met in practice. Indeed, it is said to be conservative, because if a relation H belongs to the sector $\{a,b\}$, then $g(H) = b$. Consequently, it is realized that the sector $\{-g(H), g(H)\}$, which is a conservative estimate of the system sector gain as compared to the sector $\{a,b\}$, is used throughout in the proof of the small-gain theorem. Therefore, to make use of the true sector $\{a,b\}$, it is necessary to transform the system in such a way as to reduce the gain of the system to its smallest value of $(b - a)/A$. This is accomplished by the loop transformation technique.

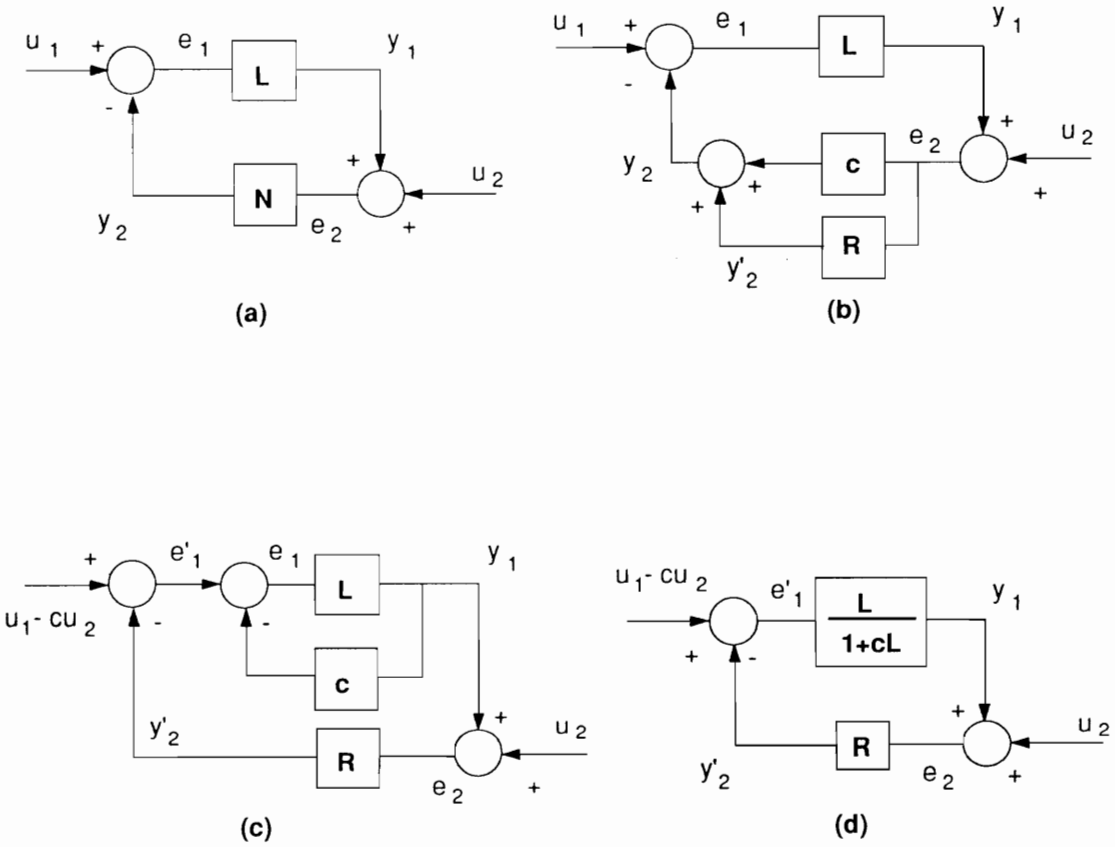

Fig. A.3: Graphical Interpretation of the Loop Transformation Technique

Consider a single-loop feedback system in Fig. A.3(a), where L is a linear relation, and N is a nonlinear relation which is interior conic $\{c,r\}$. From the definition of conicity, N can be factorized into $N = R + c$, as illustrated in Fig. A.3(b), where R is a new nonlinear system which belongs to the sector $\{-r, r\}$ (or interior conic $\{0, r\}$) and c is the center radius of N. Note that the resulting system is still equivalent to the old system. Then, through block diagram manipulations, the system in Fig. A.3(b) becomes the new equivalent systems shown in Figs. A.3(c) and A.3(d). Observe that after the transformation, a new single-loop system is obtained, where

$$y_2' = y_2 - ce_2, \tag{A.33}$$

$$e_1' = e_1 + cy_1, \tag{A.34}$$

and the open-loop systems become $L/(1+cL)$ and R. The above transformation means that the loop transformation technique performs a rotation of N about the origin so that the center c coincides with the horizontal axis and $R = N - c$ belongs to the sector $\{-r, r\}$. The loop transformation theorem is stated below:

Theorem:

If $L/(1+cL)$ is BIBO stable for a given c, then the original system and the transformed system are equivalent; namely, the original system is BIBO stable if and only if the transformed system is BIBO stable.

The proof is completed through algebraic manipulations and can be found in [Vid. 1993, Zames Part I 1966]. Under the new transformed system, it is expected that the stability condition should become less conservative when applying the small-gain theorem because the nonlinear relation N becomes R which has a smaller gain than N, and the gain of the linear block $L/(1+cL)$ must be less than or equal to $g(L)$. According to Eq. A.32, the new stability condition becomes

$$1 - g\left(\frac{L}{1+cL}\right)r \quad > 0, \tag{A.35}$$

and, the boundedness inequalities are given by [Vid. 1993]

$$\begin{bmatrix} \|e_1\| \\ \|e_2\| \end{bmatrix} \leq \frac{1}{1-g_L r} \begin{bmatrix} g_L c+1 & (g_L c+1)(r+c) \\ g_L & g_L c+1 \end{bmatrix} \begin{bmatrix} \|u_1\| \\ \|u_2\| \end{bmatrix}, \tag{A.36}$$

$$\begin{bmatrix} \|y_1\| \\ \|y_2\| \end{bmatrix} \leq \frac{1}{1-g_L r} \begin{bmatrix} g_L & g_L(r+c) \\ g_L(r+c) & (g_L c+1)(r+c) \end{bmatrix} \begin{bmatrix} \|u_1\| \\ \|u_2\| \end{bmatrix}, \tag{A.37}$$

where $g_L = g\left(\frac{L}{1+cL}\right)$. Remark that combination of the loop transformation theorem and the small-gain theorem for the stability analysis of nonlinear systems is in a sense equivalent to the classical gain and phase shift used for the stability analysis in linear time-invariant systems. However, only sufficient conditions can be obtained from the above stability result since it restricts very little information on the nonlinear relation N. The only required information is the sector $\{a, b\}$ where N belongs.

A.2.4 The Circle Criterion

Straight application of the small-gain and loop transformation theorems from the previous section offers very little usefulness. It is preferable if one can interpret these results in the frequency domain because of its versatility and elegance. The theory developed in the previous section is applicable to all norms; however, as previously mentioned, application of the theory in the frequency domain requires the 2-norm, due to Parseval's theorem. Given the transformed system in Fig. A.3, the stability condition requires that Eq. A.35 be true. Let $L(s)$ denote the frequency domain representation of the linear system L; then Eq. A.35 in the context of 2-norm is equivalent to

$$\sup_{-\infty<f<\infty}\left|\frac{L(j2\pi f)}{1+cL(j2\pi f)}\right|.r \; <1. \tag{A.38}$$

Equation A.38 has an interesting graphical interpretation. If $\{a,b\}$ denotes the sector which N belongs to, $b > 0$, $c = (a + b)/2$, and $r = (b - a)/2$, the stability condition in Eq. A.38 can be divided into three distinct cases depending on whether $a > 0$, $a = 0$ or $a < 0$.

Theorem (Circle Criterion):

Assuming that $\frac{L(s)}{1+cL(s)}$ is a BIBO stable linear system, define D(a,b) to be a disc whose center is on the real axis and which intersects the real axis at two points: $-1/a$ and $-1/b$. Then

Case 1: a > 0 *The Nyquist plot of $L(s)$ must lie outside the disc D(a,b) and encircle the disc in the counterclockwise direction as many times as there are RHP poles of $L(s)$*

Case 2: a = 0 *The Nyquist plot of $L(s)$ must stay on the right of the vertical line passing through $(-1/b, 0)$. This is a special case of case 1, when the disc D(a,b) degenerates into a half plane since $a = 0$. The condition on the Nyquist plot of $L(s)$ is equivalent to*

$$\mathrm{Re}\{L(j2\pi f)\} > -\frac{1}{b}. \tag{A.39}$$

Case 3: a < 0 *The Nyquist plot of $L(s)$ must remain inside the disc D(a,b).*

Interpretation of the three cases is shown in Fig. A.4. This Circle Criterion is powerful in a sense that no major restriction on N is made; that is, N can have memory, as long as N is inside a known sector $\{a,b\}$. Also, verification of the stability condition is made easy by plotting the Nyquist plot of $L(s)$ and checking the stability based on the sector $\{a,b\}$ of the nonlinear system N.

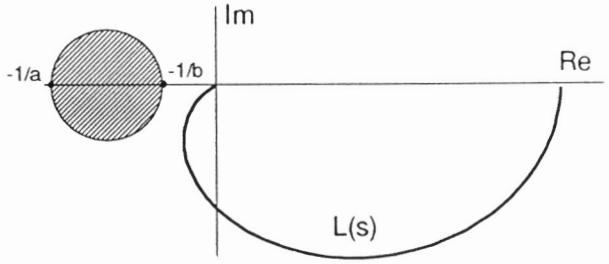

(a)

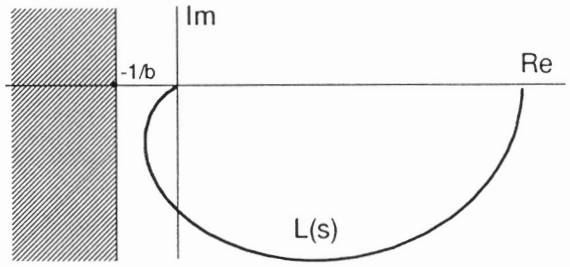

(b)

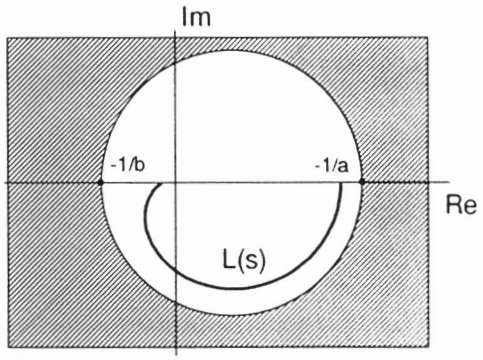

(c)

Fig. A.4: Circle Criterion
(a) $a > 0$
(b) $a = 0$
(c) $a < 0$

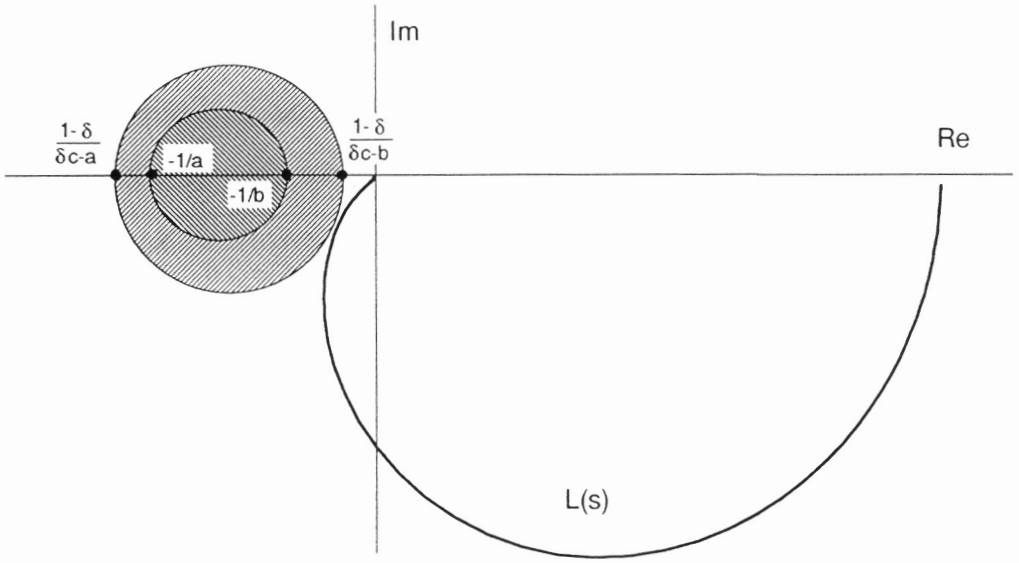

(a)

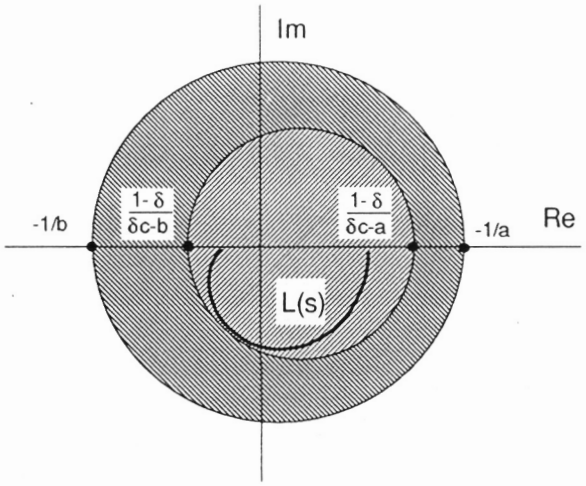

(b)

Fig. A.5: Graphical Interpretation of the Margin of Boundedness
(a) $a > 0$
(b) $a \leq 0$

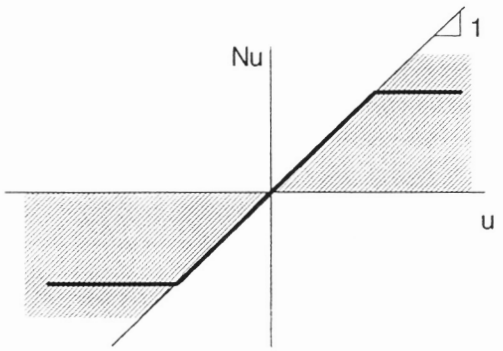

(a)

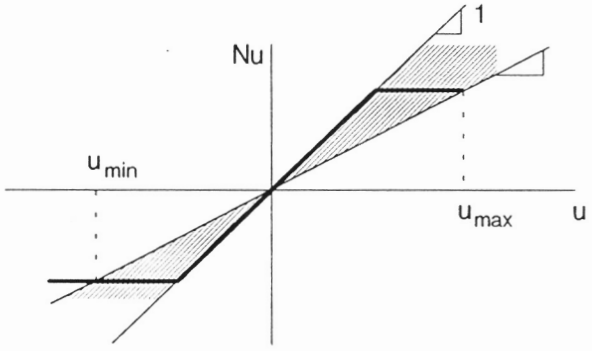

(b)

Fig. A.6: A Redefined Sector for Local Stability

A.2.5 Graphical Interpretation of the Margin of Boundedness

As already defined, the margin of boundedness is a measure of degree of stability of a system. The margin of boundedness, δ , can assume values between (0,1), where a near-one value means the closed-loop system is very stable, whereas a near-zero value implies the system is on the verge of becoming unstable. For the system in Fig. A.3, δ is defined as

$$\delta \equiv 1 - \sup_{-\infty<f<\infty} \left| \frac{L(j2\pi f)}{1 + cL(j2\pi f)} \right| .r . \tag{A.40}$$

Nevertheless, it is preferable to interpret δ straight from the Nyquist plot of $L(s)$. From Fig. A.4, the separation between the Nyquist plot of $L(s)$ and the disc $D(a,b)$ should indicate how stable the system is; therefore, δ should be a function of that separation. If the disc $D(a,b)$ is redefined as $D(a,b;\delta)$, which is a disc whose center is on the real axis and which intersects the real axis at two points $\frac{1-\delta}{\delta c - a}$ and $\frac{1-\delta}{\delta c - b}$ where c is the center conic, $c = (a + b) / 2$, then, δ is the margin of boundedness of the closed-loop system. Given the sector $\{a,b\}$ and the Nyquist plot of $L(s)$, the disc $D(a,b;\delta)$ can be plotted with various δ until $L(s)$ is almost tangent to the disc at one point. That particular value of δ will represent the margin of boundedness of the closed-loop system. The technique is illustrated in Fig. A.5. For the case where $a > 0$, the Nyquist plot of $L(s)$ must stay outside or inside the disc $D(a,b;\delta)$ depending on whether $\delta \le \frac{2a}{b+a}$ or $\delta > \frac{2a}{b+a}$, respectively. Indeed, as δ increases from 0, the disc $D(a,b;\delta)$ becomes larger, and when $\delta = \frac{2a}{b+a}$, $D(a,b;\delta)$ intersects the negative real axis at $-\infty$ at $-1/(b + a)$, which implies that the disc degenerates into a left half plane. If δ increases further, the left half plane wraps around the right half plane and shrinks into a circle. When $a \le 0$, the Nyquist plot of $L(s)$ must stay inside the disc $D(a,b;\delta)$. As observed from Fig. A.5(b), $D(a,b;\delta)$ becomes smaller as δ becomes larger, and $D(a,b;\delta)$ degenerates into a single point at the origin when $\delta = 1$. The above interpretation of the margin

of boundedness suggests that for a single loop feedback system with a linear part and a nonlinear part, maximum stability condition ($\delta \cong 1$) is achieved only if the Nyquist plot of the linear part is confined within a very small circle center at the origin. In other words, the gain of the linear part must be small.

A.2.6 Local Stability

The above stability criterion is often referred to as an absolute stability criterion. If the stability condition is met, the system is BIBO stable for any bounded inputs. However, global stability is often a stringent condition that is hard to meet in practice. Furthermore, BIBO stability for all bounded inputs– even very large inputs– is unnecessary in practical design. Usually one may be content with a more restricted but adequate bounds on the inputs, which in consequence may require a smaller sector $\{a,b\}$ for the nonlinear feedback loop N, and the stability condition can be considerably relaxed. For example, consider a saturating nonlinearity as shown in Fig. A.6. From Fig. A.6(a) it is evident that N is inside the sector $\{0,1\}$. However, the sector $\{0,1\}$ implies any bounded value of the input u. Thus, it may be necessary to restrict $U_{min} \leq u \leq U_{max}$, and a smaller sector will be obtained, as shown in Fig. A.6(b). If a sector smaller than the true sector is used for the nonlinearity, the absolute stability problem is referred to as a local stability problem. The stability region is not a whole hyperplane, but is reduced to a finite hyperplane.

A.2.7 Multiplier Theory

It has been stated that the small-gain theorem suffers a deficiency of being sign-insensitive and therefore yields conservative stability results. The reason is that the small-gain theorem uses norms of signals to establish a stability condition. Thus, in order to reduce the conservativeness of the small-gain theorem, the loop transformation theorem is introduced, and application of the

small-gain theorem after the loop transformation of the system yields a better stability result. Yet, application of both theorems yields only a sufficient stability condition and how far it is from necessity is not generally well-known. In fact, [Vid. 1993] has derived the necessity condition of the circle criterion by selecting a particular class of systems and showing that the circle criterion establishes sufficient as well as necessary conditions. Thus, the above result suggests that the circle criterion is conservative, but not too conservative.

At this stage, one may wonder whether there exist some other means of improving the conservativeness of the stability results established so far. The answer is there exists another transformation technique which involves the concept of ***multipliers***. Recall from the circle criterion that the degree of stability depends solely upon the separation of the Nyquist plot of the linear subsystem and the forbidden region due to the sectoricity of the nonlinear subsystem. Thus, stability results can be further improved if one can manipulate the subsystems L and N in such a way as to maximize the separation between $L(s)$ and N. This can be done through the use of the multiplier theory. *The basic idea behind the multiplier technique is that by multiplying the relations L and N by appropriately chosen multipliers, the product can be doctored to either shift the Nyquist plot of L(s) farther to the right or reduce the size of the forbidden region.* The concept is illustrated in Fig. A.7 where Z denotes the multiplier. Note that introduction of a multiplier yields an equivalent system, provided that Z is chosen appropriately. Indeed, there exist three classes of suitable positive real multipliers (the concept of positive real is equivalent to passivity and is explained in [Temes 1977]): (1) Popov multipliers, (2) RC multipliers, and (3) RL multipliers. They are defined as follows:

(1) **Popov multiplier:** $Z(s) = 1 + qs$, for $q > 0$. (A.41)

(2) **RC multiplier:** $Z(s) = K_\infty + \sum_{i=1}^{n} \frac{K_i}{s + p_i}$, (A.42)

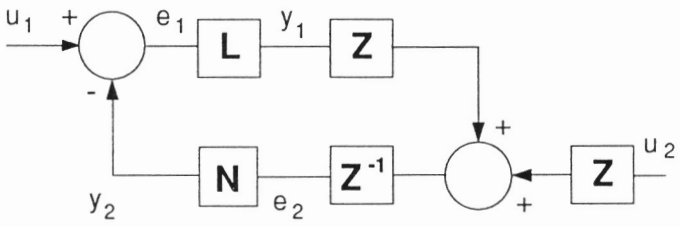

(a)

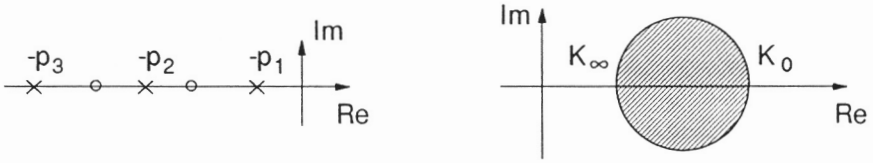

(b)

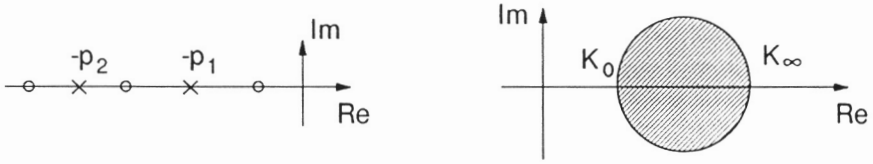

(c)

Fig. A.7: Multiplier Insertion
(a) Multiplier Technique
(b) RC Multiplier Characteristics
(c) RL Multiplier Characteristics

where $K_\infty > 0$, $K_i \geq 0$, and $p_i > 0$ for $i = 1, \ldots, n$. Also $K_0 \equiv Z(s=0) = K_\infty + \sum_{i=1}^{n} \frac{K_i}{p_i}$.

(3) **RL multiplier:** $Z(s) = K_0 + \sum_{i=1}^{n} \frac{K_i s}{s + p_i}$, (A.43)

where $K_0 > 0$, $K_i \geq 0$, and $p_i > 0$ for $i = 1, \ldots, n$; and $K_\infty \equiv Z(s \to \infty) = K_0 + \sum_{i=1}^{n} K_i$.

The multipliers of type (2) and (3) are associated with the respective names RC and RL because they can be realized using Foster expansion into a ladder of resistors and capacitors (RC type) or resistors and inductors (RL type) [Temes, 1977]. These multipliers consist of real poles and zeros that alternate on the negative real axis, as shown in Fig. A.7(b). For the RC type, the first critical frequency on the negative real axis is a pole, whereas the first critical frequency for the RL type is a zero. Furthermore, their frequency responses lie inside a circle in the right-half plane, which means that Z_{RC} belongs to the sector $\{K_\infty, K_0\}$ and Z_{RL} to the sector $\{K_0, K_\infty\}$. Finally, it is evident that if $Z(s)$ is of type RC then $Z(s)^{-1}$ is of type RL.

Also, the use of the above multipliers does not destroy the BIBO stability property of the linear system LZ. If L is known to be a stable linear system and Z is positive real, then the product LZ is still a stable linear system because all the poles of $Z(s)$ locate on the negative real axis. Therefore, LZ is BIBO stable and has a finite gain.

A.2.7.1 Sector Products

When introducing the multiplier Z to form the LZ product, the nonlinear subsystem, N, must be multiplied by Z^{-1}, as in Fig. A.7. Then, if N contains memory, it is not known in general which sector the product NZ^{-1} will belong to, unless it is computed numerically. Thus, *it is important to realize that whenthe multiplier technique is applied , N must be memoryless and time-invariant.*

If N is time varying, more restriction on N will be required [Cho, 1968]. Otherwise, if N is memoryless and belongs to the sector $\{a,b\}$, then the sector of the product NZ^{-1} is given by

(1) if Z is a Popov multiplier, then $Z^{-1} \in \{0,1\}$ and $NZ^{-1} \in \{a,b\} \times \{0,1\} = \{0,b\}$,

(2) if Z is of type RC, then $Z^{-1} \in \{1/K_0, 1/K_\infty\}$, and

$$NZ^{-1} \in \{a,b\} \times \{1/K_0, 1/K_\infty\} = \begin{cases} \{a/K_0, b/K_\infty\} & a>0 \\ \{a/K_\infty, b/K_\infty\} & a<0, \\ \{0, b/K_\infty\} & a=0 \end{cases}$$

(3) if Z if of type RL, the results is the same as (2), but with K_0 and K_∞ interchanged.

The proofs for these three cases can be found in [Zames Part II, 1966].

Using these three types of multipliers in connection with the subsystems L and N can either shift the Nyquist plot of $L(s)Z(s)$ farther to the right, or reduce the size of the forbidden region as observed from the above properties. Consequently, the multiplier technique will improve further the stability criterion derived from the small-gain theorem and the loop transformation technique, as discussed in the following section.

A.2.7.2 Improved Stability Criteria

Based on the multiplier theory, several new and less conservative stability conditions can be established by applying a multiplier Z to the system, performing the loop transformation theorem, and checking the stability based on the small-gain theorem.

Theorem:

Consider the basic single-loop feedback system in Fig. A.2. Let N be memoryless, time invariant, and inside the sector $\{0,b\}$, and L be BIBO stable; then the closed-loop system is BIBO stable if

$$\mathrm{Re}\left\{\left(L(\mathrm{j}2\pi f)+\frac{1}{b}\right)Z(\mathrm{j}2\pi f)\right\}>0. \tag{A.44}$$

Proof:

Without loss of generality, assume that Z is of RC type; then after introducing Z into the system, one obtains the equivalent system as in Fig. A.7. The linear block becomes LZ, and the nonlinear block NZ^{-1}. Since $N \in \{0,b\}$, $NZ^{-1} \in \{0, b/K_\infty\}$. Then it follows from case 2 of the Circle criterion that BIBO stability requires

$$\mathrm{Re}\{L(\mathrm{j}2\pi f)Z(\mathrm{j}2\pi f)\}>\frac{-K_\infty}{b}. \tag{A.45}$$

However, observe from Fig. A.7 that $\mathrm{Re}\{Z(\mathrm{j}2\pi f)\} \geq K_\infty$; therefore

$$-\mathrm{Re}\left\{\frac{Z(\mathrm{j}2\pi f)}{b}\right\}\leq\frac{-K_\infty}{b}. \tag{A.46}$$

After inserting Eq. A.46 into Eq. A.45 and after some simplification, Eq. A.44 is obtained.

When N belongs to $\{a,b\}$ instead of $\{0,b\}$, one can first apply the loop transformation technique to the system so that the new nonlinearity N' belongs to $\{0, b\text{-}a\}$; that is, N is expanded into two parallel block structures of $N = N' + a$, and therefore, N' belongs to the sector $\{0,b\text{-}a\}$. The application of the multiplier technique and the Circle criterion yields

$$\mathrm{Re}\left\{\frac{bL(\mathrm{j}2\pi f)+1}{aL(\mathrm{j}2\pi f)+1}Z(\mathrm{j}2\pi f)\right\}>0 \tag{A.47}$$

as a new stability condition.

A.2.7.3 The Off-Axis Circle Criterion

The Off-Axis Circle criterion is based on Eqs. A.44 and A.47 where $Z(s)$ is an RC or RL multiplier [Y. S. Cho, 1968b]. This criterion is an extension of the circle criterion and has the following graphical interpretation.

Theorem (Off-Axis Circle Criterion):

Consider the basic single loop feedback system in Fig. A.2, and let H_1 be a linear element L and H_2 be a nonlinear element, N, where N is *memoryless*, time invariant, and inside the sector $\{a,b\}$ where $b > 0$. Then the closed-loop system is BIBO stable if

Case 1: a > 0 *The Nyquist plot of L(s) lies outside a circle passing through -1/a and -1/b (note that the center need not be on the negative real axis as in the Circle criterion) and encircles it as many times as there are RHP poles of L(s)*

Case 2: a = 0 *The Nyquist plot of L(s) must stay on the right side of a line of any slope passing through (-1/b, 0).*

Case 3: a < 0 *The Nyquist plot of L(s) lies inside a circle passing through -1/a and -1/b*

Even though these new stability conditions are still sufficient conditions, experience has shown that in most cases, the stability results are very near necessary conditions. Therefore, in accessing stability of a single-loop system, it is advantageous to first apply the multiplier technique and the loop transformation technique whenever applicable and to apply the small-gain theorem afterward. However, the choice of the appropriate multiplier depends on the characteristics of the linear subsystem, and must be carefully considered to sharpen the stability condition.

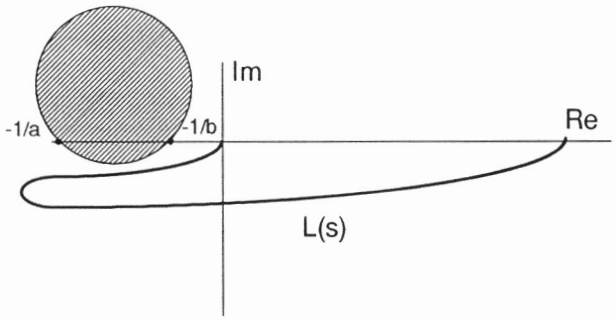

(a)

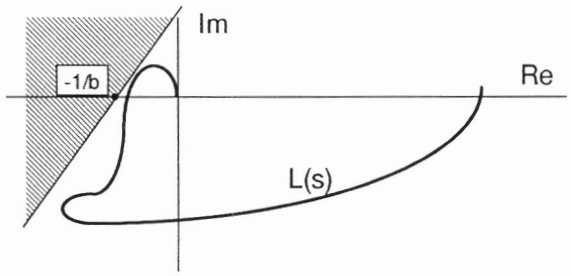

(b)

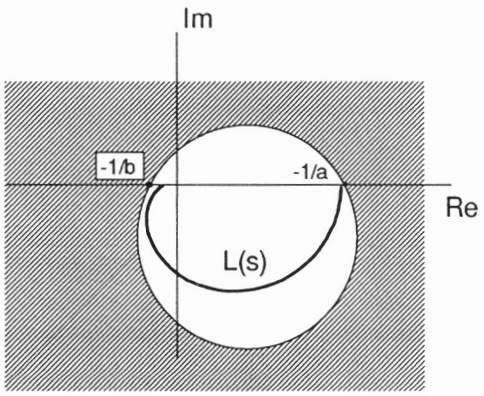

(c)

Fig. A.8: Off-Axis Circle Criterion
(a) $a > 0$
(b) $a = 0$
(c) $a < 0$

A.3 Input-Output Stability of Multiple-Loop Systems

In the previous section, several techniques have been introduced to analyze the stability of a single-loop nonlinear system. The first stability condition, based on the small-gain theorem, requires that the product of the open-loop subsystem be less than one. Also, in order to reduce the conservativeness of the small-gain theorem, the loop transformation technique and the multiplier technique are discussed, and several new stability criteria are derived. These results can be extended to systems that contain several single loops or to multiple-loop systems. In dealing with multiple-loop systems, the results obtained from the small-gain theorem are no longer in scalar form, but in vector form. Consequently, it is necessary to introduce the so-called M-matrices whose properties can be applied to derive a small-gain condition for a multiple-loop system.

A.3.1 M-Matrices

Definition:

Let $\mathbf{R} = [r_{ij}]$ be a real $n \times n$ matrix; then the principal minors, D_k, of the matrix $\mathbf{R}$ are defined as

$$D_k = \begin{vmatrix} r_{11} & \cdots & r_{1k} \\ \vdots & \ddots & \vdots \\ r_{k1} & \cdots & r_{kk} \end{vmatrix} \quad ,k = 1,\ldots,n.$$

Definition:

A real $n \times n$ matrix $\mathbf{R}$ is said to be an **M-matrix** if $r_{ij} \leq 0$ for $i \neq j$ (i.e., all the off-diagonal elements of $\mathbf{R}$ are nonpositive), and if all the principal minors of $\mathbf{R}$ are positive.

Theorem:

If $\mathbf{R}$ is an M-matrix, then the following statements are equivalent:

(*i*) *The principal minors of* $\mathbf{R}$ *are all positive.*

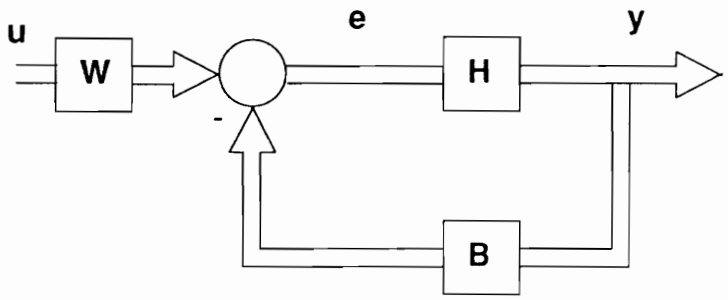

Fig. A.9: A Basic Multiple Loop System

(ii) $\boldsymbol{R}$ is non singular. All elements of $\boldsymbol{R}^{-1}$ are nonnegative and all the diagonal elements of $\boldsymbol{R}^{-1}$ are positive.

(iii) The real parts of all eigenvalues of $\boldsymbol{R}$ are positive.

A.3.2 A Small-Gain Theorem for Multiple-Loop Systems

Consider a basic multiple-loop system as shown in Fig. A.9, where $\mathbf{u} = [u_1 \ \ldots \ u_m]^T$ is an input vector, $\mathbf{e} = [e_1 \ \ldots \ e_n]^T$ is the error vector, and $\mathbf{y} = [y_1 \ \ldots \ y_p]^T$ is the output of the multiple-loop system, and $\mathbf{W}$, $\mathbf{H}$, and $\mathbf{B}$ are relation matrices such that

$$\begin{bmatrix} y_1 \\ \vdots \\ y_p \end{bmatrix} = \begin{bmatrix} h_{11} & \cdots & h_{1n} \\ \vdots & \ddots & \vdots \\ h_{p1} & \cdots & h_{pn} \end{bmatrix} \begin{bmatrix} e_1 \\ \vdots \\ e_n \end{bmatrix}, \tag{A.48}$$

$$\begin{bmatrix} e_1 \\ \vdots \\ e_n \end{bmatrix} = \begin{bmatrix} w_{11} & \cdots & w_{1m} \\ \vdots & \ddots & \vdots \\ w_{n1} & \cdots & w_{nn} \end{bmatrix} \begin{bmatrix} u_1 \\ \vdots \\ u_m \end{bmatrix} - \begin{bmatrix} b_{11} & \cdots & b_{1p} \\ \vdots & \ddots & \vdots \\ b_{n1} & \cdots & b_{np} \end{bmatrix} \begin{bmatrix} y_1 \\ \vdots \\ y_p \end{bmatrix}. \tag{A.49}$$

In terms of vector notation, the multiple-loop system can be written as

$$\mathbf{e} = -\mathbf{BH}\,\mathbf{e} + \mathbf{Wu}\,. \tag{A.50}$$

The gains of the relation matrices **H**, **B**, and **W** are defined as $g(\mathbf{H}) = [g(h_{ij})]$, $g(\mathbf{B}) = [g(b_{ij})]$, and $g(\mathbf{W}) = [g(w_{ij})]$, respectively. Let $\mathbf{R} \equiv \mathbf{I} - g(\mathbf{H})g(\mathbf{B})$, where **I** is an $n \times n$ identity matrix; then if **R** is an M-matrix, the system is BIBO stable.

Proof:

Define $\|\mathbf{e}\| = \left[\|e_1\| \ldots \|e_n\|\right]^T$, $\|\mathbf{u}\| = \left[\|u_1\| \ldots \|u_m\|\right]^T$, and $\|\mathbf{y}\| = \left[\|y_1\| \ldots \|y_p\|\right]^T$. Then it follows from the triangular inequality that Eq. A.50 becomes

$$\|\mathbf{e}\| \le g(\mathbf{H})g(\mathbf{B})\|\mathbf{e}\| + g(\mathbf{W})\|\mathbf{u}\| \tag{A.51}$$

or

$$[\mathbf{I} - g(\mathbf{H})g(\mathbf{B})]\|\mathbf{e}\| \leq g(\mathbf{W})\|\mathbf{u}\|, \tag{A.52}$$

where $\mathbf{I}$ is the $n \times n$ identity matrix. Provided that $\mathbf{R}^{-1}$ exists,

$$\|\mathbf{e}\| \leq \mathbf{R}^{-1}g(\mathbf{W})\|\mathbf{u}\| \tag{A.53}$$

and

$$\|\mathbf{y}\| \leq g(\mathbf{H})\mathbf{R}^{-1}g(\mathbf{W})\|\mathbf{u}\|. \tag{A.54}$$

According to Eq A.53, BIBO stability requires that $\mathbf{R}^{-1}$ exist and all elements of $\mathbf{R}^{-1}$ be nonnegative. Since $g(\mathbf{H})$ and $g(\mathbf{B})$ are matrices which consist of gains of relations, $g(h_{ij})$ and $g(b_{ij})$, $g(\mathbf{H})$ and $g(\mathbf{B})$ contain nonnegative elements, and therefore, $\mathbf{R}$ is a matrix whose off-diagonal elements are nonpositive. Thus, the conditions for $\mathbf{R}$ being invertible and $\mathbf{R}^{-1}$ having nonnegative elements require that $\mathbf{R}$ be an M-matrix. The easiest way for checking if $\mathbf{R}$ is an M-matrix is to verify that all the principal minors of $\mathbf{R}$ are positive. Therefore, if $\mathbf{R}$ is $n \times n$, there will be n conditions in connection with the principal minors to verify. Fortunately, it is frequent that these n conditions usually reduce to a few stability conditions, and consequently, applicability of the method seems feasible.

The above theorem is an extension of the small-gain theorem for a single-loop system. The extension of the theorem to include the loop transformation technique has been developed by Porter [Porter 1972, and Michel 1977]. However, generalization of the multiplier technique for the multiple-loop system has not been obtained anywhere in the literature.

Appendix B

Perturbation Signals for Nonlinear System Identification

Two types of signals, which can be easily generated by software or hardware, have been proposed as perturbation signals for nonlinear system identification: pseudorandom binary signals (PRBS) [Godfrey, 1993], and constant-switching-pace symmetric random signals (CSRS) [Marmarelis, 1978]. The PRBS is a binary signal that switches randomly to either the next value of A or $-A$ at every Δt time interval, as illustrated in Fig. B.1(a). However, the PRBS is not a pure random signal itself, but a periodic signal. The PRBS has the advantage of easier generation, and a technique for generating these pseudorandom sequences is a register circuit, as shown in Fig. B.1(b). Given an initial arbitrary binary sequence in the n registers, an exclusive-OR (XOR) operation is performed on the last register and a specific m^{th} register, and the outcome is feedback to the first register. The last register is the output, where 0 and 1 will correspond to values of $-A$ and A, respectively. Even though the output of the circuit appears to possess random character, the binary sequence will repeat itself after $2^n - 1$ bits. However, the maximum length sequences, i.e., those of period $2^n - 1$ bits, can only be produced if the exclusive-OR operation is performed on the last register and a specific register, as depicted in Table B.1. Also, the power spectral density of a PRBS of period $T = N.\Delta t$, where $N = 2^n - 1$, is a train of dirac delta functions appearing at discrete frequencies and is given by

$$\mathcal{P}_x(f=\frac{k}{T}) = A^2 \frac{N+1}{N^2} \frac{\sin^2(\pi k/N)}{(\pi k/N)^2}. \tag{B.1}$$

The other type of random signal used in nonlinear system identification is the CSRS, as shown in Fig. B.2. These test signals combine the stairlike form of the pseudorandom signal with the random character in amplitude distribution. Unlike the PRBS, the CSRS is not a periodic signal, and the signal amplitude distribution can be any type, such as Gaussian or uniform distributions. Thus, this type of signal can be generated easily using software and is suitable for computer simulations. The power spectral density of the CSRS is continuous in frequency and is given by [Marmarelis, 1978]

$$\mathcal{P}_x(f) = E[x^2]\Delta t \frac{\sin^2(\pi f \Delta t)}{(\pi f \Delta t)^2}, \tag{B.2}$$

where $E[x^2]$, a constant, is the variance of the random signal x with a zero mean and a probability density function $f(x)$,

$$E[x^2] = \int_{-\infty}^{\infty} x^2 f(x) dx. \tag{B.3}$$

If the amplitude of the signal x is uniformly distributed between A and $-A$, then it can be shown that $E[x^2] = A^2/C$. Likewise, if Gaussian distribution is selected for the random signal x, then one can specify an amplitude A as the standard deviation of the signal x; and therefore, $E[x^2] = A^2$. This implies that the power spectrum of a CSRS is proportional to the square of the amplitude of signal x; or in other words, the larger the amplitude of x is, the more power the signal x carries. On the other hand, the power bandwidth depends on Δt. As illustrated in Fig. B.2(b), for a large Δt, the bell shape becomes narrower, which implies that most of the power of the signal concentrates in the low frequency range. On the other hand, a small Δt results in a larger power bandwidth of the signal.

Thus, pseudorandom signals such as CSRSs and PRBSs, which have a common adjustable large power bandwidth, are more suitable for nonlinear system identification than conventional signals such as sinusoids, steps, pulses, and ramps.

Table B.1: Stages That Can Be Combined with the Last Stage to Generate Maximum-Length Pseudorandom Binary Sequence

Number of Registers, n	Register #n XOR with	Sequence length in bits
5	2	31
6	1	63
7	1, or 3	127
9	4	511
10	3	1023
11	2	2047
15	1,4, or 7	32767
18	7	262,143
20	3	1,048,575
21	2	2,097,151
22	1	4,194,303
23	5 or 9	8,388,607
25	3 or 7	33,554,431
28	3,9, or 13	268,435,455
31	3,6,7, or 13	2,147,483,647
33	13	8,589,934,591

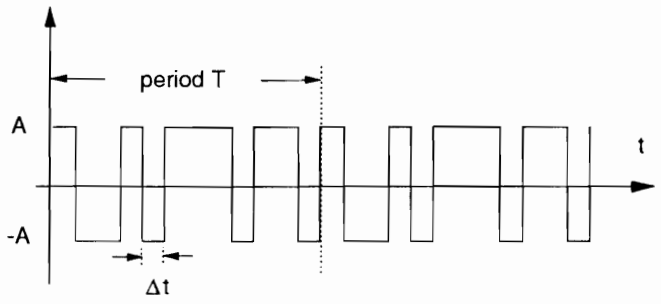

(a)

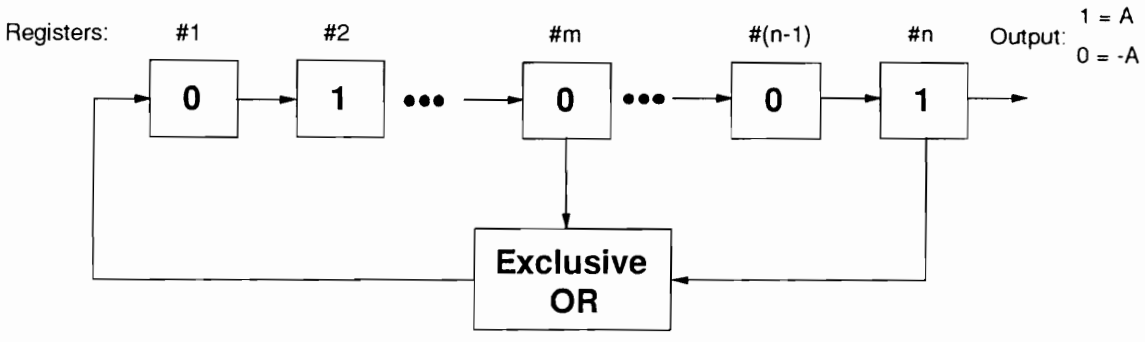

(b)

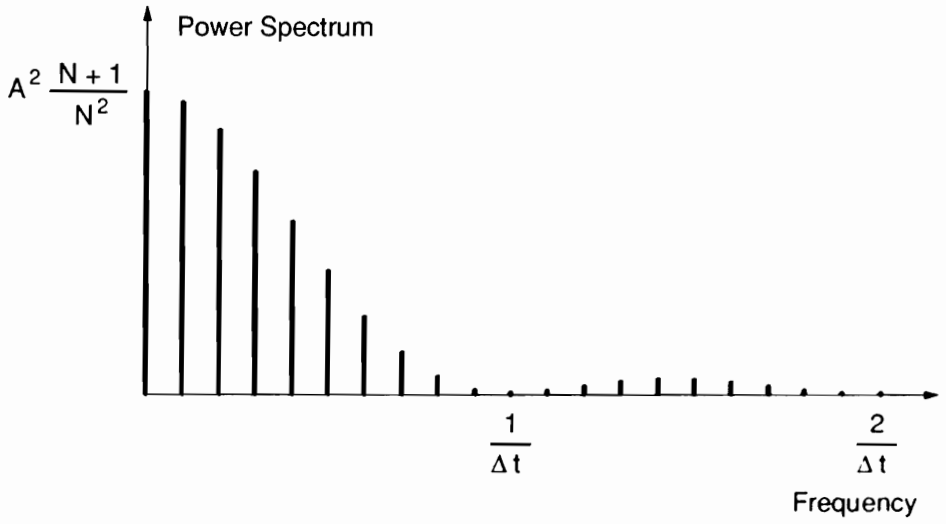

(c)

Fig. B.1: Pseudorandom Binary Signals Characteristics
(a) Sample Waveform
(b) Shift Register Circuit for Generating a PRBS
(c) Power Spectral Density of a PRBS

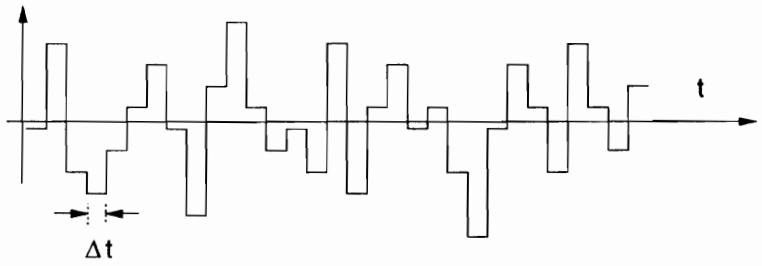

(a)

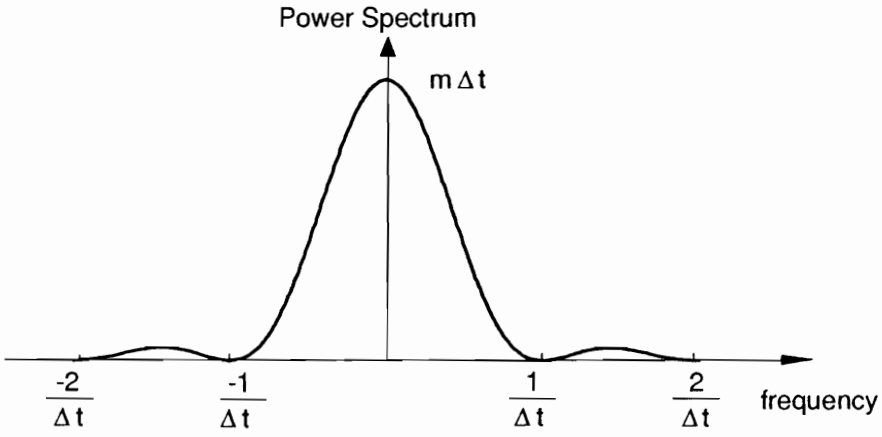

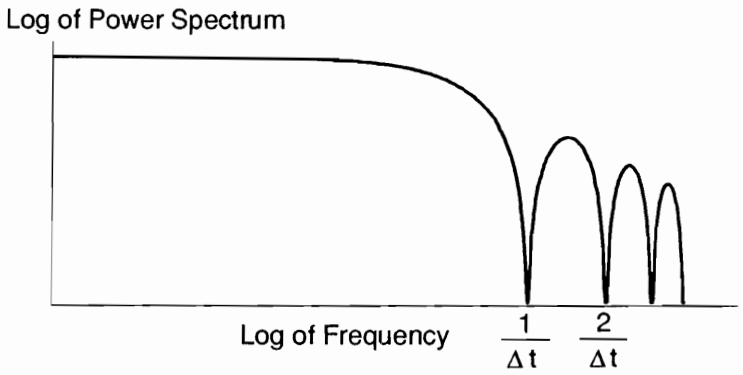

(b)

Fig. B.2: CSRS characteristics
(a) Sample Waveform
(b) Power Spectral Density of a CSRS

Appendix C

Stability of a Single-Loop Nonlinear System

Consider a single-loop nonlinear system containing a saturation nonlinearity as shown in Fig. C.1(a), where L represents a linear operator, and $k(t)$ represents a time-varying nonlinear operator. It will be shown that the stability property of the system in Fig. C.1(a) is similar to the stability property of the one in Fig. C.1(b), provided that the nonlinearity $k(t)$ is absolutely integrable.

Lemma [C.T. Chen, 1968]:

Let f_1 and f_2 be any functions defined on $[0, \infty)$. If f_1 is bounded on $[0, \infty)$ and tends to zero as $t \to \infty$ and if $\int_0^\infty |f_1(t)|dt < \infty$ then the convolution

$$(f_1 * f_2)(t) \equiv \int_0^t f_2(t-\lambda) f_1(\lambda) d\lambda \tag{C.1}$$

tends to zero as $t \to \infty$.

Theorem:

Consider the single-loop feedback system in Fig. C.1(a). If $\int_0^\infty |k(t)|dt < \infty$, and if the system in Figs. C.1(b) is BIBO stable, then the system in Fig. C.1(a) is also BIBO stable.

Proof: According to Fig. C.1(b),

$$y_a = L(u - Sy_a), \tag{C.2}$$

where S denotes the saturation nonlinearity. Assume that S belongs to the conic sector $\{c,r\}$, then expanding $S = c + R$, where R is a nonlinear operator belonging to the sector $\{r,-r\}$ yields

$$y_a = L[u - (c + R)y_a], \tag{C.3}$$

which can be simplified to

$$y_a = \frac{L}{1 + cL}(u - Ry_a). \tag{C.4}$$

It follows from the Circle criterion that one of the condition required for the feedback loop in Fig. C.1(b) to be BIBO stable is that $\frac{L}{1 + cL}$ is a stable linear operator; that is the impulse response $\left(\frac{L}{1 + cL}\right)(t)$ is stable which implies $\left(\frac{L}{1 + cL}\right)(t)$ is bounded on $[0,\infty)$ and tends to zero as $t \to \infty$.

On the other hand, according to Fig. C.1(a)

$$y = L[u - (1 + K)Sy] = L(u - Sy) + LKSy, \tag{C.5}$$

where K denotes the time-varying operator $k(t)$. Expanding $S = c + R$ yields

$$y = L[u - (c + R)y] + LKSy, \tag{C.6}$$

which can be simplified to

$$y = \frac{L}{1 + cL}(u - Ry) + \frac{L}{1 + cL}KSy. \tag{C.7}$$

Substituting Eq. C.4 into Eq. C.7 results in

$$y - y_a = \frac{L}{1 + cL}KSy, \tag{C.8}$$

or in the time domain

$$y(t) - y_a(t) = \int_0^{\infty} L'(t-\lambda)k(\lambda)Sat[y(\lambda)]d\lambda, \tag{C.9}$$

where $L' = \dfrac{L}{1+cL}$, and $Sat(.)$ denotes the saturation function which satisfies $|Sat(y)| < M < \infty$ (M is a real positive number). Applying the properties of 1-norm on Eq. C.9 yields

$$|y(t) - y_a(t)| \le M \int_0^{\infty} |L'(t-\lambda)||k(\lambda)|d\lambda. \tag{C.10}$$

since L' is bounded on $[0, \infty)$ and tends to zero as $t \to \infty$, and $k(t)$ is absolutely integrable, it follows from the above lemma that

$$\lim_{t\to\infty} |y(t) - y_a(t)| = 0. \tag{C.11}$$

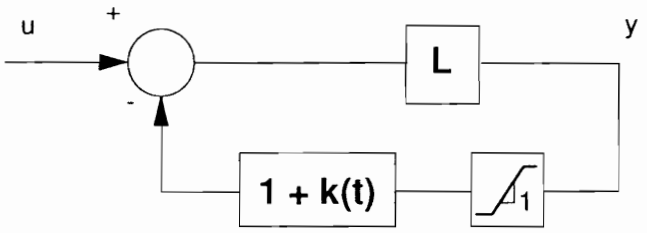

(a)

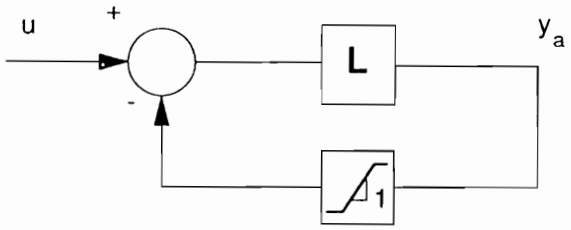

(b)

Fig. C.1: Single Loop Nonlinear Systems
(a) System Containing Two Nonlinearities
(b) System Containing one nonlinearity

Appendix D

MATLAB Programs

D.1 Small-Signal ARMA Modeling

```
%+++++++++++++++++++++++++++++++++++++++++++++++++++++++++++++++++++++++++%
%                                                                         %
%              Small-Signal Identification: ARMA Modeling                 %
%                                                                         %
%+++++++++++++++++++++++++++++++++++++++++++++++++++++++++++++++++++++++++%
load slpf0.dat            % Load data
U = slpf0(:,1);           % U = input data
Y = slpf0(:,2);           % Y = output data
Fs = 80000;               % Sampling frequency

%*************************************************************************%
% System identification for various orders                                %
%*************************************************************************%
max_order = 8;                        % maximum system order = 8 - 1 = 7
result = zeros (max_order,2);         % first column = system order
                                      % second column = LOG RMS error
for order = 2:max_order+1;            % sytem order = order - 1
   n  = length(Y) - order;
   UU = U(1:n);
   YY = Y(1:n);
   for i = 2:order;
      UU = [U(i:n+i-1) UU];
      YY = [Y(i:n+i-1) YY];
   end;

   Ye  = YY(:,1);
   Ue = [ones(n,1) UU  YY(:,2:order)];
   W = (Ue'*Ue) \ (Ue' * Ye);      %  Indentification -> ARMA model
   yd = Ue*W;
   result(order-1,:) = [order-1  log10(sqrt( mean (abs(Ye - yd).^2)))];
end;
result
```

```
%+++++++++++++++++++++++++++++++++++++++++++++++++++++++++++++++++++++++++%
%              Prompt user to select a system order                       %
%+++++++++++++++++++++++++++++++++++++++++++++++++++++++++++++++++++++++++%
system_order = input ('Select system order: ');
n  = length(Y) - system_order;
UU = U(1:n);
YY = Y(1:n);
for i = 2:system_order+1;
   UU = [U(i:n+i-1) UU];
   YY = [Y(i:n+i-1) YY];
end;
Ye  = YY(:,1);
Ue = [ones(n,1) UU  YY(:,2:system_order+1)];
W = (Ue'*Ue) \ (Ue' * Ye);        % ARMA model identification
numd = W(2:system_order+2)';
dend = [1  -W(system_order+3:length(W))'];


%*************************************************************************%
%                              Identification Result                      %
%*************************************************************************%
yd = Ue*W;
plot ([Ye(1:50) yd(1:50)]);
title ('Output Response Comparison');
pause;

%...Estimate Transfer function Z-domain -> S-domain  ...................
[num,den] = d2cm (numd,dend,1/Fs,'zoh');
%[z,p,k] = tf2zp (num,den);
%z = z(2:3);
%[num,den] = zp2tf(z,p,k);
w = logspace (1,6,300);
i = find (w > 2*pi*10);
i = i(1);
w = w(i:length(w));
i = find (w > 2*pi*1e5);
i = i(1);
w = w(1:i);
[mag,ph] = bode (num,den,w);
db = 20 * log10 (mag);
semilogx (w/2/pi,db);
grid;
title ('Transfer Function Gain [dB]');

figure
semilogx (w/2/pi,ph);
title ('Transfer Function Phase')
grid;
```

D.2 Sector Gain Identification of Nonlinear Part

```
%+++++++++++++++++++++++++++++++++++++++++++++++++++++++++++++++++++++++++%
%                                                                         %
%       Sector Gain identification of Nonlinear Part                      %
%                                                                         %
%+++++++++++++++++++++++++++++++++++++++++++++++++++++++++++++++++++++++++%
load w115_50.dat     % load linear ARMA model
W = w115_50;
Fs = 80000;          %  Sampling frequency

load l115.dat        % Load large-signal response data
U  = l115(:,1);      % U = input
Y  = l115(:,2);      % Y = output
clear l115;

%+++++++++++++++++++++++++++++++++++++++++++++++++++++++++++++++++++++++++%
%        Pass through Linear part: Input = U --> Output = Ya              %
%+++++++++++++++++++++++++++++++++++++++++++++++++++++++++++++++++++++++++%
order = length(W)/2;
Ya = Y;
UU = [U(order-1:-1:1)' 0];
YY = [Y(order-2:-1:1)' 0];
for i=order:length(Y);
  UU = [U(i) UU(1:order-1)];
  YY = [Ya(i-1) YY(1:order-2)];
  F = [1  UU  YY];
  Ya(i) = F * W;
end;

%+++++++++++++++++++++++++++++++++++++++++++++++++++++++++++++++++++++++++%
%                       Pass through mutiplier                            %
%+++++++++++++++++++++++++++++++++++++++++++++++++++++++++++++++++++++++++%
wp1 = 2*pi*24;
wz1 = 2*pi*240;
wz2 = 2*pi*240;
wp2 = 2*pi*2400;
numM = conv ([1/wz1 1],[1/wz2  1]);
denM = conv ([1/wp1 1],[1/wp2  1]);
[numM,denM] = c2dm (numM,denM,1/Fs,'zoh');
Wm = [numM -denM(2:3)]';

U = Ya;
Ya = Y;
UU = [U(2:-1:1)' 0];
YY = [Y(1)       0];
for i=3:length(Y);
  UU = [U(i) UU(1:2)];
  YY = [Ya(i-1) YY(1)];
```

```
  F = [UU  YY];
  Ya(i) = F * Wm;
end;

%+++++++++++++++++++++++++++++++++++++++++++++++++++++++++++++++++++++++++%
%                          Compute Sector Gain                            %
%+++++++++++++++++++++++++++++++++++++++++++++++++++++++++++++++++++++++++%
n = 8192
w = hanning (1024);
U = Ya(2:n+1);
Y = Y(2:n+1);
clear Ya;

[x,f] = psd (U,n,Fs,w);
c = 0:1:20;                          % this is the conic center
for i = 1:length(c);
   [y,f] = psd (Y - c(i)*U,n,Fs,w);
   r(i) = sqrt(sum(y)/sum(x));       % this is the conic radius
   [c(i)  r(i)]
end;
plot (c,r);
```

Vita

The author was born in Ban-Me-Thuot, Vietnam. He received his B.S., M.S., and Ph.D. degrees in electrical engineering from Virginia Polytechnic Institute and State University (Virginia Tech) in 1990, 1992, and 1994 respectively. Since 1990, he has been a Graduate Research Assistant at the Virginia Power Electronics Center at Virginia Tech. His research interests include modeling, design and stability analysis of switching regulators, space power systems, distributed power systems.